ICSAT 2011

Steve Hung
Aleksandar Subic
Joerg Wellnitz
Editors

Sustainable Automotive Technologies 2011

Proceedings of the
3rd International Conference

Springer

Sustainable Automotive Technologies 2011

Steve Hung · Aleksandar Subic · Jörg Wellnitz
Editors

Sustainable Automotive Technologies 2011

Proceedings of the 3rd International Conference

Springer

Editors
Professor Steve Hung
Clemson University International Center
for Automotive Research
Greenville
USA
sthung@clemson.edu

Professor Dr.-Ing. Jörg Wellnitz
UAS-Ingolstadt
Marie-Curie-Straße 6
85055 Ingolstadt
Germany
joerg.wellnitz@fh-ingolstadt.de

Professor Aleksandar Subic
RMIT University
School of Aerospace
Mechanical & Manufacturing Engineering
P.O. Box 71
Bundoora, Victoria 3083
Australia
aleksandar.subic@rmit.edu.au

ISBN 978-3-642-19052-0 e-ISBN 978-3-642-19053-7
DOI 10.1007/978-3-642-19053-7
Springer Heidelberg Dordrecht London New York

Library of Congress Control Number: 2011920836

Cover design: WMXDesign GmbH, Heidelberg

Printed on acid-free paper

Springer is part of Springer Science+Business Media (www.springer.com)

Preface

This third volume of the book on Sustainable Automotive Technologies published by Springer is a result of extensive investigations undertaken by researchers from industry, government research institutes, and universities worldwide. The book includes a selection of 17 papers from the total of 35 contributions presented at the Conference, coming from Europe, US, Hong Kong, Australia and Columbia. The contributions that have been selected for publication in this book have been peer reviewed by an international panel of experts and edited by the Editors appointed by Springer.

This publication is an important outcome of the 3rd International Conference on Sustainable Automotive Technologies, ICSAT2011 that was organised in Clemson, South Carolina, US by the Clemson University International Centre for Automotive Research (ICAR), in collaboration with the University of Applied Sciences Ingolstadt, Germany and RMIT University in Melbourne, Australia. It follows the successful launch of the first conference in this series that was held in Melbourne in 2008 and chaired by Professor Aleksandar Subic, and the subsequent second conference which was held in Chiemsee in the German Alps and chaired by Professor Joerg Wellnitz. This third conference in the series is chaired by Professor Steve Hung. The ICSAT2011 conference has attracted over 100 participants from many organisations and countries. The conference has attracted significant industry support, especially from the local automotive industry hub in South Carolina, US.

The Editors and their respective universities are proud to announce this publication that represents an important milestone for the dissemination of knowledge about sustainable automotive technologies, and in particular about the emerging and developing green car technologies. With over 900 million vehicles on world roads today contributing to around 16% of total greenhouse gas emissions (and rising), the need for strategic research in and rapid development of green cars and associated sustainable technologies is growing. The book aims to address this need by highlighting some of the key technologies and practices in this field. It also aims to provide a balanced view on the range of green car technologies considered by industry and academia.

The Editors wish to thank all authors, international reviewers and Springer for their support and contributions without which this publication would not be possible. We hope that everyone involved with sustainable automotive technologies or interested in this particular topic will find this book to be a valuable resource going forward.

The Editors

TABLE OF CONTENTS

V Materials and structures

VI Vehicle systems

I EVALUATING SUSTAINABILITY

A HOLISTIC APPROACH TO SUSTAINABILITY EVALUATIONS IN THE AUTOMOTIVE INDUSTRY

J. Weber, M. Bowler, T. Kurfess

Clemson University International Center for Automotive Research, 4 Research Drive, Greenville, SC 29607, U. S. A.; Email: mbowler@clemson.edu

Abstract: The influence of sustainability has revolutionized the automotive industry. Although the industry has made countless improvements in this arena, it is still far from being sustainable. To date the majority of sustainability efforts have focused on environmental friendliness, both of the cars and the respective production processes. However, in order for an automotive corporation to be truly sustainable in the future all business decisions will need to be driven from the view point of sustainability. A true sustainable solution must be logical economically, socially, and environmentally, both locally and globally within the corporation. This approach requires the consideration of the following four domains: mobility system, phases of the extended life cycle, level of value creation, and sustainability perspective. This paper aims to create a structure to allow cause and effect mapping between decisions made at all points in the vehicle life cycle at all levels of value creation within a given mobility system in order to determine its true sustainability. This structure allows decision makers to comprehensively understand, evaluate, and compare products, processes or business alternatives in terms of their sustainability. This will in effect facilitate localized decisions that make sustainable business sense locally and globally within the corporation, and ultimately within the automotive industry.

1 Introduction

Sustainability, or the ability to sustain or endure, was refined in terms of human sustainability by the Bruntland commission in 1987 as the "development that meets the needs of the present without compromising the ability of future generations to meet their own needs." [1] This requires a holistic approach that considers economic, environmental, and social aspects in the development of everything from manufactured goods and public policy to corporations and personal lives. Maintaining an intact environment, a society in physical and psychic health, and economically successful business are the three main targets which are mutually interdependent and hence all of equal importance (see Fig. 1) [2].

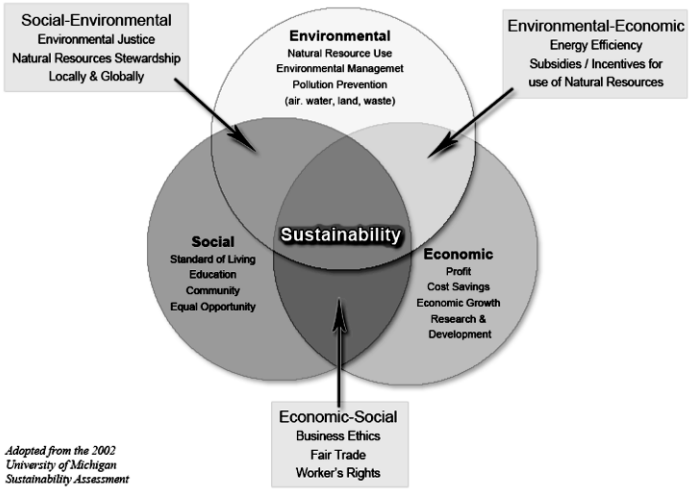

Fig. 1: The Three Spheres of Sustainability [2]

2 Sustainability in the Automotive Industry

In the automotive industry, sustainability has been primarily synonymous with environmental friendliness, initially of the vehicles and then of their respective production processes. This is achieved by methods such as life cycle analysis and design or environmental accounting. For the automakers, environmental friendliness was achieved by complying with the legal requirements, usually at the expense of undercutting their economic targets. In the past this compliance created a vehicle that was “green enough” for consumers and therefore green enough for the manufacturer [3].

Over the last decade however, sustainability has received an increasing amount of attention. A good indicator of this is the jump of corporate issued sustainability reports from around 300 in 1996 to over 3,000 in 2009 [4]. There has also been an emergence of environmental standards, best practices, and rankings such as ISO 14000, European Eco-Management and Audit Scheme (EMAS), and the Dow Jones Sustainability Index for corporations [5,6]. Since 1999, the Dow Jones sustainability indexes (DJSI) track the financial performance of the leading sustainability-driven companies worldwide and provide investors with a financial quantification of and a ranking in terms of sustainability [7]. Moreover, in the most recent years tools that allow individuals to calculate their own environmental impact or assess their personal sustainability have been made easily accessible on

the web [8,9]. Today, an integrated idea of sustainability is prevalent to all stakeholders whether it is businesses, government, or general society. This translates to the following attributes that affect the automotive industry:

- Society as a whole is not only more sustainability conscious, but also more discerning towards others and their sustainability claims.
- Customers now see ecologic friendliness of a car and the overall sustainability of the related processes as a relevant feature by which competing car offers can be differentiated just like vehicle dynamics or cabin comfort, and are therefore ready to pay a premium price for it. (e.g. hybrid or electric cars).
- Managers in the automotive industry agree that in the long run, social responsibility, ecological reasonability, and economic management represent not only the most humanitarian but also the most economic way of doing business.
- Investors and analysts use corporate sustainability as an important criterion, representing a major driver for long-term economic success and thus for long-term shareholder value. Companies with a high degree of corporate sustainability embrace opportunities to leverage their sustainable position and manage the risks deriving from economic, environmental and social development.

As a consequence, acting sustainably, and attaining the related public perception, has become an important but complex asset that requires appropriate management tools. Precarious situations might arise for companies marketing environmentally friendly or sustainable products or services. In a society where a company's image is worth billions of dollars it is important that it operates in a manner consistent with its image. Any company caught not living up to these standards runs the risk of loss market share and brand loyalty.

In addition, as environmental aspects of product, production, and corporate operation improve and become ingrained in the future, social responsibility will start to play a more significant role. It is expected that in the future social responsibility will attain a comparable amount of transparency and attention as environmental responsibility does today. Therefore, companies must begin to address these issues now so they can meet customer expectations for the future.

This paper serves as an approach to enable automotive companies to holistically assess their sustainability status by means of a practical checklist. As a multitude of methods on rating economic success is available, the checklist will focus on ecologic and social sustainability.

3 A Holistic View on Sustainability

An objective assessment of technical or business alternatives in terms of sustainability requires a holistic view that covers the multiple dimensions of sustainability as depicted in the "Sustainability Cube" (Fig. 2). The cube is constructed from the three dimensions that affect the sustainability of a product.

The first dimension is “The mobility system”, which includes not only the vehicle but also the propulsion energy and traffic infrastructure that the vehicle relies on to operate. The second dimension is the phases of the life cycle which consists of six phases: (1) Strategy, R&D, Planning (2) Marketing, (3) Production, (4) Sales and Distribution, (5) Usages, Maintenance, and Repair, (6) End of life. The final dimension is the level of value creation that, depending on industry, consists at the very minimum of the original equipment manufacturer (OEM), service provider, component supplier, and material supplier.

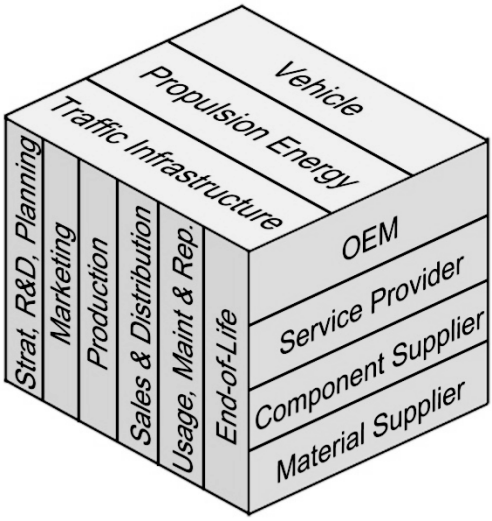

Fig. 2: Sustainability Cube

Each interface between the three dimensions of the sustainability cube represents a cell in which sustainable factors must be considered. This can only be done effectively not only considering the sustainability effect internal to the cell, but also where decisions made in that cell (or array of cells denoted by []) effect other cells within the cube. The following serve as some examples

Strategy, R&D, Planning-[Mobility System]-OEM

Even before the first car has been built and is used by a customer, the mobility system has had an economic, ecologic and social impact (e.g. treatment of people involved, development costs, risks, emissions and waste of prototype testing etc.). Working methods during this phase such as design to manufacture, design to service, or design to recycling vastly determine sustainability in following phases.

[Life Cycle]-Propulsion Energy-[Value Chain]

Here, not only the creation processes (oil production and refining, power generation, hydrogen generation) must be taken into account. A comprehensive “well to tank” analysis requires also incorporation of the distribution processes including

the required infrastructure: fuel transport on water, road and rail; pipelines, filling stations, tanks, power grids, storage power stations etc.

Usage, Maintenance, Repair-Traffic Infrastructure- OEM

The processes that create and operate the infrastructure that is required to generally enable usage of the vehicle must be considered (roads, bridges, tunnels, lighting, parking structures, traffic control, road toll collection systems etc.). These define the environment in which the vehicle will operate and thus must be considered in order to determine how the vehicle will interact with and what impact it will have socially, ecologically, and economically in its environment. A current example of this is traffic and parking problems in megacities, and the cost and maintenance associated with use by certain vehicles.

Production-[Mobility System]-[Value Chain]

The processes taking place at construction sites ("production" of the traffic environment), energy creation sites, or vehicle and components manufacturing plants are among the biggest contributors to sustainability. All along the value creation chain, emissions and waste caused by chemical or physical processes, fair treatment of workers and employees must be evaluated thoroughly.

[Life-Cycle]-Vehicle-[Value Chain]

It is not sufficient to only consider the processes carried out at OEM level. Along the value creation chain, there are multiple levels of contributing processes at 1^{st} to n^{th} tier suppliers, material suppliers, or service providers. Here, critical aspects are compliance of suppliers with regulations concerning ecological and social responsibility, especially for suppliers from developing countries which are chosen for cost reasons. This is in addition to ensuring economical health and thus continued existence of business partners is part of a sustainable business approach

Given the current industrial landscape some cells are regarded as more important than others. For example Production-Vehicle-OEM is much more relevant to an automotive OEM than Marketing-Traffic Infrastructure-Material Supplier. In the future, this might change as the industry evolves and as an example an OEM finds itself in a position of creating a purpose built vehicle for a new type of traffic infrastructure, then this cell becomes extremely relevant.

4 The Sustainability Checklist

In a holistic sustainability assessment, each cell of this Sustainability Cube has to be investigated, independent from the size of the concept that should be evaluated , be it a new production system, a new vehicle concept, new forms of propulsion energy, or even alternative mobility scenario (such as banning personal vehi-

cles from inner city areas). As explained above, acting sustainably means optimizing the resulting impact for the respective business unit (economic responsibility), the local and global environment (ecologic responsibility), and the human beings directly or indirectly affected of the product and its related processes (social responsibility).When going through the cells of the Sustainability Cube, all three dimensions have to be taken into account. This is supported by a Sustainability Checklist (Fig. 3) with general questions that in conjunction with the distinct cube cells lead to very specific answers.

As mentioned before sustainability to date has been well defined in terms of environmental and ecological aspects and is therefore relatively easy to assess from the business status point of view. Social aspects on the other hand are poorly defined and cannot be as easily, or succinctly, compared or assessed. Therefore for this area the checklist consists of two general questions in conjunction with two example questions that must be assessed in order to ensure social sustainability.

5 Summary and Next Steps

With sustainability becoming a more relevant characteristic of products, brands, and companies, a methodology is required that allows a holistic assessment of the complex notion of sustainability. For this purpose, the structure represented by the Sustainability Cube and the checklist are a pragmatic and effective tool. The logical next step would be the introduction of quantitative evaluations that would lead to a Sustainability Index by which alternative solutions could be directly compared and ranked. In addition, more prevalent social sustainability characteristics must be established.

Part 1: Environmental Sustainability: Minimizing the impact a business has on the ecological environment

- Minimized utilization of exhaustible resources (e.g. water, energy, fossil fuel …)?
- Minimum energy consumption?
- Minimum emissions (gaseous, evaporations, particulate, noise, thermal, electromagnetic …)?
- Minimum waste (toxic, non-toxic, degradable)?
- Has the basic principle of avoid – reuse – recycle – dipose been applied?

Part 2: Social Sustainability: Minimizing the impact a business has on the social environment

Generic:

- What is the impact of business practices on people associated directly to the product or production of the mobility system (e.g. employees, purchaser of vehicle)?
- What is the impact of business practices on people indirectly associated to the product or production process (e.g. communities surrounding a production plant, local governments, neighbors to people who purchase the vehicle, cities)?
- Have basic principles like those embodied in the the ILO convention (freedom of association and collective bargaining, discrimination, forced labour, child labour) been applied all along the value creation chain?

Examples:

- Workplaces are designed to ensure physical health (physical strain, ergonomics, noise, light, accessibility, climate, possibility to recover, health insurance benefits …)?
- Psychic health of workers/employees/managers is ensured by respective policies, corporate culture, management conduct, fair and predictable treatment, consideration of individual human aspects …?

Part 3: Economic Sustainability

- Is there a consistent long term strategy for this part of the business?
- Is the business governed by appropriate management methods/capabilities?

Fig. 3: Sustainability Checklist

References

[1] Brundtland G. Presentation of the report of the world commission on environment and development to UNEP's 14th governing council session. June 8,1987. Nairobi, Kenya
[2] Vanderbilt University: <http://www.vanderbilt.edu/sustainvu/sustainability.php>
[3] Weber J: Automotive Development Processes, Springer 2009
[4] "Trends in Sustainability Reporting" CRNews Monthly. February 2010. http://businessinthecommunity.newsweaver.co.uk/bitcnewsletter/vzas9fduievnkdv89usw6o
[5] ISO 1400. http://www.iso.org/iso/iso_14000_essentials
[6] EMAS. http://ec.europa.eu/environment/emas/index_en.htm
[7] Dow Jones Susatainability Index. http://www.sustainability-index.com/
[8] Source Map Open Supply Chains. http://www.sourcemap.org/_
[9] Connected Urban Development. http://urbanecomap.org/

II TECHNOLOGIES FOR PRODUCTION

FLEXURAL CREEPING ANALYSIS OF POLYURETHANE COMPOSITES PRODUCED BY AN INNOVATIVE PULTRUSION PROCESS

S. Bruckmeier[1], J. Wellnitz[1,2]

[1] Research-Institute for Technology and Artistic Design GmbH, Marie Curie Straße 6, 85055 Ingolstadt, Germany; Email: stephanie.bruckmeier@itd-in.de,

[2] University of Applied Sciences Ingolstadt, Esplanade 10, 85049 Ingolstadt, Germany; Email: joerg.wellnitz@fh-ingolstadt.de

Abstract: An innovative pultrusion process makes it possible to produce fiber reinforced polyurethane composites with superior mechanical properties that allow various applications in the automotive industry e.g. as structural lightweight parts for future e-mobility. In the new pultruded polyurethane composite more reinforcing fibers can be concentrated to achieve excellent short term mechanical properties e.g. stiffness, strength or damage tolerance. Furthermore the new cost-effective and highly automated process allows the production of profiles with very complex cross-sections. However, the knowledge on long term mechanical behaviour of this polyurethane material is limited. In the present study continuous fiber reinforced composites fabricated by the innovative pultrusion process are investigated in terms of viscoelastic creep and creep-rupture properties. Specimens of unidirectional E-glass with polyurethane, epoxy, polyester resins and a composite of polyurethane with basalt fiber have been tested in long term three-point flexure tests. For theoretical description the plate theory of E. REISSNER has been considered and simplified to derivate analytical solutions. Furthermore approaches are currently made to modify the constitutive equations in the simplified Reissner respectively thus the experimental data can be used for the mathematical description of creep behavior in thicker plates.

1 Introduction

A new pultrusion technology allows manufacturing complex profiles (see Fig. 1) with superior mechanical properties. The process makes it possible to enhance the content of reinforcing fibres up to 72 percent fiber volume fraction.

So far the pultruded reinforced material has exhibited promising short term mechanical properties in terms of e.g. stiffness, strength, elongation to failure, shear strength and impact resistance [5]. However the application as a structural part requires also investigations on long term behavior such as creep. Hence the scope of this analysis is the basic investigation of the flexural viscoelastic creep behavior. Besides the experimental program a new simplified REISSNER Theory and an approach for its solution is presented. After modifying the HOOKE`s Law according to the experimental results the plate theory is applicable for the creep analysis of thicker composites under external flexural load.

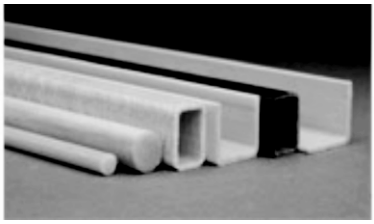

Fig. 1 Fiber reinforced polymers produced by an innovative pultrusion process [5]

2 Manufacturing process

Pultrusion is a continuous method of manufacturing various reinforced plastic shapes of complex cross sections. The unidirectional roving's are drawn through a liquid specially formulated thermosetting resin bath to thoroughly wet every fiber. A forming-shaping guide assembles the coated fibers. While the fibers are pulled through a die the resin is cured under pressure and heat. Figure 2 shows the classcal pultrusion process with two component system of polyol and isocyanate [3, 5].

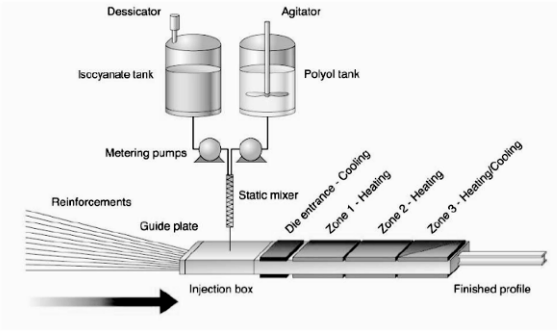

Fig. 2 Schematic of a typical polyurethane pultrusion set up [5]

3 Experimental work

Specimens of unidirectional E-glass polyurethane composites are tested in long term three-point flexure tests. The procedure closely follows the EN ISO 899-2:2003 standard. For the purpose of comparison the program includes the investigation of epoxy and polyester as resins, both with E-glass fiber reinforcement and in addition polyurethane with basalt fibre. The material combinations have been tested along and in transversal fiber direction. Almost all creep tests are performed at room temperature, temperature of 60°C with 5% relative humidity and tests with 95% humidity. Various stress levels have been applied based on the flexural strength of the E-glass polyurethane composite obtained in the respective static tests.

So far the high stress creep results for transversal and axial tests have been obtained. The maximum deformations at mid-span of the samples are measured with time and the strains as a function of time for the three point test are calculated according to the beam theory respectively. Figure 1 shows exemplify the variation in strain with time at room temperature and an axial loading of 30 percent of the flexural strength. While the polyester composite failed within the very first day the epoxy and polyurethane glass fiber composite exhibit slighter creep and maintain the load. Probably due to the not yet optimized quality regarding the fiber matrix interface, the basalt composite exhibit inferior long term properties. Tests with transversal loading have shown similar characteristics.

All in all the initial results indicate the dependency of the chosen resin and manufacturing process, whereas the pultruded glass fiber polyurethane exhibits promising substantial creeping resistance. Furthermore it is confirmed that creep and creep rupture do occur also in fiber direction. Because of limited testing stations and the wide variety of test conditions the load time was limited to 1000h.
The program is not completely conducted yet and has to be continuing and repeated also in regard to the statistical evaluations [2, 5, 6].

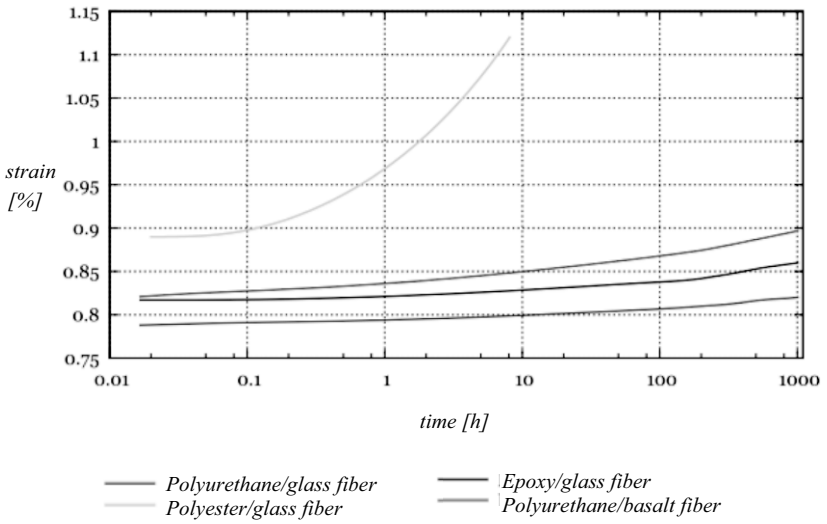

Fig. 3 Axial loading of 30 percent stress level of flexural strength of the E-glass polyurethane composite (at room temperature) [2].

4 Approach for a theoretical analysis

The experimental data obtained from short and long term tests allow to find relations between strain rate, stress, temperature and time. However for calculating and simulating the material behavior under external load, adequate theories are required.

Since innovative, very light materials as the pultruded fiberglass are usually designed with thicker walls and or show a relatively soft interlaminar shear modulus, they perform completely different under external load compared to the traditional structures for example steel or concrete parts. By applying the classical plate theory for those modern materials more stress is calculated und the deflections will be underpredicted since the structures are assumed to be too stiff.

Thus other “modern” plate theories like the REISSNER theory are necessary.
The REISSNER theory provides a higher degree of accuracy as the effects of the third dimension are taken into account. The theory considers shear and normal transverse stress, whereas in the classical theory based on the KIRCHHOFF/BERNOULLI hypothesis these stress components are neglected completely.

The REISSNER problem results in three inhomogeneous, time variant, linear, partial differential equation with constant coefficients, which are partly interconnected to each other. Because of the complexity of this system of differential equations, even for static problems, we introduced an approximation based on the GAUSSIAN curvature. The idea is to uncouple the second and third REISSNER differential equations, which is given by a specific derivation term. This term is replaced by a new constant parameter P. We suppose that the rectangle plate has a very small pre-curvature and thus the GAUSSIAN curvatures are very small. This approximated value P orientates on the small given pre-curvature of the plate. With this assumption of a plate-imperfection as show in figure 4, we construct analytical solutions with the aid of traditional mathematical methods. The solutions consist of well-known elementary functions that exactly satisfying these simplified REISSNER differential equations for the static problem [1, 4].

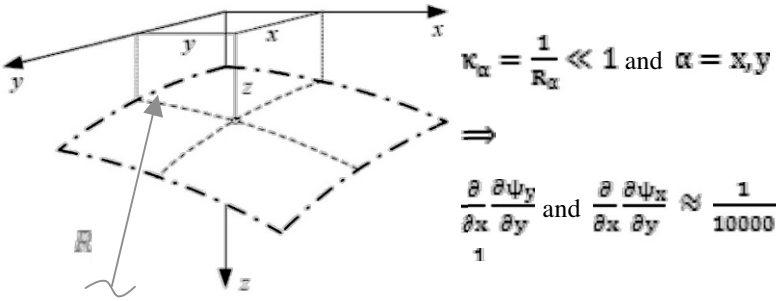

Fig. 4 Assumption of a very small imperfection of the elastic plate [1]

To reflect time dependency a reliable constitutive model must be formulated and integrated in the simplified Reissner theory which is currently been working on.

5 Core benefits and application of pultrusion profiles

The innovative pultrusion technology allows the use of a higher concentration of fiberglass, which leads to many superior properties compared to traditional materials. With the new fiber glass-reinforced pultruded polyurethane it is possible to reduce the wall thickness, which yields to lower weight of the structural construction or it can be fabricated to take advantage of the higher stiffness at constant cross-section.

In addition to the mechanical advantages the pultrusion process is environmental friendly (without styrene), cost effective and allows high-speed and automated

production with high-quality and commercialized polyurethane. Furthermore almost any constant cross-section part can be manufactured. Also excellent resin-to-fiber bonding and transverse properties have been achieved so far [5].

Because of the outlined key benefits the pultruded lightweight material is applicable for a variety of industries, e.g. aerospace and automotive. Especially the advantage in terms of the lighter weight, wide availability and high performance in combination with the highly automated mass process makes it a promising structural part (such as space frame construction) for sustainable future e-mobility.

6 Conclusion

So far the preliminary results of the long term three point bending tests indicate that the fibre-reinforced polyurethane exhibits better creep performance compared to alternative resins. The lightweight material is one of the promising key technologies in the development of efficient and sustainable e-mobility solutions.

Furthermore in this study the mathematical description of thicker plates has been considered. The REISSNER theory was simplified by introducing a constant parameter that made it is possible to derivate analytical solutions. To implement the creep behavior in the REISSNER equations the HOOKE`s law has to be modified respectively. For a complete creep modeling the end results of the long term tests which are still in progress have to be taken into account. Furthermore the verification of the applied models must be performed.

References

[1] Bruckmeier S.: *Behandlung und Lösung von Flächentragwerksproblemen moderner Plattentheorien,* Master Thesis, Hochschule Ingolstadt, Ingolstadt, Germany, 2010
[2] Bruckmeier S., Wellnitz J.: *Kriechen von Pultrudaten*, Forschungsbericht, Institut für Technik und Design GmbH, Ingolstadt, Germany, 2010
[3] Haberstroh E., Michaeli W. Meyer F., Pauling A.: *PUR – Neue Wege mit innovativem Werkstoff,* 24. IKV-Kolloquium Aachen, Germany, 2008
[4] Reissner E.: *The Effects of transverse shear deformation on the bending of elastic plates*. Journal Appl. Mech. 12., 1945
[5] http://www.bayermaterialscience.de
[6] Abdel-Magid B., R. Lopez-Anico R. Smith G., et al.: *Flexure creep properties of E-glass reinforced polymers, In: Composite Structures*, 2003, 247-253

MANUFACTURING MICROSTRUCTURED SURFACES FOR AUTOMOTIVE APPLICATIONS

A. Cannon, M. Maguire, R. Hulseman, W. King

Hoowaki LLC, 511 Westinghouse Rd, Pendleton SC 29670, U. S. A.;
Email: ralphhulseman@hoowaki.com

Abstract: Every manufactured part has a surface finish, and this finish affects many attributes of the part including: water or oil repellency, friction coefficient, or appearance. This paper describes how microstructures can be manufactured into the surface of real manufactured metal parts with a focus on the application of water repellency.

1 Introduction

Superhydrophobicity is the extreme water repelling ability of some natural surfaces like the lotus leaf [1] and synthetic surfaces that mimic the surface structure and chemistry of the lotus leaf [2]. Figure 1 illustrates the concept of how surface microstructures affect the water repelling characteristics of a surface. When a surface becomes rough with patterned microstructures, the surface microstructures affect the way that water interacts with that surface. In the presence of microstructures, a surface that repels water ("phobic") becomes more water-repelling and a surface that attracts water ("philic") becomes more attractive.

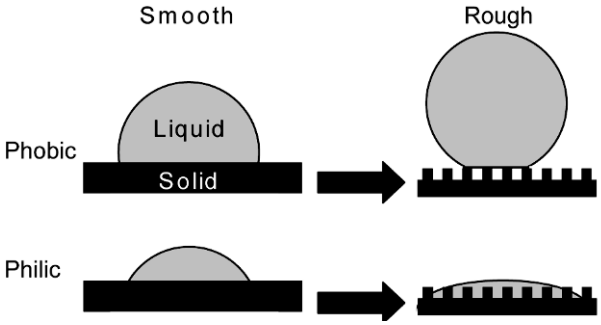

Fig. 1 Surface roughness amplifies natural surface chemistry.

2 Superhydrophobic Silicone Micropillars

Figure 2 shows fabricated silicone rubber micropillars that rendered the normally hydrophobic silicone superhydrophobic. While the smooth polymer originally had contact angle $\theta = 112°$, the microstructured polymer has $\theta = 152°$. Using inexpensively fabricated superhydrophobic products to protect expensive equipment could mitigate the cost of automobile corrosion. The National Association of Corrosion Engineers estimates corrosion consumes 3% of the Gross Domestic Product of the United States annually [3]. Superhydrophobic surfaces can also exhibit "self-cleaning" properties useful for automobiles because droplets that roll off of the surface carry away particles that are larger than microstructure spacing [1]. Superhydrophobic microstructures such as Figure 2 shows have been used to decrease drag [4, 5] and reduce ice thickness and adherence [6].

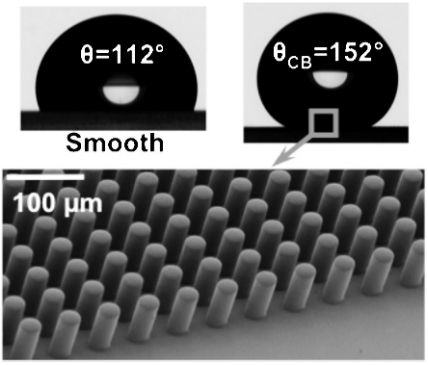

Fig. 2 Micropillars molded into silicone rubber cause an increase in contact angle and render the silicone superhydrophobic

3 Tools for Superhydrophobic Polymer Microstructures

Hoowaki produces flat and curved molding tools for molding superhydrophobic structures into polymers such as santoprene that is used extensively in automobiles. The tools can be used in a press or as an injection mold insert. As Figure 3 shows, the process of molding a superhydrophobic polymer surface begins with a mold cavity and a microstructured steel insert. The steel insert is assembled with the mold cavity, and polymer is molded in the assembly. A polymer replicate results having microstructures from the steel insert. The microstructures shown in Figure 3 cause superhydrophobicity demonstrated in Figure 2.

Microstructured tools can have microholes or micropillars depending on the specific application. Figure 4 shows a stainless steel mold insert with micropillars on a two dimensional curved surface. The microstructures Hoowaki produces range in size from 5 μm to 200 μm, and the molding tools range in macro size from 1" to 6" and can be machined to fit specific applications. The materials Hoowaki can microstructure include stainless steels, tool steel, nickel, titanium, copper, and carbide steels.

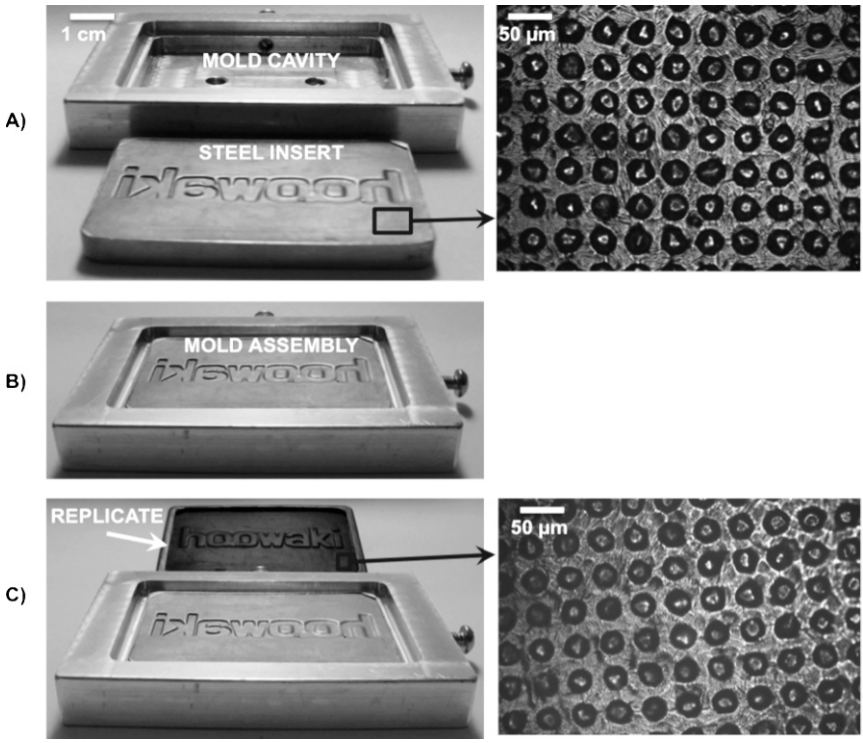

Fig. 3 Production of microstructured superhydrophobic molded parts using microstructured steel mold inserts - A) The process begins with a mold cavity and a microstructured steel insert. B) The steel insert is assembled with the mold cavity, and polymer is molded in the assembly. C) A polymer replicate results having microstructures from the steel insert. The microstructures shown here cause superhydrophobicity demonstrated in Figure 2.

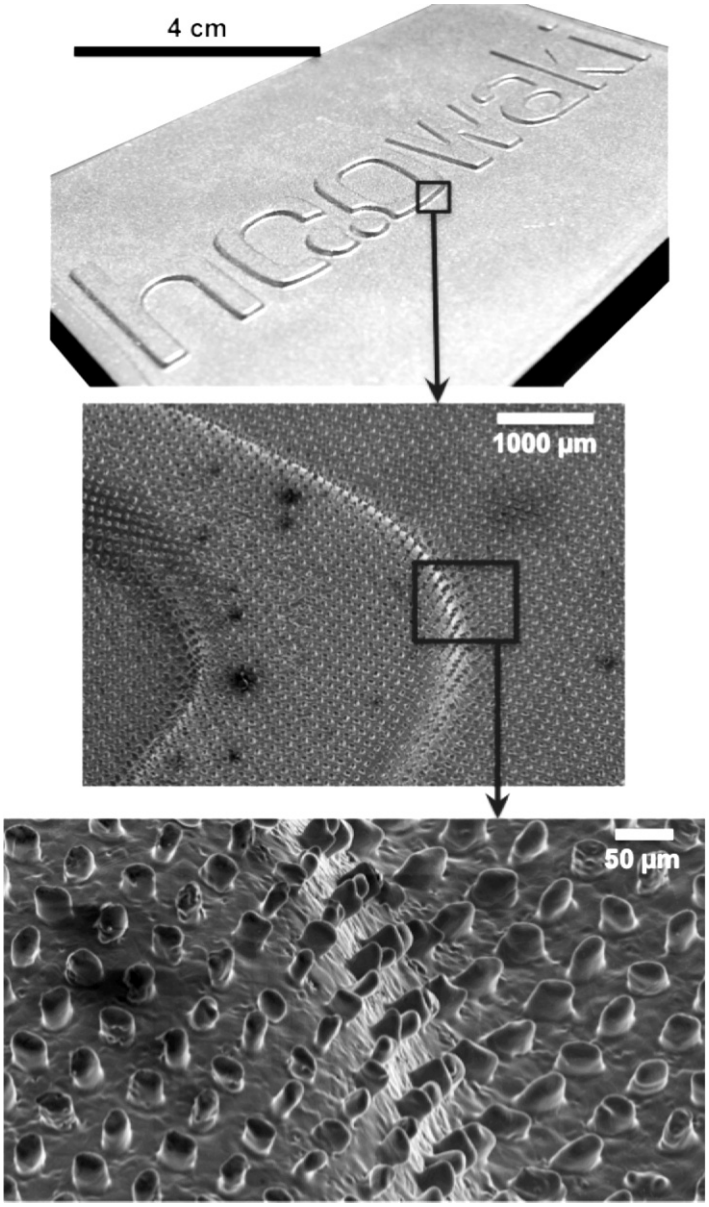

Fig. 4 Stainless steel micropillars with two dimensional curved surfaces - Hoowaki produces stainless steel tools with flat and curved surfaces with microholes and micropillars.

Acknowledgments

Hoowaki thanks the National Science Foundation and the South Carolina Research Authority for funding the present work.

References

[1] Neinhuis, C. and W. Barthlott, *Characterization and Distribution of Water-repellent, Self-cleaning Plant Surfaces*. Ann Bot, 1997. 79(6): p. 667-677.
[2] Cannon, A.H. and W.P. King, *Hydrophobicity of curved microstructured surfaces* Journal of Micromechanics and Microengineering, 2010. 20(2): p. 025018.
[3] Koch, G.H., et al., *Corrosion costs and preventative strategies in the United States*. 2002, National Association of Corrosion Engineers (NACE)
[4] Watanabe, K., *Fluid frictions of shark skin and lotus leaf - How does the drag reduction occur?* Journal of Japanese Society of Tribologists, 2000. 45(5): p. 354-359.
[5] Wilson, M., *Superhydrophobic Surfaces Reduce Drag*. Physics Today, 2009. 62(10): p. 16-19.
[6] Cao, L., et al., *Anti-icing superhydrophobic coatings*. Langmuir, 2009. 25(21): p. 12444-12448.

THE FIRST WATER BASED PRETREATMENT SYSTEM FOR DIRECT GLAZING

W.-R. Huck

Sika Technology AG, Tueffenwies 16, CH-8048 Zurich, Switzerland;
Email: huck.wolf-ruediger@ch.sika.com

Abstract: Here, the first waterborne pretreatment for Direct Glazing is presented, Sika HydroPrep®-100, a water based Activator for glass bonding including current applications in Automotive. The excellent product properties of Sika HydroPrep®-100 such as the possibility of shorter flash-off times, much lower odour, easy handling of the mixed activator and removal in case of contamination are discussed. To complete a VOC-free direct glazing process, also the adhesive has to be solvent-free and solvent free alternatives for paint treatment are required. Here, different solutions are feasible and will be discussed.

1 Introduction

Elastic bonding is a well established joining technology in the Automotive industry, especially with regards to the bonding of two different materials. In the past, all pretreatment systems in Automotive Direct Glazing, such as cleaners, activators and primers were solvent-based.

A first, significant reduction in VOC output could be achieved by implementing primerless technology. Here, the black primer is eliminated completely from the bonding process and only a specially formulated solvent-based activator is applied as glass pretreatment. This technology was first established at Automotive OEMs in 1985 and is now a well accepted process.

With the introduction of the first waterborne activators for Direct Glazing, the VOC output could be further reduced by almost 99%, due to a very low content of VOC in the product. Figure 1 illustrates this VOC reduction.

The technical properties and key data of Sika HydroPrep®-100 are comparable to the solvent-based technology such as Sika® Aktivator in terms of shelf life, adhesion performance on float glass or glass ceramic frits, as well as the maximal open time. Furthermore, the amount of material required for the activation was reduced to about 50%.

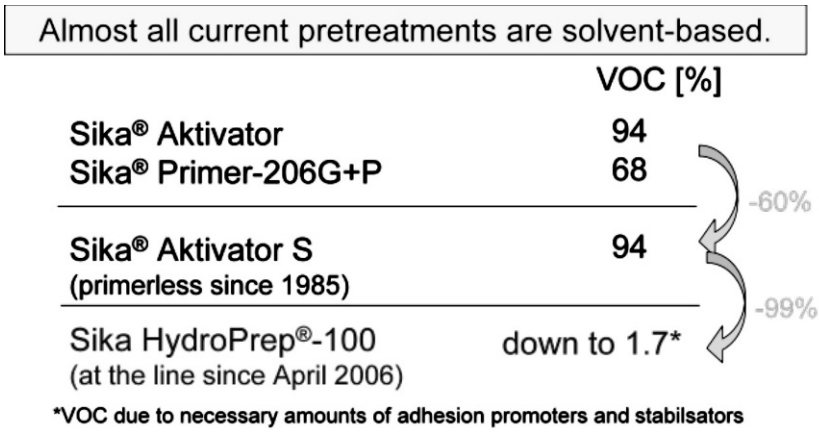

Fig. 1 VOC reduction advantage of Sika HydroPrep®-100

2 Sika HydroPrep-1: Properties

Based on water, the product is much more user-friendly with regards odour. Furthermore, handling of the mixed activator is much easier, as it is not sensitive to moisture and water evaporates much more slowly than other organic-based solvents. This information was collected from 2 different European car manufactures in various line trials and laboratory tests, where Sika Hydroprep®-100 was used daily for the serial production cars.. No ventilation is required for the removal of solvent fumes, avoiding important investments and running expenses for energy and maintenance. Figure 2 is a summary of general handling properties.

Fig. 2 Sika HydroPrep-100 general handling properties

3 Comparison of time to bonding

As the adhesion promoters are already hydrolysed, Sika HydroPrep®-100 offers the possibility of shorter flash-off times,. The adhesive can be applied as soon as the water has evaporated, which means the open time is effectively a 'visible minimum open time'. On the wet surface, the adhesive will also build up adhesion, but handling is not possible and the adhesive bead may shift when oriented horizontally. Figure 3 illustrates potential process timing impact.

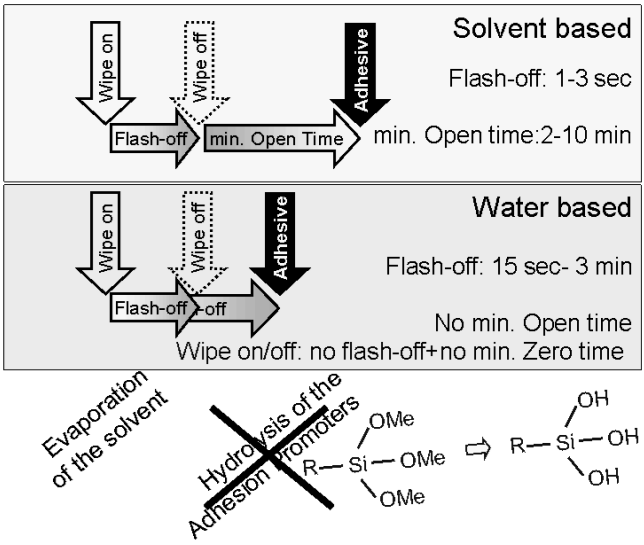

Fig. 3 Comparison of time to bonding of solvent based and water based adhesive pretreatment

4 General Overview of Ecological Study Results

In an ecological study these parameters were calculated. As a reference, the current 2-step pre-treatment, consisting of application of an activator and a primer, was used. The primerless solution, where only an activator is applied, already leads to a significant decrease on impacts of in energy demand, which in turn reduces the impact of car production on climate change, potential of overfertilisation and acidification, summer smog or raw material scarcity. Switching to the Sika HydroPrep®-100 all these effects are again significantly decreased, *e.g.* only 10% of the initial values for the cumulated energy demand or impact on climate change are obtained. Figure 4 shows comparative ecological impacts of preparation treatment options.

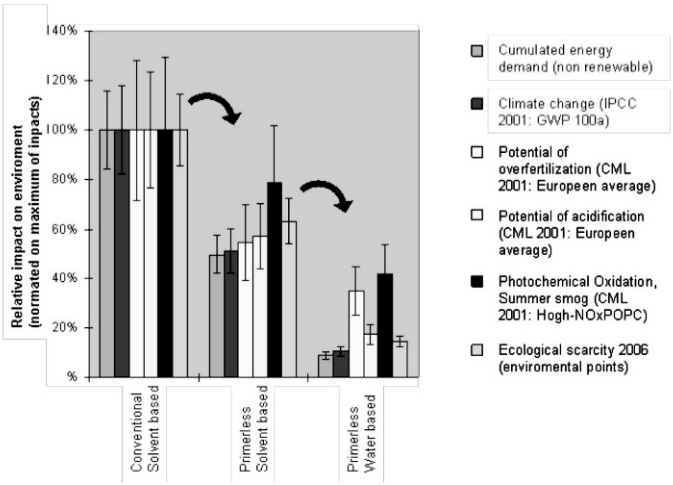

Fig. 4 Comparative ecological impacts of preparation treatments

Additional benefits are that the product is not considered as a dangerous good and does not require any safety labels. Therefore, there are advantages when using water-based activators with regards to transportation and stocking of the material. Furthermore, the standard aluminium containers which are used for solvent-based primer packaging can be replaced by an environmentally friendly plastic bottle.

To complete a VOC-free direct glazing process, the adhesive must also be solvent-free. The pretreatment of the paint and processing products such as cleaners must also be considered.

5 Sika's VOC-free Bonding Concept

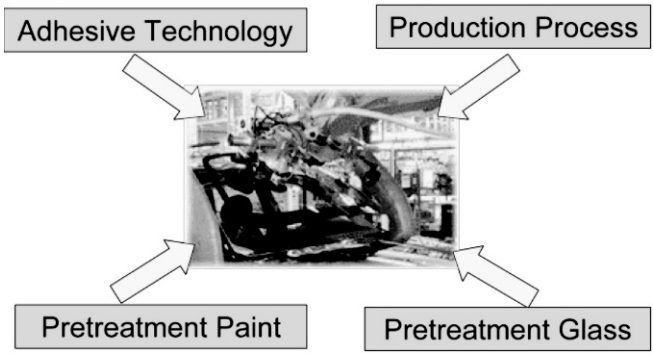

Fig. 5 Elements of Sika's strategy to achieve VOC bonding

For paint substrates there are 3 different options:

1. No pretreatment is necessary. The adhesive/paint system is adapted to build up adhesion by itself
2. A cleaner is used to remove contamination.
3. An activator is applied, in order to improve adhesion

For all concepts, water-based solutions are available.

To complete the water based products for direct glazing, Sika Clean Glass can be used for the removal of moderate contamination on windows. For the removal of silicon residues from poor window production Sika Cleaner S (II) should be used.

6 Application of Water-based activator

A very challenging task was the adaptation of the water-based activator to the increasingly frequently used spray applications. The challenge was to meet parameters which are currently used on the production line and which had been optimised over the years for solvent borne pretreatments, which evaporate very fast. Furthermore, the wetting behaviour of a solvent or water borne solution is very different.

With currently used equipment, the application width and flash-off time were not within specifications. Sika started several external and internal studies to develop a suitable solution. Finally, a special commercial nozzle was found which can be used in combination with new efficient ventilation with no additional investment required to the current state-of-the-art spraying equipment. For the manual application, today's materials such as towels, felts or foams can be used and have no negative impact on the product performance. The application characteristics appear in Figure 6.

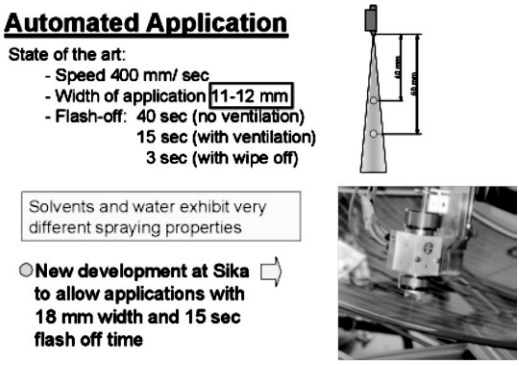

Fig 6 Sika HydroPrep-100 spray application characteristics

Conclusion

In conclusion, the water-based activators are an ecological and economical solution with many benefits. For these reasons, Sika HydroPrep®-100 is already in use on the first automotive assembly lines with great success.

HYBRID COMMAND ISSUING IN A 2-DOF SERVOMECHANISM OPERATED UNDER VISION-BASED FEEDBACK CONTROL

C. Montes, C. Wong, J. Ziegert, L. Mears

Clemson University International Center for Automotive Research,
Greenville, SC 29607 U. S. A.; E-mail: carlosm@clemson.edu

Abstract: This paper presents a new method for generating motion commands in a 2 degree-of-freedom (DOF) vision-based position control system. The control system uses a fixed digital camera to direct-observe the multi-dimensional position of a known target displayed on an Liquid Cristal Display (LCD) and determines the position of the tool based on this information. This system, implemented on an XY-stage, was first introduced in Wong [1], and further investigated in Montes & Ziegert [2] and Montes *et al*. [3]. Previous results demonstrated sensor resolutions on the order of 3 μm; however the resolution of motion commands was constrained to values on the order of hundreds of microns due to the physical characteristics of the LCD picture elements (or pixels). The new method presented here overcomes this constraint and allows generation of motion commands as small as 3 μm. Simulation results are provided.

1 Introduction

The development of cleaner and more efficient technologies in the automotive industry has come to increase quality levels in the manufacturing sector. One of the biggest challenges in the development of new machine tools is the one related to error mapping. Common servomechanisms found in computer numerical control (CNC) machines utilize complex kinematic models of the machine to compensate errors affecting machine tool accuracy. In this work a 2 degree-of-freedom (DOF) vision-based position control system for machine tools is studied. This system is implemented on an XY-stage as shown in Fig. 1 (a). A fixed vision sensor is located so that camera plane is parallel to the LCD, which moves freely in the XY plane based upon control action. In-plane motion instructions for the XY-stage are given by moving or modulating the dynamic target on the LCD, and thereby creating a position error between the target and the principal point (PP) in the camera plane (Fig. 1 (b)). Initially the control system can be thought of as a tracking device, where the control system moves the machine axes to align the target on screen with PP in the image plane. However, displacements of the target on the

screen are constrained by the size of the smallest element on the LCD, i.e. are constrained by one LCD pixel. The LCD pixel size in the experimental setup is 294x294 μm, i.e. motion commands are constrained to 294 μm along the LCD *Y*-axis and 98 μm (294/3) along the LCD *X*-axis. The difference between the size of *Y*-axis and *X*-axis displacements is due to the construction of one LCD pixels, which is made of three different color stripes, R, G and B, arranged horizontally from left to right. The possibility of individually generating blue, green or red from a single pixel, implies control of the physical location of the target to within 1/3 of a pixel along the LCD *X*-axis. A new method for generating displacement commands as small as 3 μm is presented next. The method, 2 Hybrid Command Generation Protocol, combines visual-tracking and regular servo control, where the former implies the tracking of the target on the LCD and the latter implies a non-fixed reference signal to the control loop.

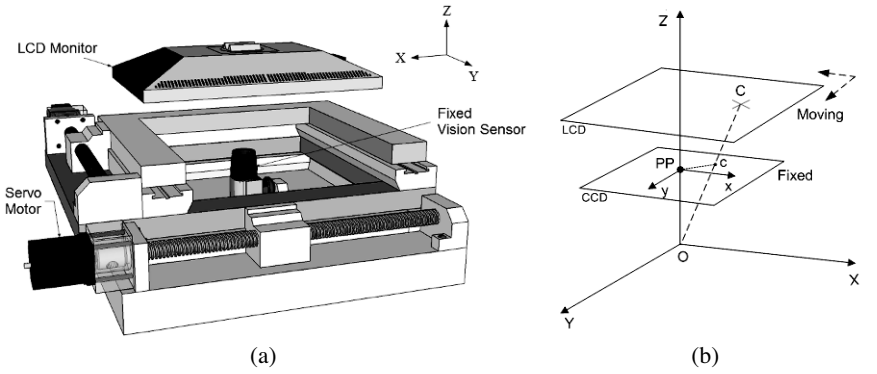

(a) (b)

Fig. 1 (a) 2-axis stage with LCD monitor and fixed CCD camera. (b) Multi-dimensional position control error calculated based on the mapping of the target position on the LCD (point C) onto the image plane (point c) and referenced to the CCD principal point, PP.

Given the fact that the dynamics of the two axes are decoupled, it is possible to represent the experimental multiple-input multiple-output (MIMO) system as two single-input single-output (SISO) servo-systems of the form $X(s) = G(s)V(s)$, where *X* is the displacement along one of the axis, *V* is the input voltage to the servo motor and *G* is the transfer function. The analysis that follows is conducted for one axis (*X*-axis), only. Modeling and other considerations for the second axis (*Y*-axis) can be obtained in a similar way as for the first one.

2 Hybrid Command Generation Protocol

Due to slow hardware frame rate and long image processing times, the feedback signal from the camera is delayed in time and intermittent with respect to the

controller's update frequency, affecting overall performance and stability. These factors are addressed through a model-based Smith predictor scheme, which relies on a mathematical model of the servo motors to predict the output of the plant between vision feedback-updates, only. **Fig. 2** shows the augmented control structure operating as a function of the discrete variable i, where $\hat{V}$ is used to model the intermittency and delay associated with the real camera dynamics, V, and C represents the controller. x_i^{Target} is the last increment of the target position on the LCD, with $x_0^{Target} = 0$; x_i is the position of the stage. Commands equal to a multiple of one LCD pixel (or 1/3 of a pixel for the case of horizontal displacement commands) are issued by moving the target on the LCD by that specific distance, and setting the reference on the image plane as the origin (i.e. PP). In this case the control system operates as a regular tracking system. For commands smaller than one LCD pixel, the target is displaced by the smallest possible amount on the LCD and the reference signal is set to a value different than PP. Full attention is now paid to issuing commands smaller than one LCD pixel and introducing the necessary adaptations to make the estimate value $\hat{x}_i$ behave as $\overline{x}_i$ in Fig. 2.

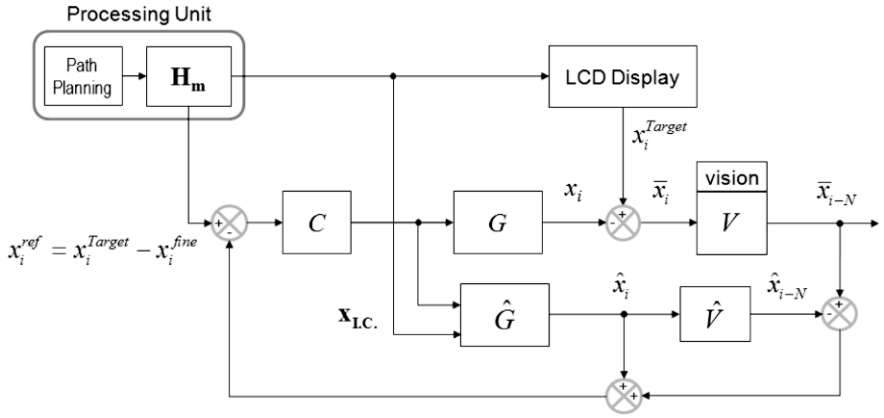

Fig. 2 Single-axis command issuing through hybrid command generation protocol.

Ignoring the Smith predictor, the controller, and the effects of the camera dynamics, the visual servo loop from Fig. 2 can be represented by either one of the diagrams in Fig. 3. The value x^{fine} is the desired displacement command, where $\left|x^{fine}\right| < 1$ LCD pixel.

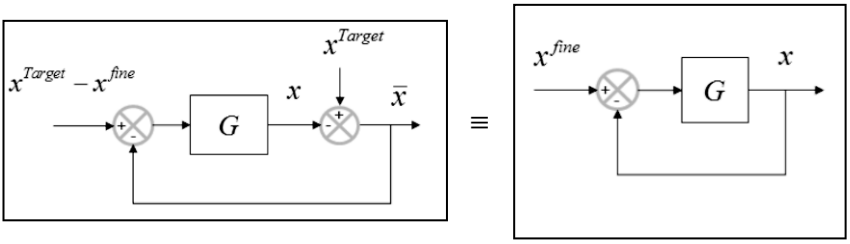

Fig. 3 Simplified visual servo loop.

The closed-loop transfer function for the right-hand side diagram in Fig. 3 is known to be of the form

$$\frac{X(s)}{X^{fine}(s)} = \frac{b_0}{s^2 + a_1 s + b_0} \tag{1}$$

with $b_0, a_1 \in \mathbb{R}$. The differential equation associated with (1) is $\ddot{x}(t) + a_1\dot{x}(t) + b_0 x(t) = b_0 x^{fine}(t)$ with $\dot{x}(t) = dx/dt$, $\ddot{x}(t) = d^2x/dt^2$. The general solution is $x(t) = C_0 e^{r_1 t} + C_1 e^{r_2 t} + x^{fine}$ with $C_0, C_1, r_1, r_2 \in \mathbb{R}$, $r_1, r_2 \leq 0$, $r_1 \neq r_2$, assuming a stable non-oscillatory system. Given the initial conditions $x(0) = 0, \dot{x}(0) = 0$, it follows that $C_0 = \left(r_2/r_1 - r_2\right)x^{fine}$ and $C_1 = \left(r_1/r_2 - r_1\right)x^{fine}$. Hence,

$$x(t) = x^{fine}\left(\frac{r_2}{r_1 - r_2}e^{r_1 t} + \frac{r_1}{r_2 - r_1}e^{r_2 t} + 1\right) \tag{2}$$

Equation (2) indicates that the position of the stage along the *X*-axis converges exponentially to x^{fine}, as desired. From the left-hand side diagram in Fig. 3, it follows that

$$\bar{x}(t) = x^{Target} - x^{fine}\left(\frac{r_2}{r_1 - r_2}e^{r_1 t} + \frac{r_1}{r_2 - r_1}e^{r_2 t} + 1\right) \tag{3}$$

The value of $\bar{x}$ is now well defined for the required reference signal $x^{ref} = x^{Target} - x^{fine}$ to command the stage to move by x^{fine} μm. It is necessary at this point to determine the conditions to make the model $\hat{G}$, in Fig. 2, provide an appropriate estimate of $\bar{x}$. Let the differential equation associated with $\hat{G}$, for a

reference signal $x^{ref} = x^{Target} - x^{fine}$, be $\hat{x}(t) = \hat{C}_0 e^{\hat{r}_1 t} + \hat{C}_1 e^{\hat{r}_2 t} + \left(x^{Target} - x^{fine}\right)$ with $\hat{C}_0, \hat{C}_1, \hat{r}_1, \hat{r}_2 \in \mathbb{R},\ \hat{r}_1, \hat{r}_2 \le 0,\ \hat{r}_1 \ne \hat{r}_2$ and $\left\|r_1 - \hat{r}_1\right\|^2 < B1,\ \left\|r_2 - \hat{r}_2\right\|^2 < B2,\ B1, B2 \in \mathbb{N}$. For initial conditions $\hat{x}(0) = x^{Target}, \dot{\hat{x}}(0) = 0$ it is possible to calculate $\hat{C}_0 = -\left(\hat{r}_2 \big/ \hat{r}_1 - \hat{r}_2\right) x^{fine}$ and $\hat{C}_1 = -\left(\hat{r}_1 \big/ \hat{r}_2 - \hat{r}_1\right) x^{fine}$, and the solution to the model becomes

$$\hat{x}(t) = x^{Target} - x^{fine}\left(\frac{\hat{r}_2}{\hat{r}_1 - \hat{r}_2} e^{\hat{r}_1 t} + \frac{\hat{r}_1}{\hat{r}_2 - \hat{r}_1} e^{\hat{r}_2 t} + 1\right) \tag{4}$$

A direct comparison between (3) and (4) demonstrates that, if the initial conditions of the model $\hat{G}$ are updated according to the latest position of the target as imaged by the camera, x^{Target}, then $\hat{x}(t)$ is indeed an estimate of $\overline{x}(t)$. It is worth pointing out that x^{Target} is known at all times. $\mathbf{H_m}$ in Fig. 2 is used to calculate the required vectors $\mathbf{x^{Target}}$ and $\mathbf{x^{fine}}$, according to a predefined path plan. The input vector $\mathbf{x_{I.C.}} = \left[x(0) \quad \dot{x}(0)\right]^{\mathrm{T}}$ illustrates the initialization of the model states according to $\mathbf{x^{Target}}$.

3 Simulation Results

A basic path plan for fine in-plane displacement is generated. Fig. 4 shows the desired motion for each axis in (a) and (c) (continuous traces), as well as the required target position on the LCD (discrete traces). The required reference signals to the control system according to the path plan are shown in (b) and (d).

Simulation is conducted by feeding the path plan in Figure 4 to the control system in Figure 2. The results are shown in Fig. 5 for a controller frequency of 1 kHz and a vision block capable of providing feedback data at 400 Hz. The frequency for the vision block is defined based on image acquisition times and image processing times obtained from previous experiments. The graph in (a) shows that it is possible to obtain an output motion that is close to the desired path through small controller gains. However, the velocity pattern in (b) presents undesired oscillations. These oscillations are associated with wait times that the control loop has to undergo in between feedback updates from the vision sensor. These oscillations can be addressed by increasing the rate at which the image is displaced on the LCD, or by adding a feed forward compensator to reduce the velocity of the control system.

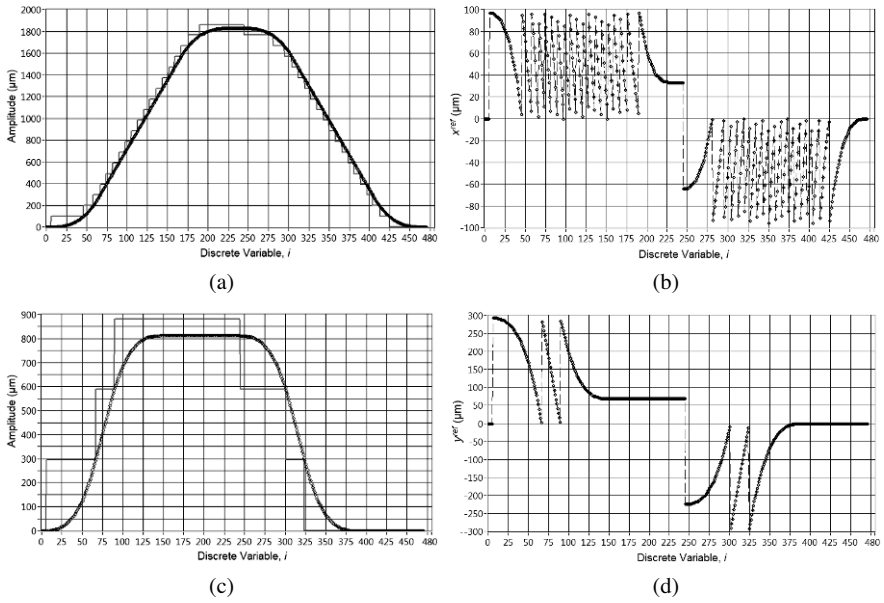

Fig. 4 (a) *X*-axis path plan (continuous trace) and corresponding (required) target position on LCD (discrete trace). (b) *X*-axis reference control-signal required for path plan. (c) *Y*-axis path plan (continuous trace) and corresponding (required) target position on LCD (discrete trace). (d) *Y*-axis reference control-signal required for path plan.

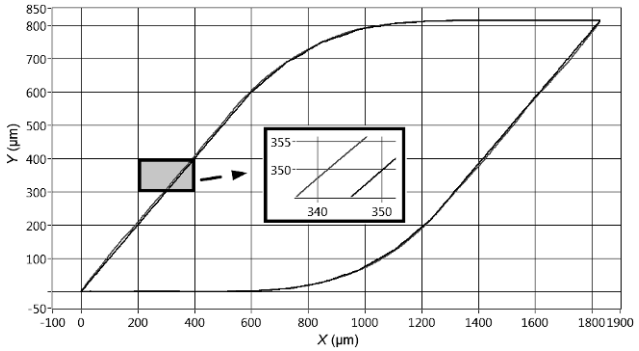

(a)

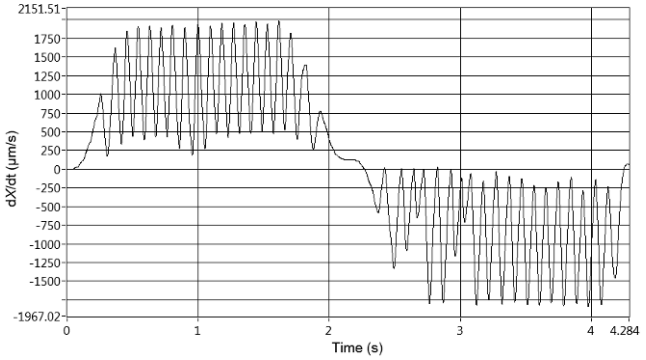

(b)

Fig. 5 Simulation results with a 1 kHz proportional controller and a vision block capable of providing feedback signals at 400 Hz. Proportional gains: P_x=30; P_y=30. (a) Desired in-plane motion and simulation output plotted on same graph. Highlighted rectangular-area shows biggest deviation between desired and simulated motion. (b) Output velocity, *X*-axis.

4 Conclusion

A method for generating motion commands as small as 3 µm for a pre-existing real time control system was presented. Simulation results indicated a need for a velocity compensator to achieve desired motion behavior.

Acknowledgements

This material is based upon work supported by the National Science Foundation under Grant No. 0800507. Any opinions, findings, and conclusions or recommendations expressed in this material are those of the author(s) and do not necessarily reflect the views of the National Science Foundation.

References

[1] C. Wong, C.A. Montes, L. Mears, J.C. Ziegert, (2008). "A New Position Feedback Method for Manufacturing Equipment." *Proceedings of the ASME International Manufacturing Science and Engineering Conference 2008* Vol. MSEC 2008, pp. 111-120. Evanston, IL, USA.

[2] Montes, C.A., J.C. Ziegert. "Vision-Aided Position Control Method for Manufacturing Machines." *International Conference on Sustainable Automotive Technologies, 2010*. Bavaria, Germany.

[3] Montes, C. A.; Ziegert, J. C.; Wong, C.; Mears, L.; and Tucker, T. "2-D Absolute Positioning System for Real Time Control Applications". *Proceedings of the Twenty-fourth Annual Meeting of the American Society for Precision Engineering, 2010*. Atlanta, GA, USA.

ALTERNATIVE METHODS TO INCREASE THE LONG TERM PERFORMANCE OF LASER-WELDED COPPER ALUMINUM CONNECTIONS FOR ELECTRONIC APPLICATIONS IN MOBILE SYSTEMS

M. Weigl[1], F. Albert[2], M. Schmidt[3]

1 Dipl.-Ing. (FH) Markus Weigl, Bayerisches Laserzentrum, Konrad-Zuse-Str. 2-6, 91052 Erlangen, Germany, phone: +49-(0)9131-97790-16, fax: +49-(0)9131-97790-11; Email: m.weigl@blz.org

2 Dipl.-Ing. (FH) Florian Albert, Bayerisches Laserzentrum, Konrad-Zuse-Str. 2-6, 91052 Erlangen, Germany, phone: +49-(0)9131-97790-21, fax: +49-(0)9131-97790-11; Email: f.albert@blz.org

3 Prof. Dr.-Ing. Michael Schmidt, Chair of Photonic Technologies, University of Erlangen-Nuremberg, Paul-Gordan-Str. 3, 91052 Erlangen, Germany, phone: +49-(0)9131-8523456, fax: +49-(0)9131-8523234; Email: michael.schmidt@lpt.uni-erlangen.de

Abstract: For the realization of modern drive concepts based on high power electronics, it is necessary to take the advantages of well-adapted materials for the respective challenges. In terms of high power electronics, mainly in the range of energy storage and distribution, the substitution of copper by aluminum seems to be adequate to reduce the mass of the overall mobile system and to lower the production costs. However, for electrical reasons a complete replacement of copper is not practicable, therefore it is necessary to contact copper and aluminum by way of metal continuity. In order to reach high operating temperatures as well as an excellent electric conductivity copper and aluminum are supposed to be joined by welding processes. For this purpose especially laser welding is a suitable technique to realize defined energy inputs, high operating speeds and good automation facilities. Nevertheless the joining of copper and aluminum by means of laser-welding causes miscellaneous difficulties. Besides worse absorption factors for the typical industrial laser wavelengths, copper and aluminum form a lot of intermetallic Cu-Al phases. Most of these phases feature high hardness values, coming along with a distinctive brittleness and effectuate minor ductility values. In this context, the present article deals with an alternative method for the laser-welding of Cu-Al connections, which avoids a direct interaction of copper and aluminum in the molten state. For this purpose, so-called roll-cladded inserts are used, in order to split one direct Cu-Al connection into two separate joints, i. e. Al-Al and Cu-Cu. The rather Cu-Al connection is transferred to the standardized roll-cladding process, whereby high-grade connections at dissimilar materials, which would form various intermetallic phases at fusion welding, are achievable.

1 Introduction

In order to optimize the characteristics of a complete high power electronic system, more and more so called tailored constructions are established for applications in high power electronics for mobile systems. Therefore it is necessary to join the respectively most suitable materials for each subsystem to an overall package. In this context, a material connection of particular interest is the combination of copper and aluminum. While copper features an outstanding electrical and thermal conductance, its comparatively high density limits the request for light-weight constructions. Furthermore copper base materials are quite expensive and their market price is supposed to once again reach the level of 9.000 USD/ton after the economic crises. In contrast to that, both the density and the market value of aluminum amounts 70% less than the one of copper. Taking into account, that depending on the relevant material composition, the electrical and thermal conductance of copper is about 20% to 40% higher, the substitution of copper by aluminum enables a reduction of the total weight and the production costs of mobile systems. As a complete replacement of copper is not practicable for electrical reasons, copper-aluminum connections by way of metal continuity are necessary. In this consequence laser beam welding offers defined energy inputs, high operating speeds and good automation facilities. Despite that, laser beam welds are challenged by miscellaneous difficulties, whereat the dominant complex of problems derives from the limited solubility of copper and aluminum within each other. According to Figure 1, an intermixture of two materials “A” and “B” can basically affect three different types of microstructures in the weld zone. In case of sufficient solubility of both materials mixed crystals are formed, while limited solubility can lead to either intermetallic phases or total mismatch in the worst case.

The binary system copper-aluminum only features very limited solid solubility values for both base materials. Any exceeding of these limits results in the formation of intermetallic phases, such as $CuAl_2$ connections in the aluminum corner of the Cu-Al phase diagram, see Figure 2. At fusion welds the distinctive hardness of these intermetallic phases typically causes an embrittlement and thereby a deformability reduction of dissimilar connections.

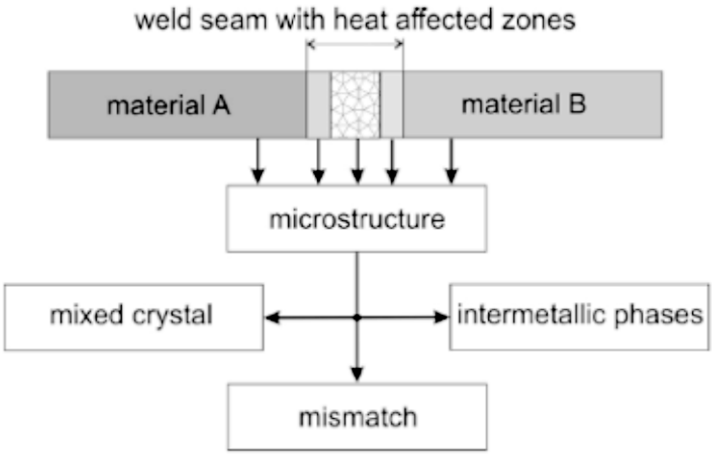

Fig. 1 Basic structural conditions in the welding zone of dissimilar material [1]

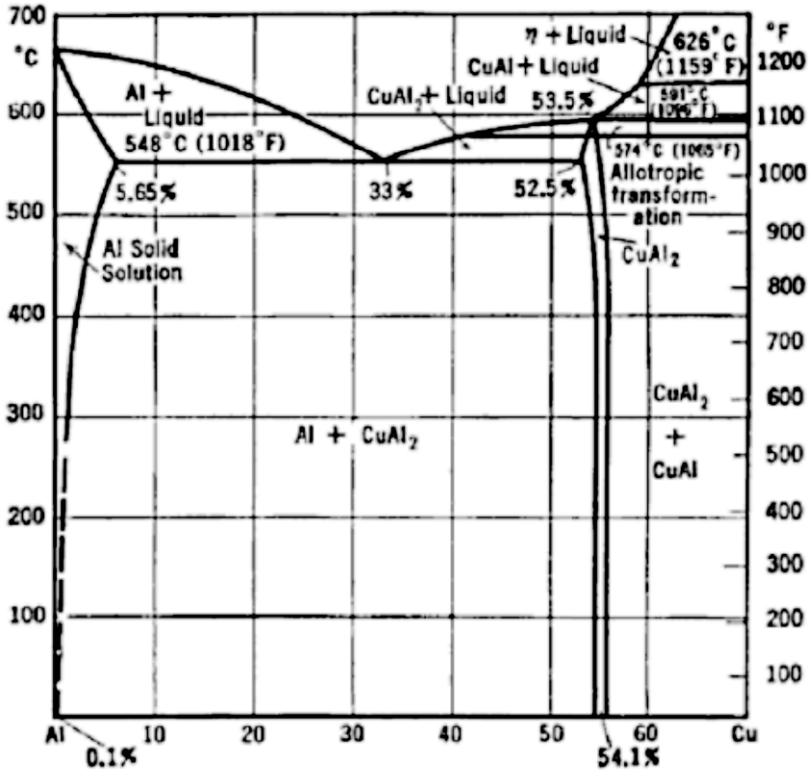

Fig. 2 Binary Al-Cu system, aluminum end of the equilibrium diagram [2]

As a consequence, the dynamic performance of such direct Cu-Al contacts with a certain intermixture zone of the base materials is often insufficient for the typical operational demands in mobile systems. In this context Figure 3 shows diverse possibilities to optimize the tensile strength of Cu-Al butt-welds. By means of a lateral beam displacement towards the aluminum base material, silver filler material and appropriate laser power modulations the connections' tensile strength can be doubled. However the ductility of the dissimilar joints is only influenced insignificantly by the implied optimization methods. That is why temperature cycling tests lead to a considerable reduction of the remaining tensile strength. Moreover corrosive loads with dilute sulphuric acid, which is similar to accumulator acid, rapidly decrease the stability of the direct Cu-Al connections, see Figure 3.

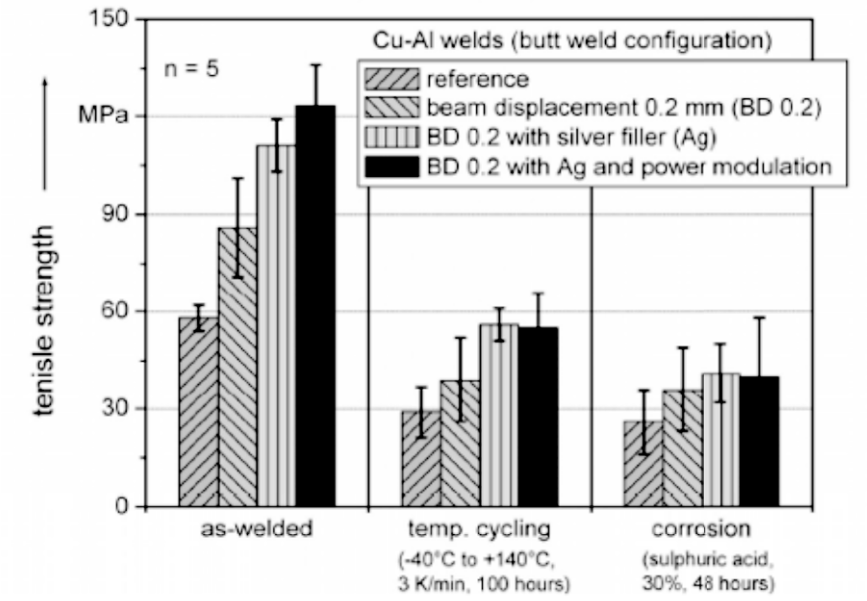

Fig. 3 Effect of diverse optimization methods and selected long-term properties; beam displacement towards aluminum base material; thickness of silver filler 50 µm [3, 4]

In order to enlarge the dynamic and chemical stability of dissimilar connections, so called rollcladded inserts can be used to split one direct Cu-Al connection into two separate joints, i. e. Al-Al and Cu-Cu. The rather Cu-Al connection is transferred to the standardized roll-cladding process, whereby high-grade connections at dissimilar materials, which would form various intermetallic phases at fusion welding, are achievable.

2 Experimental setup

For the experimental tests roll-cladded Cu-Al inserts are placed between an overlap-configuration of the base materials. The rectangular fittings are punched out of roll-cladded sheet metal with a total thickness of 1.0 mm. Roll-cladded Cu-Al sheet metal typically features an unsymmetrical proportioning of copper and aluminum, i. e. the total insert thickness divides in 70% aluminum and 30% copper. By setting different widths for the base materials and the insert, fillet welds at the intersections of the base materials and the roll-cladded insert are producible, see Figure 4.

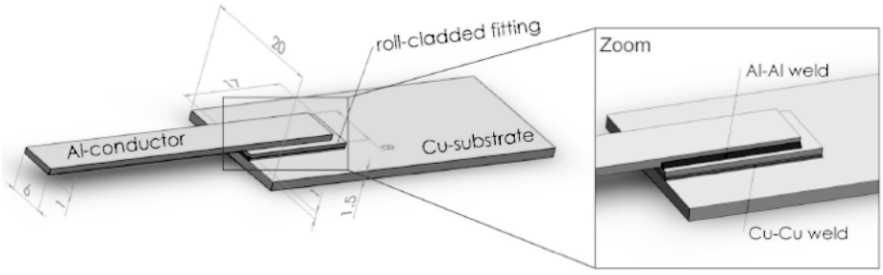

Fig. 4 Joining geometry for the welding tests with roll-cladded fittings

As laser source for the experiments the pulsed Nd:YAG laser system SLS200CL60 from the Lasag AG is used. It features a peak power of 7 kW at a pulse duration between 0.5 ms and 100 ms and a spot diameter of 400 µm. High peak power is especially needed for copper-welds with IRlasers, in order to couple into the highly-reflective material. In addition short pulse durations limit the thermal influence of the joining process on the sample, particularly at materials with a high thermal conductivity, such as copper and aluminum.

3 Results of the welding tests

In contrast to copper, aluminum features a higher absorption rate for the implied laser wavelength, combined with a lower thermal conductivity, see for example [5,6]. Therefore the Al-Al subsystem is comparatively uncritical for welding, especially in the fillets according to Figure 4. Furthermore, the higher proportion of aluminum at the roll-cladded inserts causes a further distance between the welding zone and the Cu-Al bonding zone within the insert. That is why a laser power of 2.900 W at a pulse duration of 8 ms are adaptive for the Al-Al connections, before a thermal degradation of the Cu-Al bonding zone within the roll-cladded insert may take place. On the contrary, increased laser powers and lower pulse durations are necessary for the copper welds. By enhancing the laser power up to 6.000 W,

an adequate coupling of the laser irradiation into the sample and a verification of the deep welding effect can be assured. In conjunction with an increase of the laser power, the pulse duration at Cu-Cu welds has to be reduced to 3 ms. Thereby the heat conductance within the roll-cladded inserts is limited to an uncritical extend and the thermal load on the Cu-Al bonding zone can be minimized.

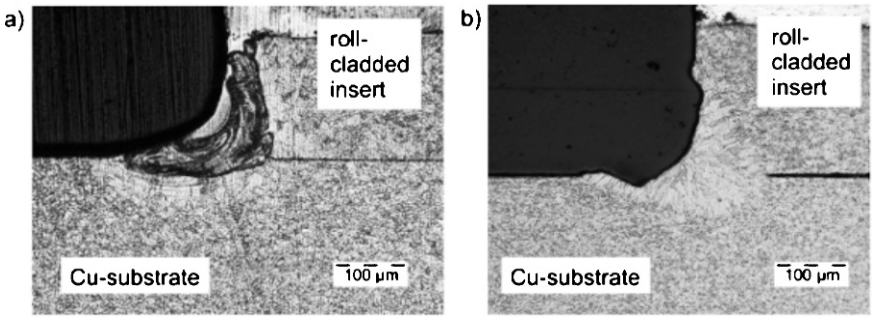

Fig. 5 Connections of the copper-substrate and the copper-side of the roll-cladded inserts:
a) Intermixture of Cu and Al, leading to the formation of intermetallic phases
b) Without intermixture of Cu and Al

In particular, a melting of copper and aluminum at the same time has to be avoided. If not, an intermixture of aluminum and copper in the molten state occurs and once again disadvantageous element distributions and hence intermetallic phases are constituted, see Figure 5a. In this context the welding of the Cu-Cu subsystem is more critical in contrast to the Al-Al joint, as the higher melting point of copper, combined with an also higher heat conductance impetuously can lead to a melting of the aluminum fraction of the roll-cladded inserts. Furthermore it has to be assured, that thermal welding process does not lead to a degradation of the bonding zone within the roll-cladded material by accelerated solid state diffusion combined with a growth of the bonding layer's thickness. In this context Figure 6 presents a closer look to the bonding zone of the roll-cladded material nearby the weld area before and after the welding process with the parameters named above. According to figure 6 no significant modification or anomaly can be detected in the microstructure. The Cu-Al diffusion zone in the bonding area features a thickness of less than 5 µm before and after the welding process, so that no growth of the critical phase seam can be seen. Therefore it can be assumed, that laser welding processes with adapted parameters do not lead to a pre-damage of the Cu-Al bonding zone.

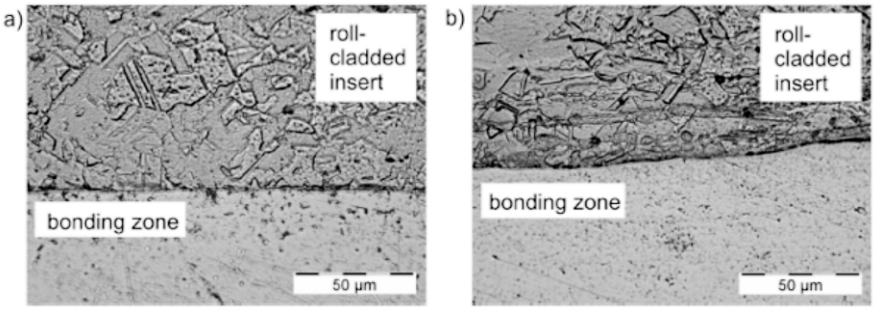

Fig. 6 Microsection of the bonding zone within the roll-cladded material:
a) As-delivered condition, before the welding process
b) After the laser beam welding process

4 Characterization of the welded samples

For an elementary characterisation of the Cu-Al connections with roll-cladded inserts mechanical and chemical / electrical tests are performed. Figure 7 a) shows the achievable tensile strength and the elongation at fracture of Cu-Al samples welded with or respectively without roll-cladded inserts. Here Al 99.5, which is the base material with the lower tensile strength but the higher ductility, serves as reference for elongation values. For clarity reasons, figure 7 does not show any error bar for the standard deviation. With a number of 5 or respectively 3 samples, the standard deviation for the tensile tests amounts ±17 MPa and on the analogy ±4% for the electrical tests

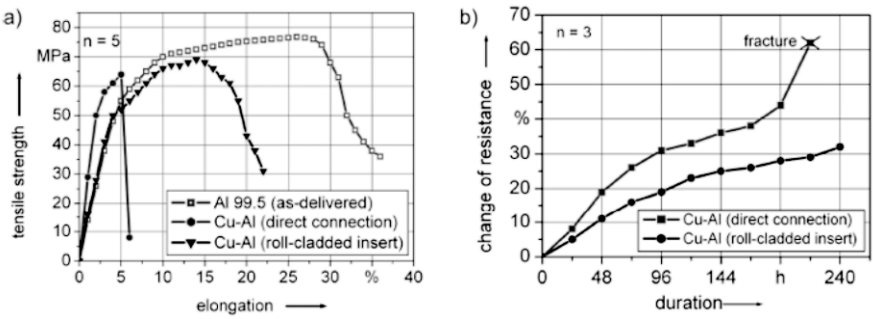

Fig. 7 Elementary characterization of Cu-Al welds with roll-cladded inserts:
a) Tensile tests with Al 99.5 as reference
b) Electrical tests under chemical load (sulphuric acid, 30%)

According to Figure 7a the ductility of Cu-Al welds can significantly be raised by means of rollcladded inserts. The fracture position of welds with cladded inserts is always placed at the beginning of the overlap zone in the aluminum base material. Up to this point the corresponding curve progression is very similar to

the one for Al 99.5 in as-delivered condition. Due to the thermal modification of the microstructure, the elongation to fracture at Cu-Al joints with inserts differs from Al 99.5, which features elongations up to 35%. By contrast, direct Cu-Al welds only exhibit elongations to fracture of less than 7%, see figure 7 a). In addition the curve for the direct Cu-Al connections displays very high gradients concerning the drop of the tensile strength shortly before the fracture. Thus only a limited reliability of direct Cu-Al welds after mechanical preload remains and all types of deformation may lead to an abrupt cracking. That is why for quasi-static mechanical purposes the use of roll-cladded inserts can be recommended. Further mechanic and dynamic tests are planned for the near future, in order to analyse also the properties of Cu-Al connections with cladded inserts under vibration and fatigue loading.

For an elementary evaluation of the time-dependent electrical characteristics, the electrical resistance of Cu-Al samples welded with roll-cladded inserts is measured under chemical load, see figure 7 b). In this context welded samples are exposed to diluted sulphuric acid (30%) over a period of 240 hours. The recording of the measurement is performed with a four-wire micro-ohmmeter at ambient temperature. At a measurement current of 1 A the resolution amounts 100 μΩ. For both variants of Cu-Al connections an increase of the electrical resistance can be observed, see figure 7 b). This effect can be explained by a chemical material removal of the dissimilar connections, which reduces the remaining conducting cross-section and enlarges the resistance. Caused by the element intermixture at direct Cu-Al joints, these weld seam are particularly susceptible to a chemical degradation. Correspondingly, the resistance of direct Cu-Al welds increases comparatively fast and after about 200 hours to 220 hours the direct connections break down. In the moment of fracture, the weld seams of the direct Cu-Al connections are completely decomposed without any remaining mechanical and respectively electrical cross-section. In contrast, Cu-Al joints with rollcladded inserts sustain uniform material removal and show no fracturing after 240 hours. In this case the steady material removal derives from the similar element composition in the Al-Al and Cu-Cu weld seams without intermetallic phases in the rather welding area.

5 Conclusions and outlook

The present article points out the possibility to achieve copper-aluminum connections by metallic continuity, without directly welding the two different base materials. Instead, one dissimilar Cu-Al joint is split up into two similar connections, i. e. Al-Al and Cu-Cu. The rather Cu-Al bonding is transferred to well-known roll-cladding processes, which effectuate very limited diffusions zone with a thickness of less than 5 μm. By means of roll-cladded inserts, an intermixture of copper and aluminum in the molten state and with it a formation of intermetallic phases can be avoided. As a consequence of the minimized proportion of intermetallic phases

in the total connection, significantly higher ductility values are achievable by this alternative welding method. Due to the reduced brittleness, also the dynamic strength of such connections is exposed to increase considerably. In this context dynamic tests according automotive standards are planned for the near future. Under acid load the material removal at Cu-Al joints welded with roll-cladded inserts continues uniformly. In addition, no abrupt break down of the connection by a complete decomposition of the weld seams has to be apprehended. Therefore the use of roll-cladded inserts for Cu-Al welds can also be recommended for electrical purposes.

Acknowledgment

The authors thank the German Research Foundation DFG for supporting parts of this work in the SFB 694 program.

References

[1] Pohle, C.: Schweißen von Werkstoffkombinationen – Metallkundliche und fertigungstechnische Grundlagen sowie Ausführungsbeispiele. DVS Fachbuchreihe Schweisstechnik, DVSVerlag, Düsseldorf, Germany, 1999
[2] Mondolfo, L. F.: Metallography of aluminum alloys, John Wiley Sons Inc, 1943
[3] Weigl, M.; Albert, F.; Schmidt, M.: Final report – Special research collaboration 694, sub project A4, Erlangen, Germany, 2006 - 2009
[4] Weigl, M.; Schmidt, M.: Modulated laser spot welding of dissimilar copper-aluminum connections. Proceedings of 4M/ICOMM conference, Karlsruhe, Germany, 2009
[5] Beyer, Eckhard: Schweißen mit Laser – Grundlagen, Springer-Verlag, Berlin Heidelberg New York, 1995
[6] VDI-Gesellschaft Verfahrenstechnik und Chemieingenieurwesen: VDI Wärmeatlas, SpringerVerlag, Berlin Heidelberg New York, 2006

III COMBUSTION ENGINES AND FUELS

INVESTIGATION AND OPTIMIZATION OF BIODIESEL CHEMISTRY FOR HCCI COMBUSTION

B. Bunting[1], M. Bunce[1], B. Joyce[2], R. Crawford[3]

[1]Fuels, Engines, and Emissions Research Center, Oak Ridge National Laboratory, National Transportation Research Center, 2360 Cherahala Blvd, Knoxville, TN 37932, U. S. A.; Email: buntingbg@ornl.gov

[2]Department of Plant Sciences, University of Tennessee, Knoxville, TN 37996-4561, U. S. A.

[3]Rincon Ranch Consulting

Abstract: Over the past 5 years, ORNL has run 95 diesel range fuels in homogeneous charge compression ignition (HCCI), including 40 bio-diesels and associated diesel fuels in their blending. The bio-diesel blends varied in oxygen content, iodine number, cetane, boiling point distribution, chemical composition, and some contained nitrogen. All fuels were run in an HCCI engine at 1800 rpm, in the power range of 2.5 to 4.5 bar IMEP, using intake air heating for combustion phasing control, and at a compression ratio of 10.6. The engine response to fuel variables has been analyzed statistically. Generally, the engine responded well to fuels with lower nitrogen and oxygen, lower cetane, and lower aromatics. Because of the wide range of fuels combined in the model, it provides only a broad overview of the engine response. It is recommended that data be truncated and re-modeled to obtain finer resolution of engine response to particular fuel variables

1 Fuels Evaluated

40 fuels were evaluated as a basis for this report, divided into 5 groups. These groups have been published previously in separate studies (ref. 1-5), and this paper is a new analysis of data combined from these papers with a particular focus on bio-fuels in the diesel range. For the purpose of this paper, bio-fuels are defined as those containing oxygen and/or derived from obviously biological sources. The 1st group of selected fuels includes four #2 ULSD diesel fuels which were used for blending of the various biofuels. The 2nd group includes 5 common methyl ester biodiesels, derived from coconut, palm, rape, soy, and mustard, and blended to B20 level in #2 ULSD, with one also blended to B10 and B50. The 3rd group is composed of 8 narrow cut methyl esters obtained from Proctor Gamble Chemical

and blended in #2 ULSD at levels from B5 to B30, for a total of 14 fuels. The 4th group includes 7 narrow cut oil shale derived fuels, which were partially hydrotreated to retain some oxygen and nitrogen content, and which were included because they may represent pyrolysis derived fuels. The 5th group consisting of 8 raw plant extracts from non-traditional plants (copaifera, aleurites, pittosporum, cymbopogon, and dictamnus), blended to B20 level in #2 ULSD. These fuel groups were obtained, analyzed, and evaluated over the time period of 2008 to 2011 and the chemistry and property data obtained were not completely consistent between the fuels.

Overall, 18 fuel related variables were considered common enough to be incorporated in the fuel data set, but not all data was available for all fuels. The matrix of 40 fuels and 18 variables is 78% complete, with only 8 variables available for all fuels and 11 variables available for 38 of the 40 fuels. This is important because selecting fuel variables which are not available for all fuels will eliminate fuels and data points from the final analysis. Variables which are complete for all fuels include cetane, T50, % oxygen, % biodiesel, % saturates, % aromatics, ppm nitrogen, and specific gravity. 38 fuels had the additional variables of T10, T90, and iodine number. These are the variables which could be reasonably selected for analysis of the type presented in this report. Complete fuel data is not included in this report, but Table 1 indicates the min, mean, and max for each of the variables.

2 Description of Engine

The engine used for this study is a simple homogeneous charge compression ignition (HCCI) engine converted from a 500 cc single cylinder commercial diesel engine. The engine has been used as a basis for many studies (ref. 1-5) and will not be explained here beyond the following description. In converting the engine to HCCI, the diesel fuel injector was removed and a heated intake port atomizing fuel injector was added. This injector is operated at temperature up to 375°C. and produces a fine fog of fuel which mixes with the incoming air before entering the cylinder. Combustion phasing is controlled by heating the intake air over the range of 100 to 400°C. and the engine operates un-throttled. Compression ratio has also been lowered from 20 to 10.5 to ensure a proper range of combustion phasing with diesel type fuels. Fuel rate is controlled with a small metering pump. Valve timing is stock from the original diesel engine. In operation, air-fuel ratio (AFR) is controlled both by intake air temperature and fuel rate. Combustion phasing is controlled by intake air temperature and AFR and engine power output is controlled by fuel rate. The simple method of combustion control employed in this engine places a great emphasis on fuel chemistry and kinetics and also make modeling of the engine very simple. The same kinetic processes occur in more complex engines, but are more mixed up in time and space.

Table 1 Range of variables for the 40 fuels used in this study.

	cetane	oxygen	biodiesel	saturates	aromatics	iodine	T10	T50	T90	nitrogen	specific gravity
	number	%	%	%	%	gm/100gm	deg.C	deg.C	deg.C	ppm	number
minimum	35.5	0.0	0.0	35.9	10.9	0.0	114	154	184	0	0.788
average	43.8	1.9	14.3	65.5	20.6	10.1	218	262	308	1159	0.857
maximum	51.8	6.2	50.0	82.7	30.9	41.1	298	319	337	9266	0.876

3 Experimental Plan

Each fuel was run at fixed fuel rates, with intake temperature varied to control combustion phasing, and data acquired included temperatures and pressures, gaseous and smoke emissions, and combustion analysis using an AVL Indicom system. This results in a timing sweep for the fuels, which can be studied to evaluate optimum performance or tradeoffs between various emission parameters. For some fuels, several fuel rates were run, and for others only one. Overall, there are 510 data points covering the 40 fuels; engine variables range from 4 to 12 grams/minute fuel rate, 0.8 to 3.7 bar IMEP, and 110 to 320 °C intake air temperature. Over this range, NOx varies from 0 to 346 ppm and smoke number from 0 to 4.6.

4 Data Analysis

Data is analyzed by using statistics, with fuel and engine control variables as input variables. Because of the simplicity of the engine it can be modeled with a minimum of variables and, in this case, we chose combustion phasing (crank angle for 50% burn or MFB50) and torque output (indicated mean effective pressure, IMEP, bar) as input variables. Using these as input variables also allows the models to be easily exercised at constant combustion phasing and power levels. For fuel variables, we choose cetane, % aromatics, T90, oxygen content, and nitrogen content. The first 3 correspond to requirements in ASTM D7467 (B6 to B20 biodiesel blends). Oxygen content was included in lieu of % biodiesel because we were uncertain how to classify the oil sands derived fuels and plant extract fuels relative to % biodiesel. Nitrogen content was included because the oil shale derived fuels contained nitrogen, as might partially upgraded pyrolysis derived fuels. These variables also have the characteristic of not being strongly correlated, so that they can be regarded as independent variables.

Data is analyzed using the statistics analysis package included in AVL Cameo, which is intended for experimental design, mapping, optimization, and control map generation for combustion engines. Models are constructed as second order polynomials with second order cross terms, using automatic selection of model terms at a 95% significance level and a forward/backwards method. Second order terms have been eliminated for the fuel variables, because many of them result in model turnover that is not logical from an engineering or chemistry viewpoint. For NOx and smoke, a square root transform is also applied to the experimental data to prevent the prediction of negative values. We have also found is that fuel characteristics very rarely fall into an orthogonal experimental design, and it is very important to track the experimental design space to avoid extrapolation of the models beyond the range of the experimental data. We should also note that a

number of models with about equal quality of fit can be constructed from the data, in order to study specific trends and that the data can also be narrowed to focus on fuels with particular characteristics. The analysis presented here is intended to provide a broad view of the analysis techniques and overall fuel effects on HCCI engine performance. The independent variables we cover in this report include emissions (NOx and smoke), fuel economy (ISFC) and control information (intake temperature).

Figure 1 compares the measured response to modeled response for each of the data points. The models provide reasonable R2s, ranging from 0.63 for smoke to 0.85 to 0.87 for intake temperature, NOx, and ISFC. The smoke model is somewhat disappointing, but when one examines Figure 2, which shows measured and modeled data vs. run order, one can see that most of the measured and modeled smoke values are zero, with spikes vs. run order generally coming from points with high fuel rate. A similar situation exists for NOx, with the run order points with high NOx corresponding to points with very advanced combustion phasing and from the points with the nitrogen containing fuels. The spiked response associated with high fuel rate or advanced timing cannot be modeled with a second order response, but we feel that the data does not support moving to higher order or more complex models. This is another example where it might be useful to truncate a data set in order to provide finer model detail in a particular area of interest.

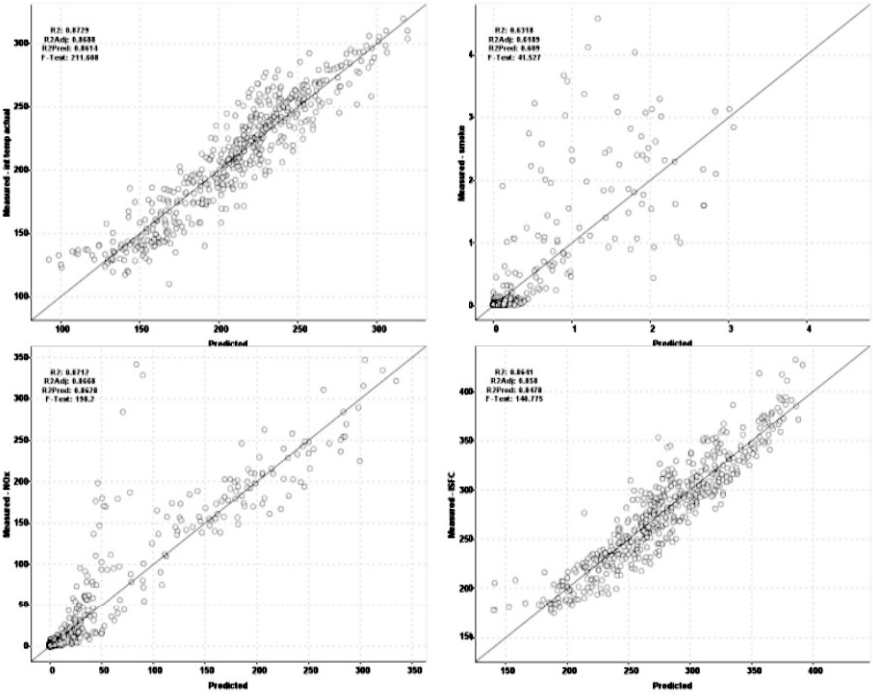

Fig. 1 Measured vs. modeled response for 4 main variable of interest, intake temperature, smoke, NOx, and ISFC, showing model ability to reproduce experimental data.

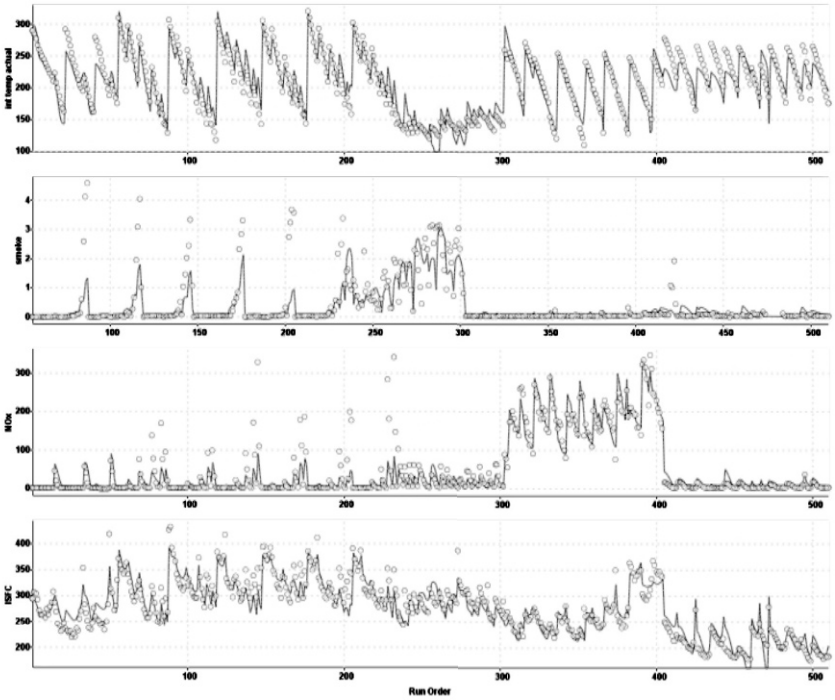

Fig 2. Measured (circles) and modeled (lines) vs. run order for 4 main variables of interest, showing ability of models to track data over timing sweeps and different fuel groups.

The overall responses of the four (4) main variables of interest to the model independent variables are shown in Figure 3. In this figure, intake temperature smoke, NOx, and ISFC are the Y-axes, and % oxygen, total aromatics, T90, cetane, nitrogen, IMEP, and MFB50 are the X-axes. Each response graph shows the effect of a single input variable on the output variables when the other fuel variables are set to their average value, IMEP is set to 3 bar, and MFB50 is set to 362. The horizontal green bars on each chart indicate the range of the experimental data and thus define the region where the model can be considered valid. The green lines on the charts indicate a 95% confidence interval for the prediction. Intake temperature provides an indication of how easy a fuel is to ignite, but is not of direct concern as long as it falls within the range of engine capability. For smoke, NOx, and ISFC, lower is better, and the majority of the graphs indicate improved performance when oxygen, aromatics, cetane, and nitrogen are lower. Optimum fuel economy for the engine is also indicated to fall at about 3 bar IMEP and 362 MFB50. Smoke and NOx both increase for advanced combustion phasing and smoke also increases rapidly at higher IMEP.

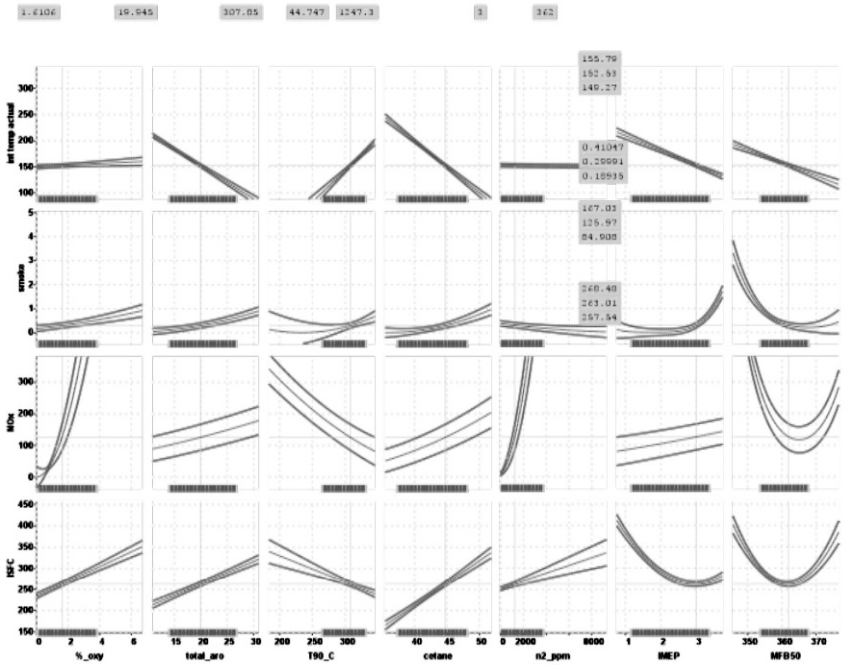

Fig. 3 Response of 4 main variables of interest to model independent variables, when each fuel variable is set to an overall average value, IMEP is set to 3 bar, and MFB50 is set to 362 (2 deg. ATDC)

5 Conclusions

Statistical models of large, varied, fuel related data sets are useful for providing a broad view of the response, but finer detail of a particular variable can probably be achieved by truncating a data set to focus in on a particular region of data. Hence, workflow should include easy access to the complete data and ability to re-model the data easily.

The following conclusions are relevant for the type of engine operation studied in this research (premixed HCCI with temperature controlled ignition in relatively light load operation), but may not apply to other engine types or operating conditions. Nitrogen, in this case from partially hydrotreated oil shale fuels, should not remain in fuels because its presence increases NOx emissions dramatically without providing other benefit. Likewise oxygen, aromatics, and high cetane were generally harmful to NOx, smoke, and ISFC.

Although not discussed in this paper, it is expected that this data could also be used to verify fuel kinetic models which then could be applied to other engine strategies using CFD modeling.

References

[1] Bruce G. Bunting, Romain Lardet, and Robert W. Crawford, Statistical Overview of 5 Years of HCCI Fuel and Engine Data from ORNL, 2010 DOE DEER Conference, 09/2010.

[2] Scott J. Eaton, Bruce G. Bunting, Samuel A. Lewis, and Craig Fairbridge, Effect of Narrow Cut Oil Shale Derived Distillates on HCCI Engine Performance, SAE paper 2009-01-2646.

[3] Bruce G. Bunting, Scott J. Eaton, Robert W. Crawford, Yi Xu, Les R. Wolf, Shankar Kumar, Don Stanton, and Howard Fang, Performance of Biodiesel Blends of Different FAME Distributions in HCCI Combustion, SAE paper 2009-01-1342.

[4] James P. Szybist, Joanna McFarlane, and Bruce G. Bunting, Comparison of Simulated and Experimental Combustion of Biodiesel Blends in a Single Cylinder Diesel HCCI Engine, SAE paper 2007-01-4010.

[5] Bruce G. Bunting, Robert W. Crawford, Les R. Wolf, and Yi Xu, The Relationships of Diesel Fuel Properties, Chemistry, and HCCI Engine Performance as Determined by Principal Components Analysis, SAE paper 2007-01-4059.

NEW POTENTIAL OF OLD WANKEL-TYPE MACHINES

B. Schapiro

Technology & Process Consulting, Kluckstraße 25, D-10785 Berlin, Germany;
Email: boris@schapiro.org

Abstract: One must acknowledge that epitrochoidal machines with circularly moving evolvent gear systems (e.g., Wankel-type machines) are indeed ingenious. Is it possible that such mathematical beauty cannot deliver corresponding utility in market-relevant applications? I will discuss the potential of bi-angular piston machines and circularly moving evolvent gear systems in applied mechanics. Bi-angular machines have some important advantages. First, the compression ratio is defined by design and not limited by the geometry. This makes it possible to employ the more efficient Diesel process in such machines. Second, the vibration resonance of the rotating piston can be suppressed in contrast to the classical tri-angular Wankel machine. This contributes to significantly less wear and tear of the working chamber. "Classical" reciprocating and rotating piston machines can also profit from advantages developed through new perspectives on Wankel-type machines. One could say that all this is well-known and simply ancient history. Granted. But perhaps we can develop new solutions to old problems by viewing and discussing them from a different perspective.

1 Rotation machines, their geometry and topology

It would be a truism to state that reciprocating piston engines dominate the power train market because, overall, they exhibit an incomparable efficiency. Nonetheless, even the fathers of today's energy technologies, such as Watt, Carnot and many others, attempted to combine the advantages of rotary motion with the efficiency of reciprocating piston machines. The famous book by Harding [1], published in 1911, contains descriptions of over 3,000 rotary machines. Ramelli [2] described a rotary compressor already in 1588.

I, too, devoted 15 years to this endeavor. And I was successful, developing the RKM technology ([3]-[5]) in which the piston's rotary motion worked with the same efficiency as reciprocating piston machines, at least theoretically. To achieve this, the RKM piston had to rotate about a periodically jumping, instantaneous

axis of rotation. Mathematical analysis of this machine proved that it belongs to the same topological class as classic reciprocating piston machines. This explains why the topologically defined characteristics of the machines should be identical with those of reciprocating piston machines. Assuming optimal utilization of thermomechanical potential, it is the topology of a machine that decisively determines its efficiency. If the advantages of rotating geometry are incorporated into the design of these machines, then, after appropriate development, the efficiency of RKM machines must be clearly superior to that of reciprocating piston machines.

While the periodically jumping, instantaneous axis of rotation contributes to a radical improvement in efficiency, it also results in a reduction of the power density of RKM machines compared with the high-speed rotating piston machines of Felix Wankel as well as turbines.

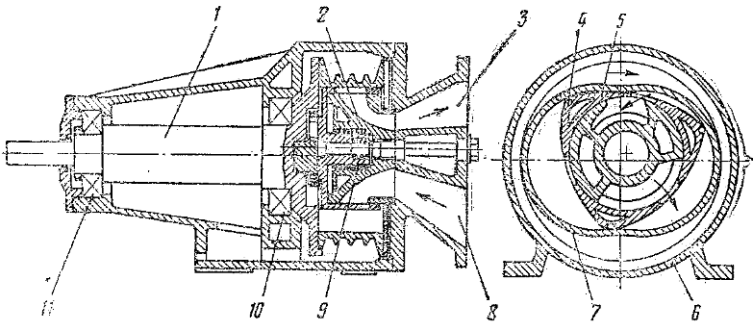

Fig. 1 Compressor, Borsig Company, Berlin 1961 (from [6], [7])
1 – Driveshaft; 2 – immovable insert with gas exchange channels; 3 – gas exhaust channel; 4 – radial seal; 5 – rotor; 6 – immovable housing; 7 – movable housing with working chamber; 8 – gas intake channel; 9 – rotor bearing; 10, 11 – movable housing bearing.

Turbines are world champions in power density because of their extremely high-speed rotation. However, they are truly efficient only when the turbine blades approach the speed of sound in the airstream. Turbines are not only extremely expensive but also achieve a high efficiency only in a relatively small operating range. Thus, they are generally cost-effective only for applications requiring megawatt or gigawatt output. They are unsuitable for mass-produced, mobile applications for use on land and water. In these areas, the technology for main and supportive motors is dependent on volume displacement machines.

2 The Efficiency of Wankel Machines

Felix Wankel devoted his life almost exclusively to planetary piston machines, because they achieve very large volume power densities through the continuously circular motion about the instantaneous axes of their pistons, which attain exceedingly high rotation speeds (on the order of 15,000 – 20,000 rpms). On the one hand, it is sad that the exceptional work of Felix Wankel and his team has never received the market attention it deserves. Both economic-political and understandable special interests of automotive giants contributed to that. On the other hand, the deplorable efficiency of Wankel machines and their resulting excessive fuel consumption played a disastrous role. The advantage of their power density could not compensate for their disadvantages in times of energy scarcity.

There are two major reasons for the Wankel motor's low efficiency: first is the geometry chosen for the famous Wankel machine, with its Reuleaux triangle in the piston's cross section and the epitrochoidal contour of the working chamber with changing algebraic sign of curvature along the chamber contour. The classic Wankel machine's maximum possible compression is wholly defined by its geometry. This geometry limits the machine's compression ratio to a number in the range of 10. As a result, this machine can be realized as a combustion engine only when employing the Otto process and similar processes in a single compression stage. The much more efficient Diesel process requires a compression ratio no less than the range of 20. Two-stage diesel Wankel engines exist, in which one stage serves as a pre-compresssor and the other as actual motor. This approach has not proved economical as the pre-compressor devours more energy than the efficiency difference between the Otto and Diesel processes can yield.

Second, the problem of sealing the rotating piston against the chamber wall has not yet been solved satisfactorily. Compared to reciprocating piston engines with their surface-to-surface seal between piston and cylinder wall, the seal between the rotating piston and the chamber wall of the trochoidal machine is a line-to-surface seal. Trochoidal machines can be realized with n orders of rotor symmetry, $n = 2$, 3, ... The piston's spring-loaded sealing lip slides along the chamber wall at a permanently changing angle during piston rotation. This angle's amplitude is defined by the piston's order of symmetry. This amplitude is greatest at $n = 2$ and is approximately equal to π minus the angle between the tangents to the piston's contours at the sealing point. It is approximately equal to $\frac{2}{3}\pi$. At $n = 3$ (the classic Wankel machine), the amplitude is approximately $\frac{1}{2}\pi$. Thus, it is clear why Felix Wankel chose the third order symmetry for his machine's piston – the sealing quality of this machine is roughly 30% better than that of a machine with the piston symmetry of the second order. In the following, we will devote our attention to these trochoidal machines with second order symmetry pistons (PPM2, Planetary Piston Machine with 2nd order piston symmetry).

3 Planetary Piston Machines with 2nd Order Piston Symmetry (PPM2)

Let us imagine that the sealing problem for planetary piston engines has been solved by means of an independent sealing technology. Which of the almost inifinite variety of planetary piston machines would be most interesting economically as a combustion engine? In my opinion, given the assumption above, a planetary piston machine with 2nd order piston symmetry (PPM2) would emerge as the clear victor.

The reasons for this are simple. First, the contour of the PPM2 piston, a trochoidal arc, conforms to at least one similar arc in the contour of the working chamber. If we build a combustion chamber into the arc portion of the chamber wall that conforms to the PPM2 piston, then the machine's compression will equal the relation between the maximum volume defined by the PPM2 geometry and the geometry-independent volume of the combustion chamber. Thus, the compression of a PPM2 motor is not defined solely by the trochoidal geometry but, contrary to the Wankel machine, together with the designed size of the combustion chamber. Consequently, the PPM2 machine can definitely be designed as a one-stage diesel with concomitant significantly improved efficiency.

Second, the piston's rotation speed and, thereby, the power density of the PPM2, is limited only be the fuel's rate of combustion. That, in turn, means that the PPM2 engine should be able to achieve the maximum power density possible for any fuel used.

With PPM2 machines, I hope to maximize both efficiency and power density.

Incidentally, all the usual advantages of planetary piston machines also accrue to the PPM2 machine. Among them are:

- small, light and simple construction requiring little space,
- few moving parts with less wear,
- outstanding power density.
- dynamic balancing provides quiet and smooth operation.

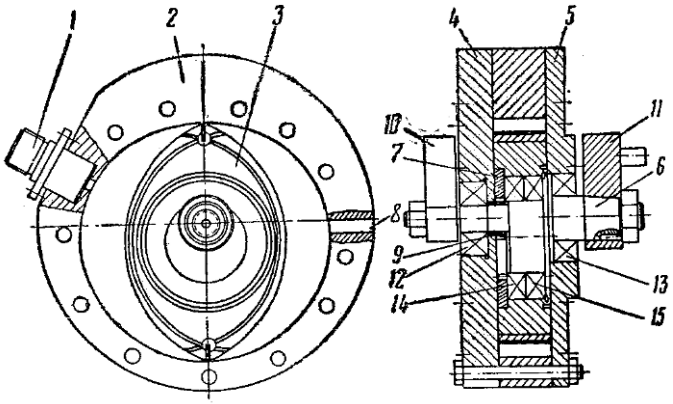

Fig. 2 Compressor RPK-160, Zhukovsky Kharkover Aeronautical Institute, Kharkov 1967 (from [8])
1 – gas exhaust valve; 2 – immovable housing; 3 – rotor; 4, 5 – facing plates; 6 – eccentric shaft; 7 – gearwheel, internal gearing; 8 – intake channel; 9 – immovable gearwheel; 10, 11 – dynamic balancing weight; 12, 13 – drive shaft bearing; 14, 15 – rotor bearing.

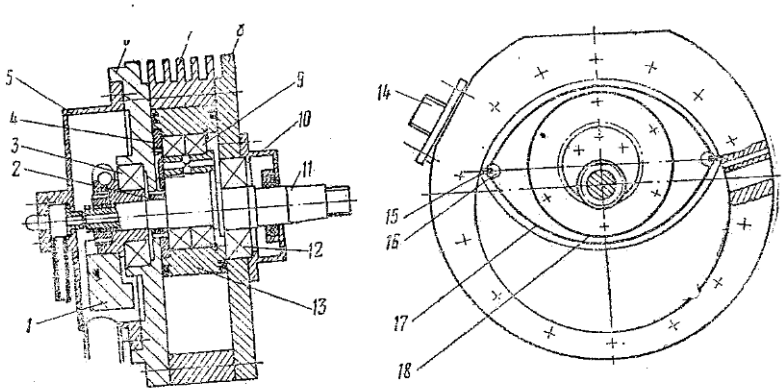

Fig. 3 Compressor RPK-300, Zhukovsky Kharkover Aeronautical Institute, Kharkov 1969 (from [8])
1 – dynamic balancing weight; 2 – immovable gearwheel; 3, 12 – driveshaft bearing; 4, gearwheel, internal gearing; 5, 10 – oil capture housing; 6, 8 – facing plates; 7 – housing; 9 – rotor bearing; 11 – eccentric shaft; 13 – rotor; 14 – gas exhaust valve; 15 – sealing strip; 16 – triple point sealing element; 17 – facing plate sealing strip; 18 – oil separation ring.

4 Desired Qualities of a Seal

The vision developed in the previous section rests on the assumption that the planetary piston machine's well-known sealing problems can be solved. I believe I have solved this problem – although only theoretically, at the moment. The solution is based on a new composite material I have invented. This material can be used as an elastically deformable element for a seal that will adapt to every curvature.

This material has the following properties decisive for the economic efficiency of PPM2 machines:

- design of the material can set its elasticity across a extremely wide parameter range by,
- the material can be formed into almost any shape and will conform to every curvature under pressure,
- this material's reaction speed to deformation should be at least 4 x 10^5 cm/sec. Sealing the piston with this material against the chamber wall of a PPM2 with a chamber diameter of 30 cm would theoretically allow rotation speeds of up to 240,000 rpm,
- the wear on this material should be comparable to the wear on today's sealing materials,
- its elasticity characteristics will remain virtually unchanged up to temperatures approaching 1,200 °C.

I ask for the esteemed readers' understanding that I do not disclose the know how for producing this miraculous material at this point. This know how is not yet protected, being currently in the assessment phase.

Acknowledgements

The author has the honor of thanking in special measure Karl Sittler for his furthering of this work, for his almost boundless patience, for his moral support and his help with the English version of this article.

I also thank Mr. Ivan Pyatov for his cordiality and the effort he expended in providing me with the difficult to attain information on trochoidal machines in industrial use.

References

[1] Harding, William Joshua, From Barker's Mills to Turbines, G.H. Woods (London), 1911

[2] Ramelli, Agostino, Le diverse et artificiose machine, 1588

[3] Schapiro, B. (2008), The RPM Rotary Piston Machines (in Eng.), in: Proceedings of "Vernetzte Wissenschaften, International Workshop Galtür-Wirl-Zejnisjoch March 26 – April 2, 2006 ", Pages 61-72, Eds. Peter Joerg Plath and Ernst-Christoph Hass, LOGOS Verlag, Berlin 2008

[4] Schapiro, B. and Terlitsky L. (2008), *RKMs: New Class of Machines*. In: Subic A., Leary M. and Wellnitz J. (Edrs), Meeting the Challenges to Sustainable Mobility, Proceedings ICSAT 2008, International Conference of Sustainable Technologies, November 2008, Melbourne, Australia

[5] Schapiro B. and Gotter A. (2010), *Analysis of Potential Increases in Energy Efficiency for Piston Combustion Machines with Unconventional Geometry*. In: Subic A., Leary M. and Wellnitz J. (Edrs), Proceedings ICSAT 2010, Second International Conference on Sustainable Automotive Technologies, February, 24 to 26, 2010; Gut Ising, Chiemsee in Germany

[6] Ansdale, R. F., Wankel Rotary Piston Compressor. In: Design and Components in Engineering, 1967, **20**, Nr. 9, pp. 52-54

[7] Ansdale, R. F., The Wankel Engine Design and Performance, Iliffe Books Ltd, London, 1968

[8] Sukhomlinov, Rostislav, Trochoidale Rotor Compressors, Publishing Houses Union "Vishcha Shkola", Kharkov, 1975

RPM – ROTARY PISTON MACHINES: NEW CLASS OF INNOVATIVE MACHINES

E. Wilhelm[1], J. Wellnitz[2]

[1]Institute for Technology and Artistic Design GmbH (ITD), Marie-Curie-Str. 6, 85055 Ingolstadt, Germany; PH 0049 (0) 841 - 9315896; FAX 0049 (0) 841 - 9517443; E-Mail: eva.wilhelm@itd-in.de

[2]University of Applied Sciences Ingolstadt, Esplanade 10, 85055 Ingolstadt, Germany; PH 0049 (0) 841 - 9348369; FAX 0049 (0) 841 - 934899369; E-Mail: joerg.wellnitz@fh-ingolstadt.de

Abstract Rotary Piston Machines (RPM) are a new class of machines for transforming stored chemical or physical energy into rotary motion or, vice versa, to use rotary motion to produce pressure or a vacuum concerning compressors or pumps. This new class of machines uses completely new principles of piston motion and of transmitting work from the piston to the driven shaft or from the drive shaft to the piston.

Compared to conventional reciprocating piston aggregates, RPM technology holds out the promise of a greater power density and a concomitant increase in efficiency. An additional reduction of the constructed space and the total weight is an outcome of this. At the same time the longevity of the machine is increasing due to a reduction in the use of fixed and movable components. Therefore, the manufacturing and maintenance costs are reduced in general.

Based on this new machine technology a focused combustion process of fuel can be carried out, this in turn is reflected in the quality and quantity of the exhaust gases and pollutant emissions.

1 Introduction

The concept of rotary piston machines is, on the one hand, radically new and, on the other, generically related to classic reciprocating piston machines and forming a topological class with them. The familiar reciprocating piston machines are an extreme limit in the mathematical sense within the RPM class of machines. For this reason, all the advances in reciprocating piston machines, including those of fuel consumption, exhaust, diesel suitability and much more, are in principle transferable to RPMs.

Comparing with existing motor/generator systems, this innovative technol-

ogy delivers a much wider range of applications and offers an promising potential for further research.

2 Current state of the art

The mathematical and theoretical feasibility of the newly developed principle is already shown in several patents, see [1], [2]. Among other things, they are related to the geometric dimension of the piston and the chamber based on mathematical considerations. There have been a realization of two different basic versions, with one or two shafts respectively.

Because of the extensive material on this subject a further embodiment is not elaborated in this paper. Moreover, the current project work deals with the scientific validation of the existing theoretical body of thought and evaluation of pilot productions.

2.1 Schematical functional principle

Figure 1 presents a two-chamber model, or better, a two-cylindrical engine to illustrate the functional principle. The schematic structure as an internal combustion engine and the basic movements of the two-axle version is illustrated in the two subsequent sequences.

In these representations the placement of various elements such as seals, valves and ignition plugs are already integrated. Nevertheless, this arrangement is not to be understood as the final one, it serves only for better orientation.

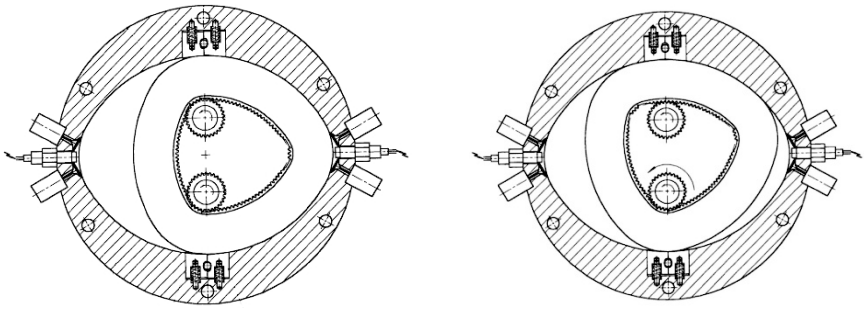

Fig. 1 Schematic drawing showing the functional principle and the movement of a RPM motor with a tri-oval piston in a bi-oval working chamber and two power transfer shafts [2]

The chamber and the rotation axes of both shafts are localized, only the piston

performs a circular motion and activates the two single shafts by an internal gear. About the vertical distance of the shafts to each other, which can be adjusted by the wall thickness of the piston or the rack height, the transmission ratio of the engine can be varied.

The velocities of the two shafts are different at each time during the motion, but sat together in the sum to a constant speed. With that type of transfer it
requires an additional transmission. In this case the two axes have to be synchronized by an additional gear. A combination with the regular gear box is conceivable. However, the bending moment within the machine should be as small as possible with regard to the material components and the dimensioning in general.

There are also relevant derivatives of both axis configurations of this technology. Which influence, in the case of the two-axis variant, on the one hand, the transition within the inner translation into a smoother movement and cause on the other hand a reduction of the workroom what affects an increase of the compression.

For a better understanding of the above-mentioned points, two derivatives of the two-axis rotary piston engine are shown in Figure 2. The shape of the piston and the chamber geometry always increase by two numbers of the oval-order with respect to the previous version.

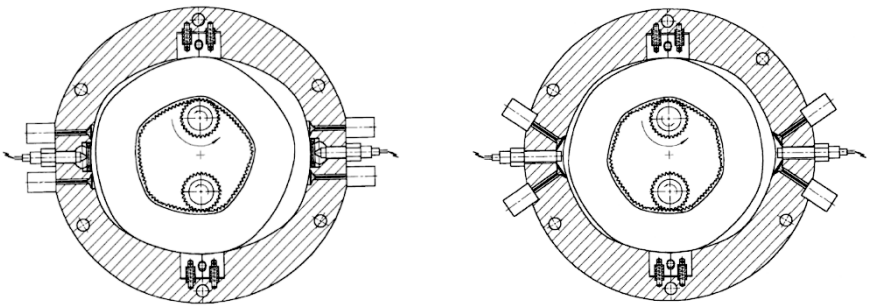

Fig. 2 Derivates of the two-axis version of the newly developed rotary piston machine; Left: piston fifth oval-order, Right: piston seventh oval-order [2]

2.2 Key benefits

Rotary piston machines are generally characterized with respect to the reciprocating piston machines by a smoother behavior, this results from the different functionality and the related movement of the individual components.

Furthermore, this technology in comparison to customary aggregates prom-

ises the possibility of a 3 to 5 times higher power density with a corresponding increase in efficiency. These advantages are accompanied by a simultaneous reduction in constructed space volume and weight of the engine.

Not only the rotation principle itself, but also the topic of the workroom sealing and the combustion chamber geometry can be represented by innovative new developments. So the determining difference to a surely known and often criticized rotation piston motor, the Wankel engine and its history, can be shown.

To give a brief insight into its set of problems, for example, it was always used a line sealing. In our case the sealing is substituted a plain for a line one. This provides on the basis of its flexibility and adaptability essential advantages.

In addition, the combustion chamber and the working chamber in the new engine concept are considered separately from each other and are geometrically designed optimally with respect to the specific needs.

2.2.1 Combustion

Due to the high two-axis ratio of 1:7 is desired, the motor of the same power turns slower than, for example, a standard reciprocating piston machine or the Wankel engine. The filling is related to the transmission of the piston, so these relatively slow revolutions per minute in turn affect the filling of the combustion chamber and the entire chamber as well as the combustion process in a positive way. Usually a complete combustion is always preferred in the sense of operating efficiency and can be achieved when the chamber is sufficiently filled with fuel mixture so this in turn has more time to burn completely.

All the effects named above are reflected to the fuel consumption and the minimization of the exhaust gases or pollutant emissions respectively.

Nowadays it is more important than ever to develop machines that are environmentally friendly and to integrate this topic actively into the process of development.

2.2.2 Lightweight construction issues

First of all, be mentioned that one can dispense with a rotary engine to the crankshaft, because a conversion of a translational in a rotational motion in this case is no longer necessary. This huge component saving affects the weight balance of the core engine and so the absence of a crankshaft is of course a positive effect on weight reduction.

Second, in addition to the surrender of the crankshaft, a 3 to 5 times smaller dimension of the constructed size is feasible. The total volume of the

motor can be reduced because of the increased engine performance potential. These savings happen all from the point of a constant power output.

Combining these advantages parallel to the use of new lightweight materials for the design of the piston, the chamber and the driving mechanism, the weight reduction and power density can be additionally improved.

2.2.3 Economic value

The aimed longevity of the engine as well as the reduction in costs is caused primary by a reduction of the fixed and movable parts, such as the lack of the crankshaft and associated connecting rods.

Secondly, based on the smooth running of the engine and the low velocities in the general phase of work, materials related to the prevailing forces and moments will be charged less and can be laid out accordingly more filigree.

From the beginning, these measures have a direct influence on the production process of the engine, the product as well as the following maintenance costs become more attractive.

3 Applications

The machine principle described here is primarily designed as a combustion engine and should be analyzed and interpreted as such, because in this area a very far-reaching spectrum can be served. Compared to existing prospective power-generation technologies, the RPM technology offers a much greater flexibility for an exceptionally wide range of potential applications, including engines and power units for motor vehicles, helicopters and fixed-wing aircrafts, marine crafts of various sizes, large stationary and portable power generators. Furthermore, applications are conceivable in the component sector, such as Range Extender, or also the use in the scope of compressor and pump technology. The usage in hydraulic and pneumatic systems, actuators, also falls into the pattern of the range of applications.

As further possible applications besides the field of internal combustion engines the overall transport and compression of media or other thermodynamic benefits would be realizable.

This newly developed rotary machine has the ability to cover an enormous range of applications and can therefore be used in a wide product field.

References

[1] Patent application DE 101 39 286 A1
[2] Patent specification DE103 08 831 B3

IV HYDROGEN AND ELECTRIC VEHICLE TECHNOLOGIES

INDUCTIVE POWER TRANSFER SYSTEM INTEGRATION FOR BATTERY-ELECTRIC VEHICLES

A. Lorico, J. Taiber, T. Yanni

Clemson University International Center for Automotive Research, Greenville SC 29607, U.S. A.; Email: alorico@clemson.edu

Abstract: As battery-electric vehicle technology advances as a viable alternative to internal combustion engine vehicles, consumer acceptance becomes a critical factor for the future of these vehicles, with driving range and vehicle cost being the preeminent parameters of concern. Unique to battery-electric vehicles is the direct inverse relationship between these parameters. Battery pack costs often account for over one half of the vehicle cost, with the vehicle range determined by the capacity (and thus cost) of the battery pack as well. An increase in vehicle range would therefore result in a significant increase in battery pack cost, and vice versa. In addition, the relationship between overall vehicle mass and total range further inversely couples vehicle cost and range. It is apparent then that a fundamental trade-off will always exist between the two parameters, unless an additional factor is added to decouple the direct relationship between them. This paper presents results of an analytical investigation of the aforementioned relationships unique to battery-electric vehicles and proposes inductively coupled power transfer (ICPT) as a potential solution and decoupling method for the vehicle range – vehicle cost relationship. The proposed inductively coupled power transfer (ICPT) system was found to be very effective by allowing the battery pack size to be reduced by up to 48%.

1 Introduction

Electric vehicles are becoming increasingly popular as an alternative to internal combustion engine (ICE) vehicles due to their zero-emission operation. While conventional powertrains are reaching new levels of efficiency and emissions amid increasingly stringent environmental regulations, many original equipment manufacturers (OEMs) are investing heavily in battery electric vehicle technology as the near-future solution for clean transportation.

In 2003, the Energy Information Administration (EIA) estimated there would be 55,852 full-electric vehicles in 2004, with an average annual growth rate from years 2000-2004 of 53.2% [1]. More recent estimates of electric vehicles in use in

the US shows a significant decrease in annual growth rate (Table 1). Another more recent study anticipates volume sales of battery-electric vehicles to be 3.1% of total vehicle sales, or 465,000 vehicles by 2020 [2]. These numbers show that mass adoption of electric vehicles is still in the early stages, with several key issues still to be solved.

Table 1: Estimated number of electric vehicles (excluding hybrids) in use in the US [1]

Year	Number of Electric Vehicles	Annual Growth Rate
2003	**47,485**	**NA**
2004	**49,536**	**4.32%**
2005	**51,398**	**3.76%**
2006	**53,526**	**4.14%**
2007	**55,730**	**4.12%**
2008	**56,901**	**2.10%**

According to the same study, two keys to mass adoption of battery electric vehicles from a consumer perspective are: Manufacturer's Suggested Retail Price MSRP reduction and a driving experience equivalent to ICE vehicles. The vehicle battery pack is critical in determining the vehicle price as well as range and performance, making it a predominant factor in both keys. The current average cost for Li-ion battery packs used in electric vehicles is $650 per kWh [3], with typical battery pack capacities in the range of 25-50 kWh for battery-electric vehicles. This equates to approximate battery pack costs of $16,250-$32,500, respectively, in many cases accounting for over one-half of the vehicle MSRP. In terms of vehicle range and performance, the battery pack determines the total range of the vehicle on a single charge, as well as the maximum power output from the battery. With the specific energy density by mass of Li-Ion batteries being 60-140 times lower than gasoline, the effect of vehicle range and performance as a function of battery pack mass is significant for an electric vehicle. This presents a critical trade-off between the battery mass, cost and total capacity, unique to battery-electric vehicles.

This paper presents an analytical study of the mass compounding effect on battery-electric vehicles. The energy storage medium for plug-in electric vehicles which constrains the range and performance is most commonly in the form of a battery pack. Previous research has shown that hybrid vehicle energy consumption decreases dramatically as vehicle mass decreases. A 100 kg decrease in vehicle mass resulted in a 4.5 mpg fuel economy increase, according to one study [5].Depending on the battery pack type, the tradeoff between mass, cost and capacity is the main motivation for the ongoing research of energy storage alternatives.

One such alternative is the use of inductively-coupled power transfer (ICPT) as a means to increase the range of an electric vehicle without substantial impact on the weight or cost of the vehicle. Recent research initiatives in the ICPT area suggest that ICPT continuous power transfer to moving vehicles is possible. While many research initiatives demonstrated ICPT capabilities in small-scale models, the potential for scalability to meet power demands for electric vehicles has been proven successful [6]. In Turin, Italy, a stationary ICPT system has been success-

fully implemented with twenty commercial busses since 2003, each charged with 60kW maximum power [7]. Similarly, in Berlin, Germany, there are plans for the implementation of an ICPT tramway system comprising of twenty-seven vehicles.

ICPT presents a technique that can efficiently transfer power without physical connection between vehicle and energy source. The transfer of energy for ICPT has been shown to be on average 75% efficient [5]. The basic ICPT system consists of three main components: the power supply, the power track (Primary coil), and the Pick-up (Secondary coil). The power track embedded into a road surface allows an ICPT-enabled vehicle (with integrated pick-up) to receive electric energy through electromagnetic induction. The energy received can be used to directly power the vehicle or charge the battery pack, according to the battery management system (BMS). Strategic placement of the power track allows for optimal utilization, which is a function of average vehicle speed, traffic flow density and track power rating. The track power rating determines the vehicle battery pack level of charging. Conventional charging levels set by the Society of Automotive Engineers Standards Committee are Level 1 (120V AC Single-Phase, 16A peak), and Level 2 (240V AC Singe-Phase, 80A peak). These levels equate to power ratings of 1.92kW and 19.2kW, respectively. For the purpose of this paper, power ratings of 20kW and 40kW were chosen for analysis. The rating of 20kW closely represents level 2 charging, while 40kW represents high-voltage fast-rate DC charging. High-voltage fast-rate DC charging has currently not been standardized by the Society of Automotive Engineers Standards Committee.

ICPT charging of vehicles has been demonstrated for certain applications in recent years; however a comprehensive analysis of the ICPT vehicle integration and infrastructure integration is needed. Due to the varying power requirements between vehicles, as well as infrastructure characteristics, the parameters for the implementation of an ICPT system need to be considered carefully for efficient deployment of an ICPT infrastructure.

2 Drive cycles

A drive cycle is a set of data points representing a desired vehicle speed versus time. They are commonly used to assess the performance, fuel consumption or emissions of vehicles in a standardized manner. In this study, several drive cycles were considered for the simulation analyses (Table 2). Both the federal highway driving schedule (FHDS) and the federal urban driving schedule (FUDS) were chosen to represent standard vehicle driving scenarios for highway and city conditions, respectively.

Table 2: Comparison of drive cycles used for simulation analyses

Drive cycle	Length (km)	Average speed (km/hr)	Duration (sec)
FUDS	**12.0**	**31.5**	**1369.0**
FHDS	**16.5**	**77.0**	**765.0**

3 Simulation Model

Computer simulations are frequently used in the automotive industry to drive down development time and cost. The ability to accurately simulate vehicle systems and subsystems without the need for a physical model leads to a more efficient vehicle development process. For the purpose of this paper, a model of an electric ICPT-enabled vehicle was developed in the MATLAB/SIMULINK environment, based on actual vehicle parameters. The model takes into account vehicle parameters, and also considers environmental parameters such as road grade, ambient temperature, etc… The vehicle parameters considered in the model are:

- Mass
- Aerodynamics
- Drivetrain efficiencies
- Battery & tire parameters

The model consists of three main components, the vehicle dynamics component, the battery-electric drivetrain, and the driver control model. The vehicle dynamics component calculates the longitudinal dynamics based on simple equations of motion and the forces acting on the vehicle during motion.

$$F_{traction} = F_{inertia} + F_{rolling} + F_{aero} + F_{grade} \quad (1)$$

Equation 1 represents the sum of the forces acting on the vehicle during motion. $F_{traction}$ represents the required tractive force at the wheels at a given instant, $F_{inertia}$ represents the force due to the linear acceleration of the vehicle mass, $F_{rolling}$ is the resisting force due to rolling of the tires, F_{aero} represents the aerodynamic drag force on the vehicle, and F_{grade} represents the gravitational force acting on the vehicle from road grades.

The battery-electric powertrain component consists of the battery pack, electric motor, driveline and electric motor controller. The battery pack performance is simulated with an electrical and thermal model to analyze the performance parameters. The driver control model simulates driver inputs based on actual vehicle speed compared to drive cycle input reference speed. The result is accelerator and brake pedal position outputs to follow the given instantaneous input speed. All subsystems combined, the model accurately simulates the vehicle longitudinal dynamics and energy management system over the specified drive cycle.

4 ICPT Track Positioning

The location of ICPT needs to be carefully considered to optimize the efficiency of energy transfer from road to vehicle. There are several factors that are critical in the optimization, such as battery state-of-charge (SOC), and vehicle av-

erage speed over the length of ICPT track. The ICPT track should be located such that the vehicle battery pack can accept the maximum possible charge energy. If the ICPT track is located at an early stage in the drive cycle, the battery SOC upper limit may stop the charge to prevent over-charging of the batteries. For the purpose of this research, a constant ICPT efficiency of 75% was used in the simulation model.

The energy transferred from ICPT is determined by power of the ICPT system and the duration of energy transfer (Equation 2). Since the duration of energy transfer is a direct function of average vehicle speed over length of ICPT track, the maximum energy transfer is achieved at the location of lowest average vehicle speed. For the purpose of this research, an ICPT track length of 500 meters was selected for both drive cycles to investigate the performance of the ICPT system. Also, an algorithm based on the equation below (Equation 2) was used to determine the location of lowest average vehicle speed was used for each drive cycle, with the constraint of battery SOC limits.

$$E_{ICPT} = \int_0^t P_{ICPT} \cdot dt \tag{2}$$

Using the optimization algorithm, the ICPT track locations for the FUDS and FHDS drive cycles were optimized for lowest average speed, thus giving the maximum energy transfer potential for the drive cycle. Figures 1 and 2 show the result of the optimization for the FUDS and FHDS drive cycles, respectively.

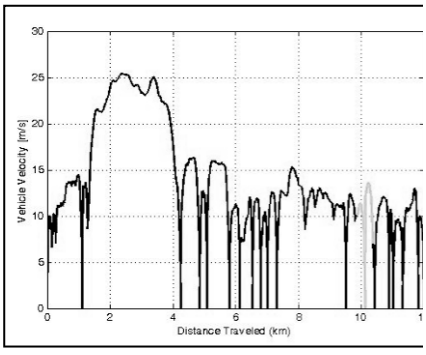

Fig. 1 ICPT track location for FUDS

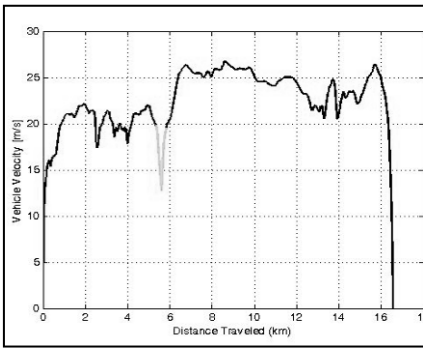

Fig. 2 ICPT track location for FHDS

The model simulation was run over both drive cycles for three cases, No ICPT, 20kW ICPT, and 40 kW ICPT. The vehicle battery pack SOC was monitored to demonstrate the power transfer from the ICPT system for the FUDS and FHDS drive cycles (Figures 3, and 4 respectively). The SOC increase due to the power transfer from ICPT is easily visible from the SOC plots. The significantly reduced

power transfer for the FHDS cycle case is attributed to the higher average speed of the drive cycle. As previously mentioned, the duration of energy transfer, and thus average vehicle speed is a primary factor of total energy transferred from ICPT.

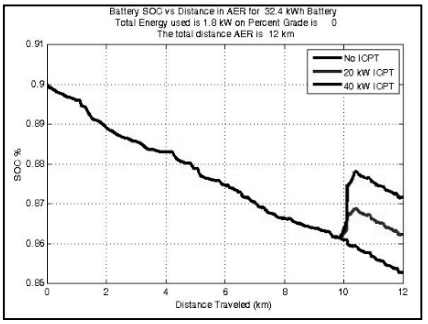

Fig. 3 SOC over FUDS Drive cycle

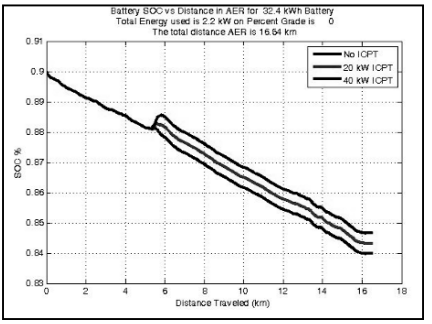

Fig. 4 SOC over FHDS Drive cycle

5 Vehicle Mass Compounding Effects

Mass tracking is a critical aspect of vehicle design engineering not merely due to the primary effects of reducing the mass of a component or structure. More importantly, the secondary mass savings from the mass reduction of the primary component further contributes to the overall mass reduction. This effect, also known as the mass compounding effect, is a means to quantify the secondary mass reduction. The compounded vehicle mass (m_{comp}) can be calculated by the following equation (Equation 3):

$$m_{comp} = m_v + \Delta m_p + \Delta m_s \tag{3}$$

Where m_v is the original vehicle mass, Δm_p the primary mass change, and Δm_s the secondary mass change (Equation 4). The secondary mass change is calculated using a secondary mass coefficient (δ_s). A recent research study has found, for typical ICE vehicles, typical secondary mass coefficients to be between 0.8 and 1.5 [8]. Equation 5 represents the compounded vehicle mass for a battery-electric vehicle, taking into consideration the tertiary mass change (Δm_t).

$$\Delta m_s = \Delta m_p * \delta_s \tag{4}$$

$$m_{comp\_BEV} = m_v + \Delta m_p + \Delta m_s + \Delta m_t \tag{5}$$

The mass compounding effect for battery-electric vehicles also has a significant effect on the vehicle cost, given the potential for decrease in battery pack capacity. Battery pack costs in the order of $650/kWh, and assuming a battery pack

capacity of 28 kWh, will show that a 5% decrease of battery pack capacity (or 1.4 kWh) results in a $910 decrease in battery pack cost. The effect that the battery pack cost alone has on the total vehicle cost presents an opportunity for alternative energy transfer methods in order to meet range requirements, while maintaining a competitive vehicle cost.

One such alternative is the use of ICPT to decrease the battery pack capacity requirements, and thus vehicle mass and cost. The effects of a potential ICPT implementation for battery-electric vehicles were analyzed using the simulation model for the two power ratings of 20 kW and 40 kW, as discussed previously. The ICPT system allows for energy transfer to an electric vehicle without the need to wait for a recharge. While the amount of energy transfer to the vehicle is a function of ICPT power rating and ICPT availability, two cases for ICPT were considered based on the driving cycles (FUDS and FHDS). The chosen ICPT length of 500 meters per single drive cycle (See table 2) represents ICPT availability per unit length of 4.2%, and 3%, respectively.

The total ranges of the vehicle model for each drive cycle without any ICPT were found to be 152.1 km and 165 km, respectively (Figure 5). These values represent the range that the vehicle used for this research can achieve with the 28 kWh battery pack. The effect of the ICPT on the total range of the vehicle is shown in figure 5 as well, with an increase in range of up to 23.7% and 62.6% for the 20kW and 40kW ICPT ratings, respectively. The findings in Figure 5 suggest that an ICPT implementation should be located in a low vehicle speed area to increase the effectiveness of the ICPT system. The mass compounding effect of ICPT implementation was found using the original vehicle range as a target. The vehicle secondary mass coefficient was assumed to be 0.5 [9]. The result was a gross vehicle mass decrease of up to 7.4% for the 20 kW ICPT case and up to 14.5% for the 40kW ICPT case (Figure 6).

As mentioned earlier, one of the driving keys for mass adoption of battery-electric vehicles is the vehicle cost, of which a main component is the battery pack. By combining the use of an ICPT system with between 3 and 4.2% ICPT coverage and the decreased mass due to mass compounding effects, a significant reduction in battery pack capacity and cost is possible. Figure 7 shows the vehicle battery pack cost for the cases of no ICPT, 20kW rating and 40kW rating. For the FUDS drive cycle, a resulting battery pack cost decrease of 25% for the 20kW ICPT case, and 48% for the 40kW ICPT case is shown.

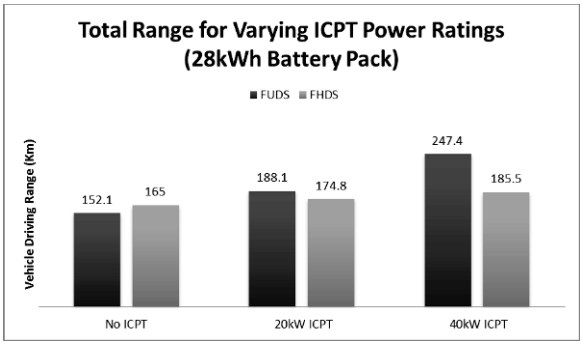

Fig. 5 Total range for varying ICPT power ratings

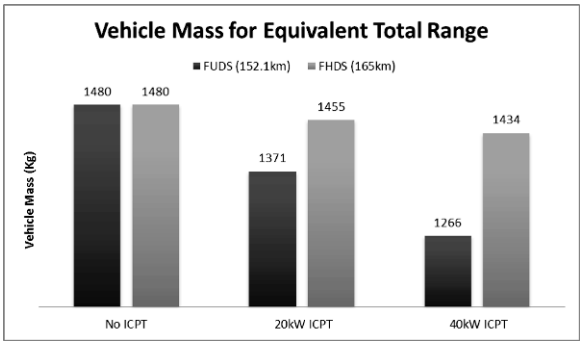

Fig. 6 Vehicle mass for equivalent total range

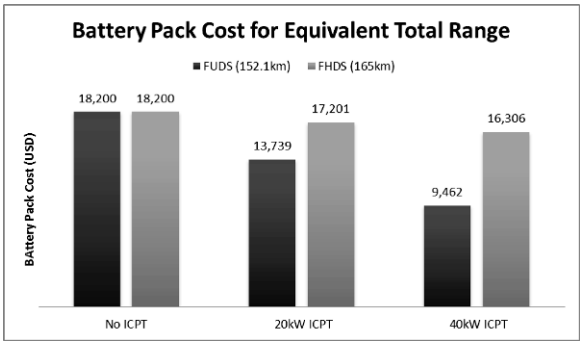

Fig. 7 Battery pack cost for equivalent total range

6 Conclusion

This paper investigated the relationships between vehicle cost, mass, total range, and battery pack mass, unique to battery-electric vehicles. The mass compounding effect for battery electric vehicles was investigated and found to be of significant importance to understand the potential mass savings and systems integration of battery-electric technology. The proposed inductively coupled power transfer (ICPT) system as a potential solution for decoupling the vehicle range – vehicle cost relationship was found to be very effective by allowing the battery pack size to be reduced considerably.

For this study, an ICPT track length of 500 meters was selected to investigate the performance of the ICPT system. Future work should be done to investigate the optimal track length based on ICPT track implementation costs and traffic density in order to propose a cost-effective solution. Future work should also include an investigation of experimental ICPT efficiency for a full-scale as a function of vehicle speed and primary-secondary alignment cases.

References

[1] U.S Energy Information Administration (EIA), “Historical Data: Alternative Transportation Fuels (ATF) and Alternative Fueled Vehicles (AFV)” US Department of Energy, 2010.

[2] Deloitte Consulting, “Gaining Traction: A customer view of electric vehicle mass adoption in the US automotive market”, *Deloitte Consulting LLP*, 2010.

[3] R. Lache, D. Galves, R. Nolan “Vehicle Electrification: More rapid growth; steeper price decline for batteries”, *Deutsche Bank Industry Update*, 2010.

[4] C.Fellner, J. Newman, “High-power batteries for use in hybrid vehicles” *Journal of Power Sources* vol. 85, pp. 229-236, 2000.

[5] S. Hung, S.M. Lukic, J. Taiber, and M. Saunders "Use of Inductively Coupled Power Transfer (ICPT) for Electric Vehicles", *IEEE PES General Meeting,* 2010.

[6] G.A.Covic, G.Elliott,O.H.Stielau,R.M.Green, J.T.Boys, “The design of contact-less energy transfer system for a people mover system”, Proc. of Int. Conf. on Power Syst. Tech., Perth, Australia, pp. 79-84, 2000.

[7] “Product Overview: Inductive Power Transfer-IPT”, Industrial Power & Control Inc., 2010.

[8] D.E.Malen, K.Reddy, “Preliminary Vehicle Mass Estimation Using Empirical Subsystem Influence Coefficients” *FGPC-Mass Compounding Project Team Auto/Steel Partnership*, 2007.

[9] M.A.Kromer, J.B.Heywood, “Electric Powertrains: Opportunities and Challenges in the U.S. Light-Duty Vehicle Fleet”, MIT LFEE 2007-03 RP, 2007.

PERFORMANCE COMPARISON OF HYDROGEN FUEL CELL AND HYDROGEN INTERNAL COMBUSTION ENGINE RACING CARS

G. Pearson[1], M. Leary[1], A. Subic [1], J. Wellnitz[2]

[1]School of Aerospace Mechanical and Manufacturing Engineering, RMIT University, Bundoora Victoria 3083 Australia; Email: geoff.pearson@rmit.edu.au

[2]University of Applied Sciences Ingolstadt, Esplanade 10, Ingolstadt Germany, E-mail: joerg.wellnitz@fh-ingolstadt.de

Abstract: Students from RMIT University and the University of Applied Sciences Ingolstadt have collaborated to build a hydrogen-powered racing car. As part of the initial conceptual design, a lap simulation was developed to compare performance and fuel usage of hydrogen internal combustion engine and hydrogen fuel cell vehicles. For the vehicle and track specifications analyzed, it was found that fuel cells require a power density of 5kg/kW to be competitive with the hydrogen internal combustion engine. The study also highlighted the complex nature of the alternative fuels debate.

1 Introduction

1.1 The case for hydrogen vehicles

Mankind's dependence on personal transport is increasing as economies grow and as emerging nations move towards a more Western lifestyle. However the transport sector relies heavily on petroleum products as a fuel source, resulting in the production of large quantities of greenhouse gases, and exposure of the transport sector to great uncertainty in the face of diminishing oil supplies.

A possible alternative fuel is hydrogen. When hydrogen reacts with oxygen in the air the only product of reaction is water, and therefore it offers the potential of carbon-free transport. Two available power units for hydrogen vehicles are the fuel cell (H_2FC) and the internal combustion engine (H_2ICE). Of the two options, the fuel cell offers advantages in potential efficiency as the chemical reaction energy is directly harnessed as an electric current to drive a motor. In comparison,

the H_2ICE cycle includes an intermediary heat phase, restricting potential efficiency to ideal heat cycle limits. From these efficiency considerations, fuel cell vehicles are often seen as the ideal "end-goal" for hydrogen powered transport.

However fuel cells can be heavier and more expensive than internal combustion engines, and require high purity hydrogen to prevent the cell from being poisoned. Hydrogen internal combustion engines are less efficient, but offer weight and cost advantages and can be run on multiple or impure fuels.

A motor vehicle is a dynamic system and therefore a vehicle's powertrain must use some of its available power to accelerate itself. This leads to the question: in an automotive situation, how much is the potential efficiency advantage of a fuel cell offset by the additional mass of the fuel cell itself?

1.2 Formula H

RMIT University (Australia) and Hochschule Ingolstadt (Germany) have collaborated to build a hydrogen powered racing car. Known as Formula H, the objectives of the project were to prove that alternative fuel vehicles are achievable with existing technologies, and to expose the student team to a real-world multinational design project. The project delivered a fully functioning LeMans prototype style racing car, powered by a BMW 800cc motorcycle engine running on hydrogen fuel, and featuring a 200bar compressed gas hydrogen supply system.

2 Vehicle Comparison Methodology

2.1 Lap Simulation

Early conceptual design process required the Formula H team to assess the relative performance of internal combustion engines and fuel cells for racetrack use. A preliminary study was undertaken in the form of a quasi-static lap simulation, based on the 3 km long Winton racetrack in Victoria Australia. A vehicle model representing a benchmark H_2ICE vehicle was simulated, with predicted lap time and fuel consumption results recorded. These results were then compared against fuel cell vehicle models of varying powers and weights.

The simulation was constructed as follows:

- The vehicle path was modeled as a string of straight lines and constant radius arcs, broken into 1 metre increments.
- Each vehicle was modeled as a point mass with representative tyre grip and power output characteristics.

- Vehicles travelled at constant speed through corners, at the tyre grip limit. Cornering speed defined entry and exit speeds for each straight.
- Forward acceleration was calculated as a function of engine power (P_{ENGINE}), driveline efficiency (η), resistance power ($P_{RESISTANCE}$, the combined aerodynamic drag and rolling resistance), velocity (v) and vehicle mass (m):

$$\eta P_{ENGINE} - P_{RESISTANCE} = mav \qquad \text{(Gillespie, 1992)}$$

- Velocity under braking was calculated using combined wind resistance and maximum tyre grip force.
- Vehicle power was assumed constant and independent of engine speed.
- Aerodynamic drag was calculated as a function of velocity (v), frontal area (A), drag coefficient (C_D) and air density (ϱ), as described in [1]:

$$F_{DRAG} = 0.5\rho A C_D v^2$$

- Vehicle energy requirements were calculated by summing kinetic energy changes, air resistance and rolling resistance energies across each track increment.
- Relative fuel used was calculated as a function of the total energy required, and overall thermodynamic efficiency. Thermodynamic efficiency of the H_2ICE was estimated at 25%, and the fuel cell at 40%.

The modeling of detailed vehicle dynamics such as cornering transients, weight transfer, or suspension dynamics were considered unnecessary for this preliminary study.

2.2 Tyre Grip

A critical modeling requirement was to capture the effect that varying vehicle weights would have on tyre performance. Whilst a tyre's grip force increases with vertical load, the relationship is not linear and the grip coefficient actually falls with increasing normal force [2]. This is known as tyre load sensitivity, and published test data [3] for Goodyear tyres similar to those used on the Formula H vehicle confirms this characteristic. The grip coefficient is seen to fall by approximately 0.03% per Newton of load (Fig. 1).

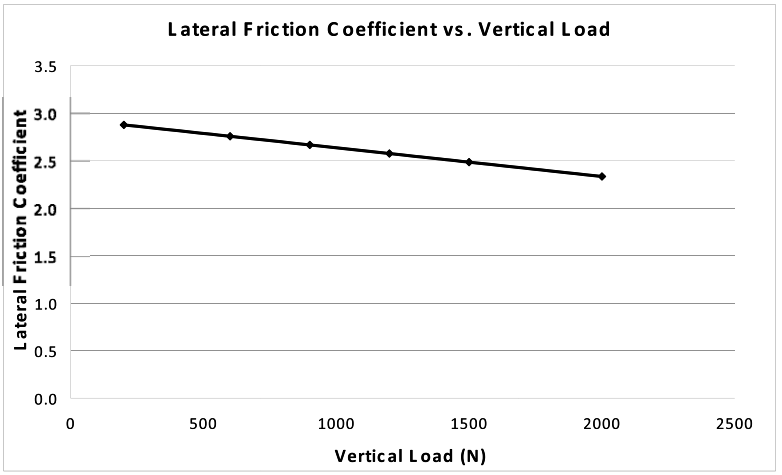

Fig. 1 Friction data, Goodyear 20.0-7.0x13 D2509 FSAE tyre ([3]).

Note that the above data were taken in controlled laboratory tests on a rolling drum tyre testing machine, and are believed to overestimate absolute friction coefficient values. A more representative value of friction coefficient is estimated at approximately 1.4-1.5, based on observations of the cornering performance of the RMIT Formula SAE vehicle using similar tyres. Tyre load sensitivity is expressed in terms of percentage variance per Newton of load, so is unaffected by this adjustment of scale.

2.3 Vehicle Specifications: H_2ICE Benchmark Vehicle

The benchmark H_2ICE vehicle was modeled on the Formula H vehicle, with the following specifications:

Table 1. H_2ICE vehicle specifications.

Specification	Value
Total vehicle mass (including driver and engine)	600kg
Engine system mass (not including H_2 supply system)	80kg
Tractive power (rear wheels)	30kW
Tyre grip coefficient (all directions)	1.4
Frontal area	1.2m^2
Drag coefficient (CFD estimate)	0.62
Rolling resistance (assumed constant)	200N
Thermodynamic efficiency	25%

The above vehicle model completed one lap of the circuit in 105.1 seconds, with a maximum speed of 129.8kmh. Note that the top speed of the actual Formula H car has been measured at 133kmh, confirming that the simulation is of reasonable accuracy.

2.4 Vehicle Specifications: Fuel Cell Vehicle

Fuel cell vehicles were simulated by replacing the IC engine system mass and output in the baseline vehicle model with each combination of the following fuel cell attributes:

- Power output: 30-80kW, in 10kW increments.
- Fuel cell unit power to weight ratio: 5-10 kg/kW, in 1kg/kW increments.

It was assumed that the compressed gas hydrogen supply system would be common to fuel cell and H_2ICE vehicles. In each case a modified tyre friction coefficient was calculated, using a tyre load sensitivity of 0.03% reduction in friction coefficient per Newton of total vehicle weight (relative to the baseline vehicle).

3 Vehicle Comparison Results

Inspection of the results highlights the importance of fuel cell weight reduction. The only fuel cell vehicles to achieve equivalent or faster lap times than the H_2ICE vehicle were those with a fuel cell mass to power ratio of 5kg/kW, and only those with power outputs of around 45kW or greater (Fig. 2). The effect of additional mass of the heavier vehicles slowed them sufficiently in the corners that any advantage on the straights was negated. This was despite the fact that in many cases the higher powered fuel cell vehicles had a greater overall power to weight ratio than the benchmark H_2ICE vehicle.

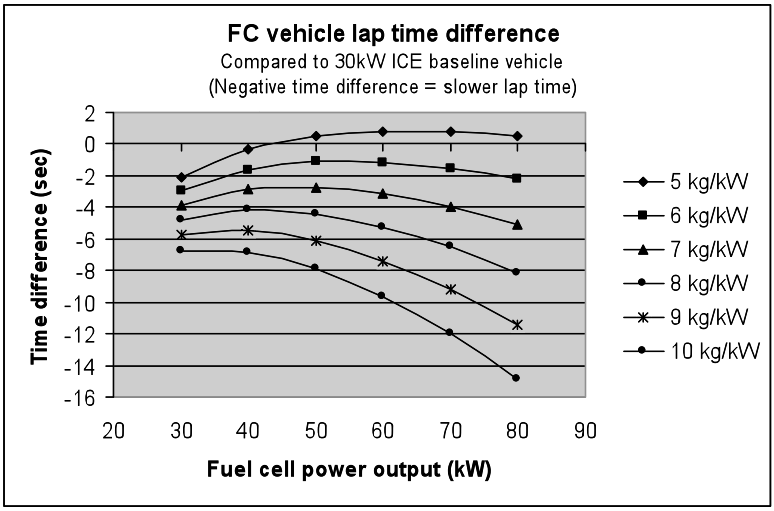

Fig 2. Comparative lap times.

All fuel cell vehicles showed a similar trend of increased fuel usage at higher power outputs, as lesser cornering speeds and higher top speeds created greater kinetic energy and aerodynamic drag energy demand (Fig. 3). Of the variants tested, only the 50kW and 60kW fuel cell design options of 5kg/kW power density were calculated to offer faster lap times and lower fuel consumption.

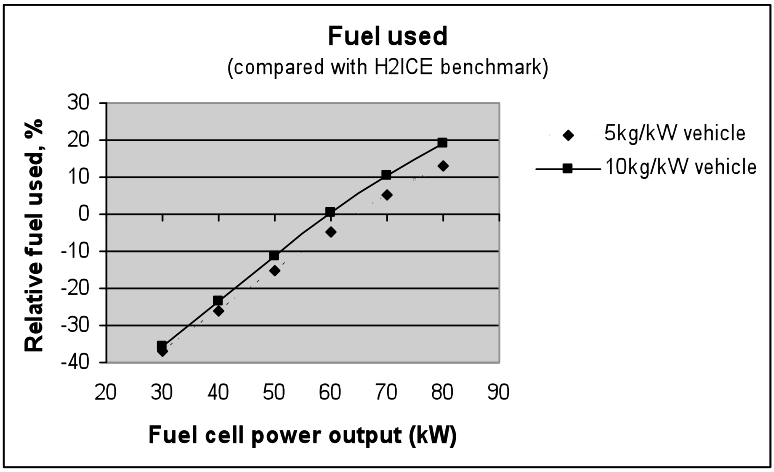

Fig. 3 Comparative fuel used

It is interesting to note that lap times show a distinct negative trend at higher power outputs. The vehicle designer would need to be aware that increasing pow-

ertrain output in an attempt to gain competitiveness can in fact result in both worse lap times and greater fuel consumption. This is particularly dependant on the tyre's load sensitivity characteristics.

4 Conclusions

The above work is a preliminary study only, and the presented results are relevant only to the particular vehicle, tyres and racetrack used in the study. Moreover, the results presented are for race conditions at the limits of a vehicle's performance, and would not be representative of common passenger vehicle usage.

However the study highlights the danger of focusing on individual parameters when assessing vehicle performance. A motor vehicle is a complex system, and decisions made on the basis of isolated criteria such as thermodynamic efficiency or power density may be poorly informed when observed at a system level. It is recommended that further investigation be undertaken into the relative merits of hydrogen fuel cell and hydrogen internal combustion engine vehicles.

References

[1] Gillespie, T.D. (1992) *Fundamentals of Vehicle Dynamics*, SAE International, Warrendale, Pa

[2] Milliken W.F. and Milliken D.L. (1995) *Race Car Vehicle Dynamics*. SAE International, Warrendale, Pa

[3] Milliken & Associates (2008) *Formula SAE Tyre Testing Consortium test data*. Available: http://www.millikenresearch.com/fsaettc.html (Accessed: 24 February, 2009).

V MATERIALS AND STRUCTURES

DESIGN OF BASIC STRUCTURAL COMPOSITE ELEMENTS

H. Bansemir

Consulting for Composites, Light Weight Structures and Knowledge Management,
Geitnerweg 4, D-81825 München, GERMANY; Email: horst@bansemir.eu

Abstract: Composite structures with basic fibre reinforced elements are widely used in the design of aerospace structures. In 1967, the BO 105, a product of the former helicopter division of MBB, now Eurocopter Deutschland GmbH, flew for the first time. This innovative helicopter was equipped with the first serial "hingeless" rotor system. The fibre composite blades were attached to the head with the help of the "lug" element. This allowed the simple design of the rotor, without damper element. These "lug" elements were later also used for the attachment of liquid helium tanks to satellite structures, such as ISO and HERSCHEL, operating in the low temperature range for the scientific observation of the sky. The thermal conductivity could be minimized and thus the lifetime could be extended. In this paper several load introduction elements derived from the „lug" element are described. The stress situation due to the load transfer is quite complicated and has to be calculated by a detailed analysis. The mechanical behaviour of composite materials allows the design of outstanding basic structural elements such as plates and shells having a high range of different stiffness, in plane and out of plane. These elements are often used for the attachment of vibration absorbing structures. In this paper several applications of anisotropic structures are described and possible use is shown. Furthermore outstanding possibilities of designing with composites will allow us to integrate electrical elements into the structures to improve their abilities.

1 Introduction

With fibre composites, outstanding new designs are possible. The early developments in the 60´s at MBB, now Eurocopter Germany, show an intensive use of composites in the design. The attachment of the composite blade to the rotor head with the help of one simple lug fastened to a titanium structure allowed the transfer of the loads. The damping behaviour of this load introduction element was such that no additional damper was necessary for the dynamic lead-lag motion.

The “hingeless” BO 105 rotor system was also used for the design of the helicopters BK 117 and EC 145. The design of the EC 135 is a “bearingless” rotor system including a “flexbeam” with a special cross section for the torsion element, shown in figure 5.

Special elements are used for damping vibrations of a structure such as the airframe of a helicopter. The elastic wall structure forming a tube-shaped hollow body supports a weighted vibrating object. The soft elastic out of plane behaviour of the wall, together with the stiff in plane behaviour can be used for several spring elements. The lug as load introduction element is also used for the suspension of cryogenic tanks of satellites. In this case the low thermal conductivity of the composite materials is used. The open net face sheet sandwich is used for the solar arrays of communication satellites. Low weight and high stiffness are the main advantages of this sandwich design.

2 Material Properties of Unidirectional Composites

Light weight structural components are of special importance for the design of helicopters. The use of composite materials is therefore recommended. The rotor blades are designed with the help of glass and carbon fibre composites. In Figure 1 the normalized properties of unidirectional composites divided by the specific weight factor indicate high strength and stiffness compared to the data of metals and wood.

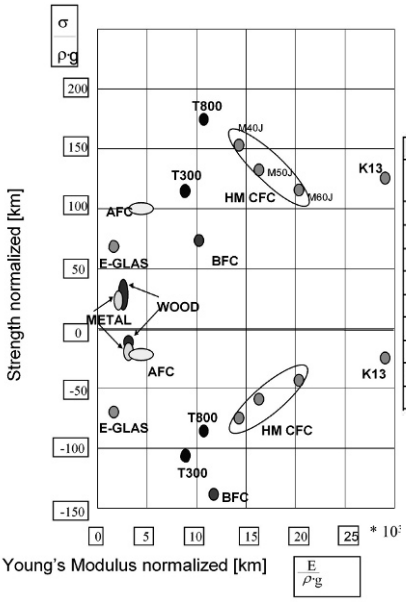

Fiber type	S2-Glass	T300	M55J	K13
	Properties of unidirectional composites			
$E_{\parallel}$ N/mm²	54000	133000	300000	500000
$E_{\perp}$ N/mm²	14000	10800	6400	5700
G_{ν} N/mm²	5400	5700	3900	3500
$\sigma_{\parallel Zug}$ N/mm²	1690	1610	1860	2100
$\sigma_{\parallel Druck}$ N/mm²	1220	1810	835	410
$\alpha_{T\parallel}$ E-6 1/K	6,5	0,4	-0,7	-1,4
$\alpha_{T\perp}$ E-6 1/K	35,8	42	35,2	32,2
$\lambda_{T\parallel}$ W/Kcm (293K)	0.01	0.05	0.544	8
$\lambda_{T\parallel}$ W/Kcm (4K)	0.002	0.0003		

Fig. 1 Properties of unidirectional composites

The normalized tension strength of the composites is in the same range, whereas the compressive strength decreases with the stiffness of the carbon composite. Kevlar (AFC) and the pitch fibre composite K13 have a very low compressive strength. The right hand side table shows the properties for different composites in figures. The unidirectional composites (60 fibre vol. %) show a high range of stiffness. The unidirectional carbon material K13 has about three times the Young´s modulus of steel in fibre direction. The thermal coefficients of carbon composite can become negative and the thermal conductivity is low. Only K13 has a very high thermal conductivity (three times the value of copper). The transverse properties are dominated by the properties of the resin, and are therefore similar for all composites as shown in Figure 1.

3 The "Lug" Load Introduction Element for Several Helicopter and Space Applications

The "lug" for the attachment of the blade to the rotor head was a key element of the BO 105 "hingeless" rotor design. The fixation of the "lug" with the help of the titanium fitting (whose cutaway picture appears in Figure 2) allowed some damped movement of the rotor blade. This rotor concept was used with success for the helicopters BO 105, BK 117 and EC 145 [2].

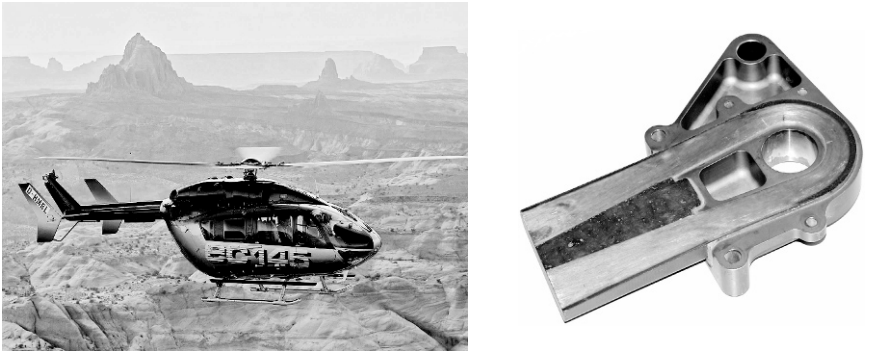

Fig. 2 The commercial EC 145 helicopter with the components glass fibre composite lug and titanium fitting

The reinforcement "lug" elements that appear in Figure 3 introduce high transverse local loads into 2-dimensional areas. Figure 4 shows the reinforcement straps of the liquid helium tanks for the space observatory HERSCHEL. The outstanding low thermal conductivity of composites allows optimization of the design of the chain of straps with respect to thermal conductivity to take into account the local temperature of the chain. At helium temperature the carbon composite lugs show a very low conductivity, whereas the glass fibre composite support strap has

a low conductivity at room temperature. Several further applications of load introduction elements are used in the automotive and aeronautical world.

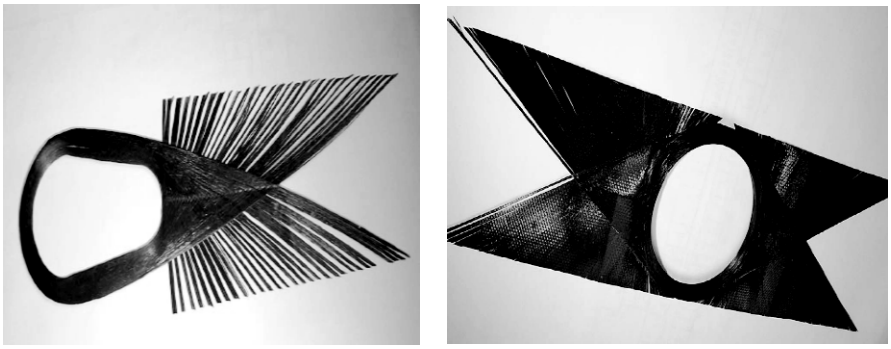

Fig. 3 Load introduction glass- and carbon fibre composite elements

Fig. 4 Space Observatory HERSCHEL and liquid helium tank glass fibre composite support straps

4 The Cross Section of the "Flexbeam" of the Helicopter EC 135

The EC 135 has a "bearingless" main rotor system with the basic "flexbeam" (see Figure 5 [3]). The design of the "flexbeam" includes several fundamental functions such as the attachment area, the flap bending section and the torsion structure. The attachment consists of two double "lugs" bonded together establishing a fail safe component.

The flap bending section has the function of a hinge, having a low flapping bending stiffness and a high strength. The torsion section was optimized with respect to many parameters, such as high torsion strength and low torsion stiffness. Its "warping free" cross section does not induce longitudinal stresses into the "flexbeam". Transverse shear loads, centrifugal loads, bending and torsion moments are transferred by the element. The geometry of the main axes is kept in order to avoid additional stresses. The design also includes elements of new rules for damage tolerance. After the dynamic test, the residual strength including higher temperature and moisture was demonstrated. The complicated design of the complete rotor blade is shown in [5].

Fig. 5 The commercial EC 135 helicopter with the "flexbeam" main blade structure and torsion cross section

5 Spring Elements for Reducing Vibrations of a Helicopter

Due to the oscillations induced by the main- and tail-rotor, the use of vibration absorbers are of essential importance for the flight behaviour and the passenger comfort. The vibration absorbers include spring and mass elements as shown in Figure 6. The apparatus for damping vibrations of a structure, such as the airframe of a helicopter, consists of a mass element, e.g. a battery, and an elastic wall structure forming a tube-shaped hollow body which supports the mass. The elastic wall elements have an in-plane spring stiffness tuned to the frequency of the

vibration to be damped. The wall elements are soft in out of plane direction due to the longitudinal strips which are loaded with torsion moments. The vibration damper containing the battery is installed at a location where clear structural vibrations occur in two directions perpendicular to each other. The damper is tuned to the vibration frequencies in both directions. This patented technology [6] can be used to reduce vibrations of a structure, for example the tail-shake of a helicopter.

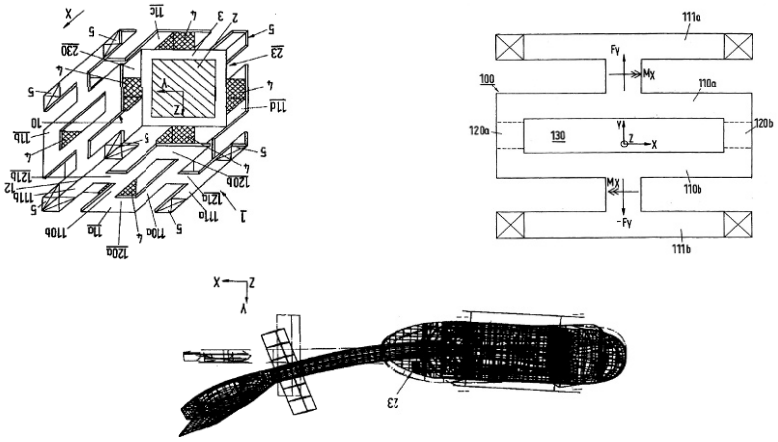

Fig. 6 Apparatus for reducing vibrations of a helicopter

6 The Open Net Face Sheet for Sandwich Structures

The electric power supply is of essential importance for the satellites in space. In the course of time mainly the communication satellites needed more and more electrical power up to 20 kW presently. So the area for the application of solar cells increased. High modulus carbon fibre components are necessary for covering the stiffness and strength demands of the wing. As high modulus carbon fibre fabrics were not available in 1970, the designers had the idea to use the filament winding process to create the “open net face sheet” fabric.

As shown in Figure 7 the sandwich of the solar arrays is composed by several elements such as “open net face sheet”, Al-honeycombs, film adhesive, doublers and “Capton” foil. Very light stiff panels provide a big area for the application of solar cells. The total wing is stiff enough for the demands of dynamic and strength

specifications. The open net sandwich allows the transfer of air during the starting phase of the spacecraft flight [9].

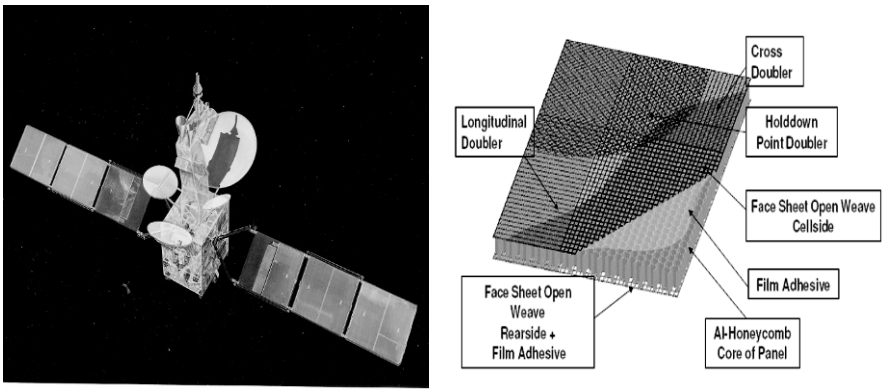

Fig. 7 Communication satellite solar arrays using "open net face sheet" sandwich

7 Summary

Light weight components are essential for the design of helicopters. In 1967, the BO 105 flew for the first time using composite blades for a "hingeless" rotor design. Special attachment "lugs" were created to connect the composite blade to the metallic rotor head. Later the "bearingless" and also "hingeless" rotor of the EC 135 used the "flexbeam" with elastic torsion elements. Other special elements were used for the design of vibration absorbers. The stiff in plane and soft out of plane spring elements connected with mass elements can improve the flight behaviour and the passenger comfort of a helicopter. Another important composite component is the filament wound open net face sheet. These face sheets can be integrated to a sandwich light weight structure for space solar arrays of communication satellites. In summary it can be stated that the use of composites can create innovative light weight structures.

Acknowledgements

The author would like to thank Karl Pfeifer, Eurocopter, for the help of formulating and correcting main elements of the paper. In addition the author would like to thank Eurocopter for the given photos.

References

[1] Schürmann H. (2004) *Konstruieren mit Faser-Kunststoff-Verbunden*, Springer-Verlag Berlin Heidelberg New York, ISBN 3-540-40283-7

[2] Humpert A. (2003) *Design of the new EUROCOPTER Medium Twin Helicopter EC145,* American Helicopter Society, 59th Annual Forum, Phoenix, Arizona, May 6 – 8.

[3] Bansemir H., Mueller R. (1997) *The EC135 – Applied Advanced Technology,* AHS, 53rd Annual Forum, Virginia Beach, USA, 29 April – 1 May 1997

[4] Wörndle R., Daschner W., (1980) *Rechnerische Untersuchung von zug- und druckbelasteten FVW-Strangschlaufen,* Z. Flugwiss. Weltraumforsch. 4 (1980), Heft 1

[5] Bansemir H., Emmerling, S. (1999) *Fatigue Substantiation and Damage Tolerance Evaluation of Fibre Composite Helicopter Components,* Corfu Greece, Applied Vehicle Technology Panel: Applications of Damage Tolerance Principles for Improved Airworthiness of Rotorcraft

[6] Bansemir H., Bongers B. (1998) *Apparatus and method for reducing vibrations of a structure particularly a helicopter,* United States Patent No 6,286,782 B1.

[7] Bansemir H., Schnell H.-G., Weiß W. (2003) *Faserverbundstrukturen für die Raumfahrt*, Deutscher Luft- und Raumfahrtkongress 2003, 17.-20. November in München

[8] Bansemir H., Bauer M., Schnell H.-G. (2001) *Großflächige Solargeneratoren in Faserverbundbauweise für Nachrichten-satelliten*, Deutscher Luft- und Raumfahrtkongress 2001, 17. – 20. Sept. in Hamburg

[9] Bansemir H., Pfeifer K. (1983) *Local stability of sandwich structures with thin fibre reinforced face skins for space application,* Engineering with Composites, SAMPE European Chapter, Third Technology Conference, London.

ENHANCING SUSTAINABILITY THROUGH THE TARGETED USE OF SYNERGY EFFECTS BETWEEN MATERIAL CONFIGURATION, PROCESS DEVELOPMENT AND LIGHTWEIGHT DESIGN AT THE EXAMPLE OF A COMPOSITE SEAT SHELL

W. Hufenbach, M. Krahl, R. Kupfer, S. Rothenberg, T. Weber, P. Lucas

Technische Universität Dresden, Institute of Lightweight Engineering and Polymer Technology, 01062 Dresden, Germany; Email: ilk@ilk.mw.tu-dresden.de

Abstract Focus of this paper is the sustainable lightweight design of a composite seat shell and the development of a fully-automated high-volume production process for lightweight-optimized automotive structures made from fibre-reinforced thermoplastics. It was shown, that the lightweight component was able to meet all static and crash-relevant requirements in combination with a weight reduction of nearly 50 %. Accompanying analyses of the economical and ecological key figures pointed out that the designed lightweight seat shell can be produced at equal costs with less resource demands than the original steel part.

1 Introduction

Considering the growth rate of the global population and the therewith associated enormous increase in resource demands – resource-poor countries like Germany – are forced to explore new ways of resource usage in order to ensure their wealth. Lightweight engineering with its inherent material and energy efficiency offers the potential to combine high technological requirements with resource conservation and cost effectiveness. Thus lightweight engineering can strengthen the vision of a sustainable economical growth. Especially in the mobility industry – as a key industry of the German economy – these issues are currently highly focused.

The “Dresdner Modell” with its vision of function integrated lightweight system engineering in multi-material design has set the benchmark in the development of efficient lightweight products. By extending the constructive development methodology in respect to resource conservation, future lightweight products are developed technologically and economically sophisticated as well as resource ef-

ficient. Within the Collaborative Research Centre 639 (SFB 639) and the associated transfer unit 639 a new fibre rein-forced thermoplastic seat shell for the VW Golf plus and VW Tiguan has been developed. The development was performed at the Institute of Lightweight Engineering and Polymer Technology (ILK) and its tight linked development partner, the R&D Department of the Volkswagen AG. Within this paper the new process technology for structural interior part will be introduced and a resource orientated analyses on both parts will be performed.

2 Development of a Lightweight Seat Shell

The task for the development was to design a novel lightweight seat shell which permits the highest possible weight reduction without impairing mechanical properties and production costs. After analyzing the basic conditions the use of textile-reinforced thermo-plastic materials seems to be an appealing approach to achieve the stated requirements. Due to their good mechanical properties and short cycle times during processing, textile-reinforced thermoplastic composites gain increasing relevance for high-volume lightweight applications. Using fast-stroke presses in combination with efficient pre-heating systems, complex structural parts can be produced within a few process steps as demanded in automotive applications.

The seat shell was chosen as a reference object for the new process technology since it is a complex and well elaborated structural part, which in addition is highly stressed in case of a crash. Furthermore it was intended that the results of the development shall indicate the novel technology potential. Therefore it was necessary to conduct studies on the mechanical and economical key figures to compare the results with the already known details of conventional steel seat shells.

In view of the fact that the lightweight seat shell was developed in respect to the holistic design approach of the “Dresdner Modell” the design was not only determined by mechanical and economical aspects. In order to enhance the sustainability of the novel seat shell parallel to the engineering process a prospective resource-orientated product assessment was carried out. By the means of this approach the life cycles of the steel and lightweight seat shells were analyzed in respect to their resource demand.

3.1 The Seat Shell Development in Detail

Typically seat shells used in modern cars are made of steel. The reference part used in the 2010 VW Golf plus and Tiguan is made of one steel pipe and four spot welded plates which are all coated by cataphoretic painting. In total the mass of

the reference part is 4.6 kg. The multistage manufacturing process for this part with several forming and joining steps is time and cost intensive.

The design concept of the new lightweight shell pursued an integrated design approach by combining semi-finished textile-reinforced thermoplastic hybrids (TRTP) and long-fibre reinforced thermoplastics (LFRT)[1]. The developed process technology allows to manufacture the whole lightweight seat shell within a single step. Furthermore the composite seat shell already features a stress optimized design. In particular this means that variable wall thicknesses in highly stressed load introduction areas are realized by applying additional local textile patches as well as forming complex stiffening structures out of the LFRT. In total this leads to a drastically cut of weight to 2.4 kg. The differences in structural design can be seen in Figure 1.

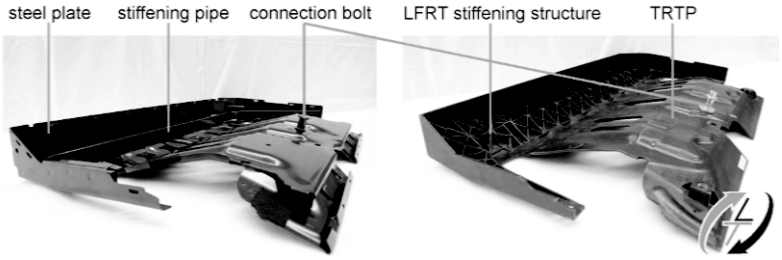

Common steel seat shell

Fibre-reinforced lightweight seat shell

Fig. 1 Comparison of the seat shell designs.

Since the structure of the original steel part needed a stiffening pipe in order to cope with the crash requirements large efforts in terms of simulating and mechanical testing under static and highly dynamic loads were carried out to evolve a LFRT stiffening structure which guaranties a highly stressable link to the TRTP ply stack. For this purpose different semi-finished products made of thermoplastic hybrid yarns, e.g. fabrics, knitted fabrics and multiaxial multilayered fabrics were assessed in respect to their potential usability for the lightweight seat shell. [1-3] Therefore material properties where obtained which served as input parameters for LS-Dyna analyses. The comparison of simulated and tested mechanical deflections under load showed a deviation of not more than 3 %.

[1] Within the development process it was decided to use glass fibre reinforced polypropylene (GF/PP).

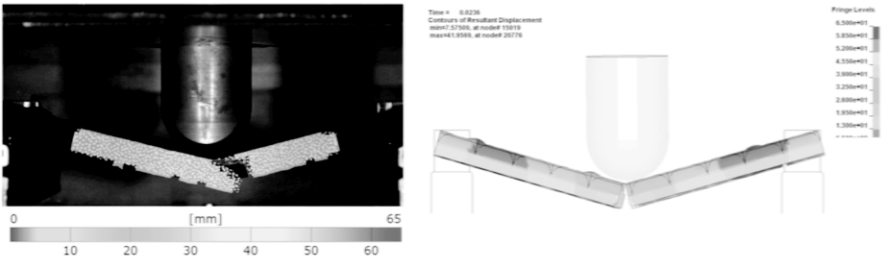

Fig. 2 Comparison of tested and simulated fibre reinforced stiffening structures in a 3 point bending crash bench.

Further failure analyses revealed the need of a surface layer made of fibre-reinforced thermoplastic fabrics to avoid unintended failure behaviour. In order to trace back influences of the manufacturing process on the fracture behaviour different failure modes were localized by the means of 3D computed tomography analysis.

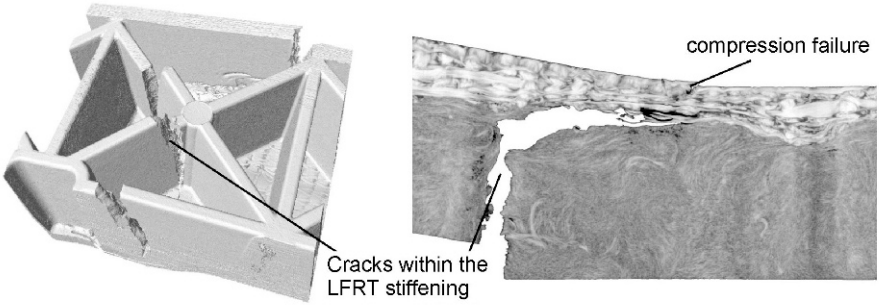

Fig. 3 Investigations on the failure modes of the stiffening structure using a CT scanner.

To establish a stable high-volume capable production process for the light-weight optimized seat shell a fully automated manufacturing process chain was designed and built. The developed process begins with the positioning of the pre-formed textile surface layer and the individual reinforcing patches. The ply stack is then heated in an infrared emitter field up to a processing temperature of 180 °C, meanwhile the LFRT-compound is extruded. By the means of a fully automated handling system, both components are simultaneously inserted into the moulding tool. For the handling system and pressing mould adapted fixing elements had been developed to prevent a slipping of the textile surface layer during the transfer and press process. The trimming of the consolidated seat shell to the final shape takes place in a subsequent stamping process. Several optimizations of the process parameters lead to an entire process time of less than 45 s.

3.2 Analyses of the Resource Efficiency of the Seat Shells

Within the "Material Efficiency and Resource Conservation" (MaRess-) Project founded by the German Federal Ministry for the Environment, Nature Conservation and Nuclear Safety and the Federal Environment Agency several analyses on the resource efficiency of the novel process technology were carried out. Therefore the production chains of the steel and composite seat shell were analysed via the "Material Input per Service Unit" (MIPS-) Concept.[4] MIPS features an input orientated approach which allows to estimate the resource productivity of complex systems within a short period of time. Studies on the result quality of different abridged lifecycle oriented concepts in comparison to the life cycle analyses (LCA) showed that MIPS was able to achieve result equality. [5]

Analogous to LCA in the first step it is mandatory to determine the objectives of the analyses. In case of the seat shells the resource demand of both products with regard to the service units 'lightweight seat shell' (LWSS) and 'lightweight-kilogram' (LWKG) ought to be analysed. Under that perspective an inventory analysis was carried out. Therefore it was necessary to analyse the production processes, define realistic product life cycles, measure process times and energy consumptions for both seat shells. Table 1 gives an overview of the collected data set and the live cycle specific assumptions.

By the means of the collected data the energy and material inputs of the different life cycle phases were aggregated and multiplied with the material input factor (MI-factor). This factor represents a material intensity value for individual input materials and energy quantities (also known as "rucksack factor"). The resulting resource consumptions are related to the preliminary defined service units.

Referring to the service unit LWSS the novel composite seat shell shows higher resource preservations in every aspect of the analyses (Figure 4). It can be observed that the resource demand of the steel part is dominated by the raw material acquisition- and use-phase. In contrast the resource consumption of the lightweight seat shell is primarily influenced by the production- and use-phase. It appears that due to the higher energy demands for heating up the thermoplastics the production phase of the lightweight seat shell is more resource intensive. However within the use phase the resource demand could be traced back to the weight related fuel consumptions, hence the lightweight part passively helps to lower the CO_2 emissions.

Table 1 Overview of the assumptions for the MIPS analyses

Type of the seat shell	Life cycle phase	Energy & Materials Inputs, Assumptions
Lightweight seat shell	Raw Material Acquisition	Input of Polypropylene
		Input of E-glass fibres
		Distinction of energy input for the production of

		LFRT & TRTP
		30 % of the LFRT can be obtained as recycling product [6]
	Production	Energy input via infrared emitter field
		Energy input via extruder
		Energy input via tool heating
		Energy input via handling robot
		Recycling of the stamp scrap
	Use	Estimated lifetime 150.000 km
		0.12 l Diesel saving through the reduction of 100 kg per 100 km [7]
	Recycling	After the use phase it is possible to recycle the fibre reinforced thermoplastic seat shell
Common steel seat shell	Raw Material	55 % Input via hot rolled, blast furnace steel
	Acquisition	45 % Input via electric arc finance road steel [8]
	Production	Energy input trough the cathodic electrophoretic coating
		Energy input via spot welding is negligible
	Use	Estimated lifetime 150.000 km
		0.12 l Diesel saving through the reduction of 100 kg per 100 km [7]
	Recycling	After the use phase it is possible to recycle the whole steel seat shell

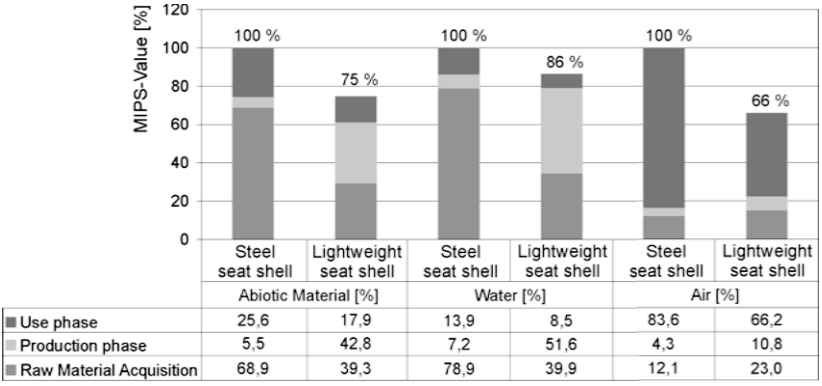

Fig. 4 Distribution of resource demands over the entire life cycle, referring to LWSS

Under the perspective of LWKG a sensitivity analyses was performed under the perspective of analysing the resource demand for 1 kg seat shell produced in the described manner (Figure 5). The analysis shows that if the seat shells would have an equal weight, the steel seat shell would be less resource demanding. Anyhow through a targeted exploitation of the mechanical properties of the fibre re-

inforced plastic it is possible to lower the weight even further than what would have been necessary for equilibrium in resource consumption.

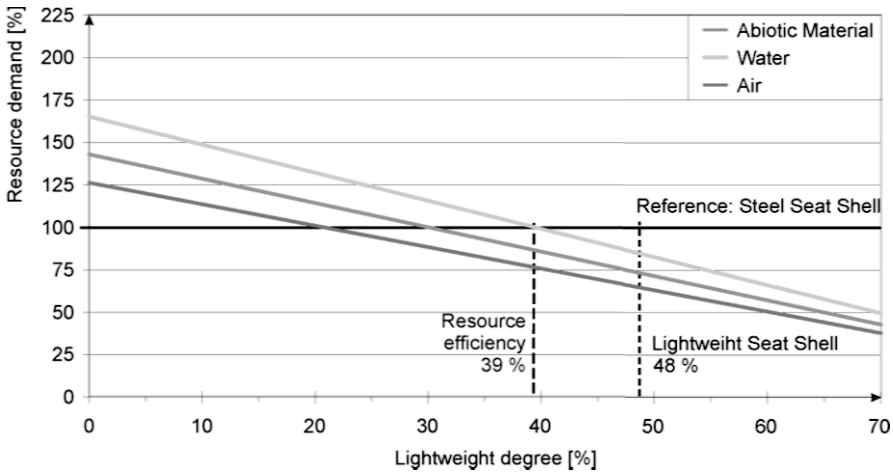

Fig. 5 Influence of the lightweight degree on the resource demand, referring to LWKG.

4 Summary

Within the frame of research of the SFB 639 and the MaRess project a novel process technology for the production of fibre-reinforced thermoplastic structural parts was developed and assessed in respect to the caused resource demand. The conducted studies on technological, economical and ecological issues acknowledge that the developed composite seat shell offers superior characteristics in respect to all aspects of the conventional steel counterpart. Although the weight of the lightweight seat shell was reduced by nearly 50 % it was shown, that the lightweight component was able to meet all static and crash-relevant requirements. Additionally it was indicated that these improvements were generated without impairing economical key figures. Furthermore a life cycle analysis regarding the resource consumptions of the seat shells was performed. For this purpose the MIPS concept with its “cradle to grave” approach was used. The results of the analysis showed that the lightweight seat shell can significantly lower the resource consumption by a range of 14 to 34 % relative to the steel part. This gives powerful arguments for the novel lightweight-design and manufacturing technique to be applied for prospective high-volume production.

Acknowledgments

The authors would like to express their gratitude towards the Deutsche Forschungsgemeinschaft (DFG) for supporting the research within the Collaborative Research Centre SFB 639 “Textile-Reinforced Composite Components in Function-Integrating Multi-Material Design for Complex Lightweight Applications.” Likewise the authors would like to express their special thanks to the German Federal Ministry for the Environment, Nature Conservation and Nuclear Safety, the Federal Environment Agency and the Wuppertal Institute for supporting the research within the “Material Efficiency and Resource Conservation” Project.

References

[1] HUFENBACH, W.; GUDE, M.; EBERT, CH.: Hybrid 3D-textile reinforced composites with tailored property profiles for crash and impact applications. Composites Science and Technology 69 (2009) 9, S.1422-1426.

[2] HUFENBACH, W.; GUDE, M.; BÖHM, ET.AL.: Numerical and experimental deformation and failure analysis of 3D-textile reinforced lightweight structures under impact loads. Tagungsband 13th European Conference on Composite Materials (ECCM-13), Stockholm, 02.-05. Juni 2008.

[3] HUFENBACH, W.: Textile Verbundbauweisen und Fertigungstechnologien für Leichtbaustrukturen des Maschinen- und Fahrzeugbaus. Progressmedia Verlag und Werbeagentur GmbH, Dresden 2007.

[4] LETTENMEIER, M., ROHN, H., ET. AL.: Resource Productivity in 7 Steps, Wuppertal Institute, Umwelt, Energie GmbH, online: http://www.wupperinst.org /uploads/tx_wibeitrag/ws41.pdf, 2010.

[5] ATIK, A.: Entscheidungsunterstützende Methoden für die Entwicklung umweltgerechter Produkte, Dissertation, Darmstadt, 2000.

[6] Diebold, K.: Vom Produktabfall zum „Abfall"-Produkt, in: Industrieanzeiger, Ausgabe02/2010, 2010.

[7] KOFFLER, C.; ROHDE-BRANDENBURGER, K.: On the calculation of fuel savings trough lightweight design in automotive life cycle assessments. International Journal of Life Cycle Assessments. 2010, Nr. 1, S. 128-135.

[8] STAHL ZENTRUM: Engagement für Stahl 2009, Düsseldorf, online: www.stahl-online.de/stahl_zentrum/Jahresbericht2009rzAnsicht.pdf, 2009.

SUSTAINABLE DESIGN OF A SIDE DOOR REINFORCING ASSEMBLY – EXPLORATORY OPTIMISATION

M. Kajtaz

School of Aerospace, Mechanical and Manufacturing Engineering, RMIT University, PO Box 71, Bundoora VIC 3083, Melbourne Australia; Email: mladenko.kajtaz@rmit.edu.au

Abstract An optimization study of a door reinforcing assembly is presented. The objective of the study, apart from an alternative material search, is to find an optimal assembly configuration and an optimal topology, whereby the topology optimisation allows for topologies to be produced by unconventional manufacturing processes. A factor analysis was conducted to investigate the effects of multiple input parameters. The thicknesses of the components were observed to be the most influential input parameters. The chosen optimum improved the crush resistance by more than 80%, while reducing the mass by 1.2%. However, the material volume increased by 80% and material utilisation decreased 7%.

1 Introduction

Buying a car is a complex decision making process influenced by many reasons including economic, environmental and social. As customers are becoming more environmentally aware and they demand greener cars. In addition to this heightened environmental awareness, the automotive industry has been affected by with more stringent legislations as well. The reduction of fuel consumption and exhaust gas emissions has become a priority whereby many countries have introduced motor vehicle taxes designed to realise the set reduction targets ([1]).

Substituting alternative materials for conventional materials in vehicle design is an important strategy for reducing environmental burdens over the entire life cycle through weight reduction. Studies have shown that 10% reduction of vehicle weight results in 5 to 8% increase in fuel efficiency ([2], [3]). Lightweight materials such as composites, aluminium and titanium have been investigated as steel substitutes for different vehicle components, resulting in potentially more sustainable vehicle designs. According to Finkbeiner and Hoffmann ([4]), and Gibson ([2]), sustainable vehicle design process should also include other criteria like technical performance, design, vehicle production, cost, quality, etc. Their view on the need to integrate sustainable design principles sooner into the development process to achieve greater benefits in terms of minimised environmental load and cost, is largely accepted in industry and the research community ([5]-[8]).

However, a range of possible alternatives is often limited by other factors such as manufacturability. In this study, computer aided engineering (CAE) and finite element analysis (FEA) in particular, were utilised as rapid design tools in a sustainable virtual design and development of a side door intrusion bar assembly. An extensive exploratory optmisation exercise was conducted to search for a lightweight assembly which would not compromise the strength and stiffness requirements for side doors of passenger cars. In addition, the search for the optimal assembly will not be limited to the conventional manufacturing processes.

It is, therefore, the objective of this study, apart from an alternative material search, to find an optimal assembly configuration and an optimal topology, whereby the topology optimisation allows for topologies to be produced by unconventional manufacturing processes.

2 FEA Model

2.1 Side Door Reinforcing Assembly

Generally, a passenger car door is mounted on a passenger car by a number of vertically spaced hinges attached to a substantially vertical edge of the door. The door can be locked in closed position by a lock incorporated in the door, which is another mounting point. Passenger car doors are required to have a sufficient degree of rigidity to resist external forces applied from front and side areas. Reinforcements, also known as impact beams, are usually placed in the passenger car doors for additional protection against large external forces that are applied upon vehicle collisions. Such impact beams are, however, responsible for an increase in the weight of the doors, resulting in an increase in the total weight of motor vehicles. It is, therefore, an objective to provide a passenger car door having lightweight reinforcing beams, or assembly, arranged effectively to increase the rigidity of the passenger car door, but add a relatively small weight.

The side door reinforcing assembly investigated in this study consisted of four parts (see **Fig. 1.**):

- *Bracket*, a short extrusion that encloses and reinforces the door lock;
- *Post,* a long, curved convexly outwardly extrusion that houses the door hinges
- *Upper* and *Lower Cross-Bars,* two long extrusions disposed in the door body joining the door hinges and the lock

2.2 Requirements and Specifications

The strength and stiffness requirements for side doors of passenger cars are specified by the Australian Design Rule (ADR) 29/00 – Side Door Strength [9]. This standard is applicable to all passenger vehicles in Australia. The crush resistance is determined as an integral of the applied load with respect to the crush distance. The test procedure guidelines for establishing the crush resistance, described in the standards, were used to create a representative FEA model.

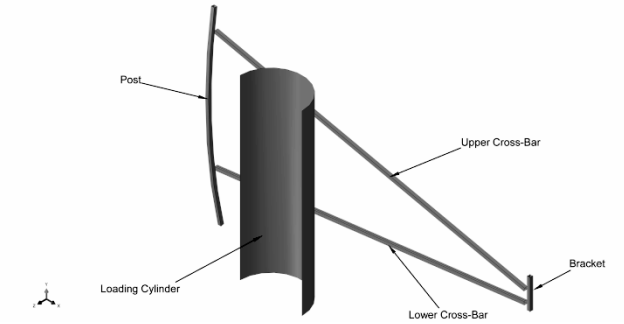

Fig. 1. Side door reinforcement assembly – Representative FEA Model as per ADR 29/00

3 Exploratory Optimisation

3.1 Description of Parameters

The optimisation consisted of coupling the ABAQUS ([10]) solver with the optimisation engine provided by modeFrontier ([11]), a commercial optimisation software package. A total of 83 parameters, summarised in **Table 1**, were used in the optimisation process to fully define the materials, geometry and assembly configurations.

The materials were parameterised as *Density, Elastic Modulus* and *Elastic Limit* triplets. The geometry parameters were used to define extrusion profiles of the components. Each profile was defined by eight control points whose x and y coordinates were input parameters (see **Fig. 2.**). Finally, the assembly configuration was varied by changing the hinge location with respect to the horizontal centre line. In **Fig. 3.**, these parameters are labelled as *uxB_VA* and *lxB_VA*.

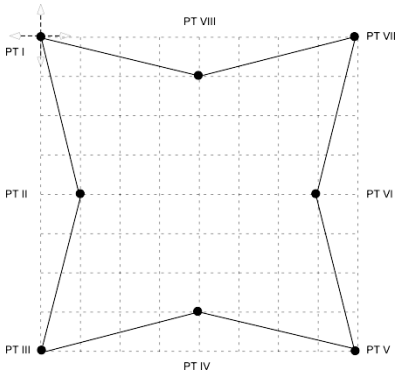

Fig. 2. Extrusion profile – Eight control points

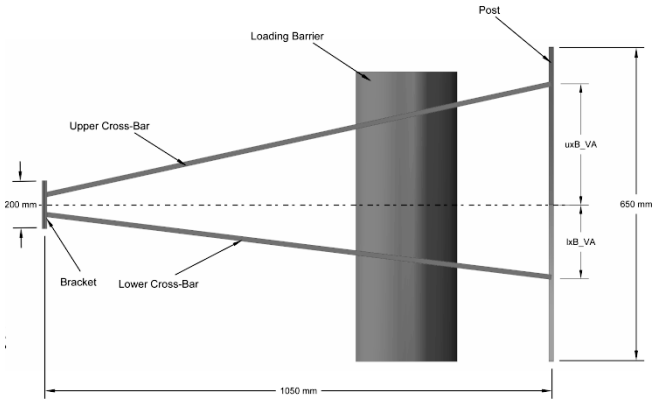

Fig. 3. Assembly configuration parameters

3.2 Description of Constraints and Objectives

The FEA results were assessed by the constraints and rated by the objective functions. The constraints were associated with combinations of the geometry coordinates to ensure feasible profile extrusions. They were treated as an additional objective.

The objective of the optimisation was to find the lightest design that maximised the crush resistance and the Utilisation Factor. The Utilisation Factor was a derived parameter measuring a percentage of elements that exceeded a set value of Mises stress. The twofold roles of the parameter were to monitor and eliminate potential stress concentration and to increase material utilisation.

3.3 Optimisation Scheduler

A proprietary version of Multi-Objective Genetic Algorithm, MOGA-II, was used as the optimisation algorithm in this study. MOGA-II is an efficient multi-objective genetic algorithm (MOGA) that uses a smart multi-search elitism ([12]). Genetic algorithms are designed to mimic an evolutionary selection. A population of candidate designs is evaluated at each iteration, and the candidates compete to contribute to the production of new designs. Each individual is represented by a string, which is a coded listing of the values of the design variables. The entire string is analogous to a chromosome, with genes for the different features (or variables). When individuals are selected to be parents for offspring designs, their genetic strings are recombined in a crossover operation, so that the new designs have elements of two earlier designs. A mutation operation also allows random modification of elements of the new individual so that it may include new features that were not present in either parent. Therefore, there were several user-defines parameters required to provide robustness and efficiency to the optimisation and the values used in this study are summarised in **Table 2.**

Table 1. Summary of input variables

Parameter	Range	Step
Geometry		
Coordinates: PT_Ix, PT_Iy, PT_IIx, PT_IIy, PT_IIIx, PT_IIIy, PT_IVx, PT_IVy, PT_Vx, PT_Vy, PT_VIx, PT_VIy, PT_VIIx, PT_VIIy, PT_VIIIx, PT_VIIIy	-75 – 75 [mm]	1
Thickness	1 – 20 [mm]	1
Material		
Elastic Modulus	30,000 – 250,000 [MPa]	5,000
Elastic Limit	100 – 700 [MPa]	50
Density	7.8E-10 – 7.8E-09 [tonnes/mm^3]	1E-10
Configuration		
Location of upper hinge	30 – 300 [mm]	3
Location of lower hinge	30 – 270 [mm]	4

Table 2. Optimisation algorithm parameters

Parameter	Value	Parameter	Value
Number of Generations	5000	Probability of Selection	0.05
Probability of Cross-Over	0.5	Probability of Mutation	0.1

4 Optimisation Findings

4.1 Factor Analysis

Factor Analysis is an exploratory data analysis which investigates the effects of multiple factors simultaneously. The main feature of this analysis is the Effects Chart, also called DOE or DEX mean plot (DOE and DEX stand for design of experiments). It is a sequence of box-whiskers plots useful for determining a ranking list of the important input parameters. Every experimental design is considered with all input parameters set at two levels, called "high" ("+1" or simply "[+]") and "low" ("-1" or simply "[-]"), respectively. The data are split into two equal-sized groups and a mean value is generated for these groups to see if the mean is increasing or decreasing over time. The means for a single input parameter are connected by a straight line. An input parameter is important if it leads to a significant shift in the location of the response variable or if it leads to a significant change in variation of the parameter.

4.1.1 Effects of Configuration Input Parameters

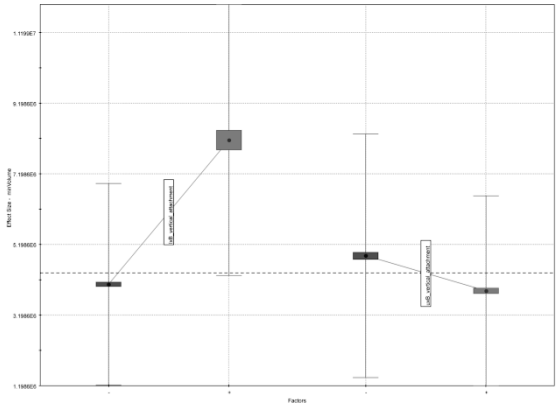

Fig. 4. Effect of configuration parameters on volume (the lower hinge on the left, the upper on the right)

The effects of changing the locations of hinges with the respect to the horizontal centre line are shown in **Fig. 4**. The lower hinge location dominated the upper hinge location when the amount of material present in the model was considered. It was observed that closer the lower hinge is to the centre line, less of the material volume was present in the model. Furthermore, the crush resistance improved as both hinges were closer to the centre line. However, the material utilisation dete-

riorated as the hinges got closer. Improvements of the material utilisation were observed as the lower hinge moved away from the centre line.

4.1.2 Effects of Material Input Parameters

Graphs, similar to that in **Fig. 4.,** were derived for the material input parameters as well. It was observed that a material selection for the *Bracket* was very critical. The effect of the *Bracket* elastic modulus was at least two times more significant than any other material parameter with the respect to the crush resistance. The material utilisation and material volume were significantly influenced by the elastic limits of the *Upper* and *Lower Cross-Bars*, which was expected since these components were mostly deformed. Surprisingly, the effects of material elastic moduli were insignificant with the respect to these two objectives.

4.1.3 Effects of Geometry Input Parameters

For the *Bracket*, all parameters that define dimensions in the direction of the loading were dominant. This was observed for all three objectives. On the other hand, all parameters that define dimensions in the direction parallel to the loading were dominant in the case of the *Post* component, especially with the respect to the crush resistance objective. The dominating geometry parameters in the case of the *Cross-Bars* were obviously parameters that define the surface area perpendicular to the loading direction.

The thicknesses of the components were observed to be the most influential parameter out all input parameters. The findings of the factor analysis are summarised in **Table 3.**

Table 3. Summary of Effects of Input Parameters

Parameter	max(Mat. Util.)	max(Crush R.)	min(Vol.)
Location of upper hinge	–	Close to CL	–
Location of lower hinge	Away from CL	Close to CL	Close to CL
Elastic Modulus	–	Bracket	–
Elastic Limit	Cross-Bars	–	Cross-Bars
Dimensions perpendicular to the loading	Bracket, Cross-Bars	Bracket, Cross-Bars	Bracket, Cross-Bars
Dimensions parallel to the loading	–	Post	–
Thickness	YES	YES	YES

4.2 Optimal Design

The gauge lengths for the baseline model in this study were taken from Wu *et al*. ([13]). Their rectangular cross section optimum design was considered.

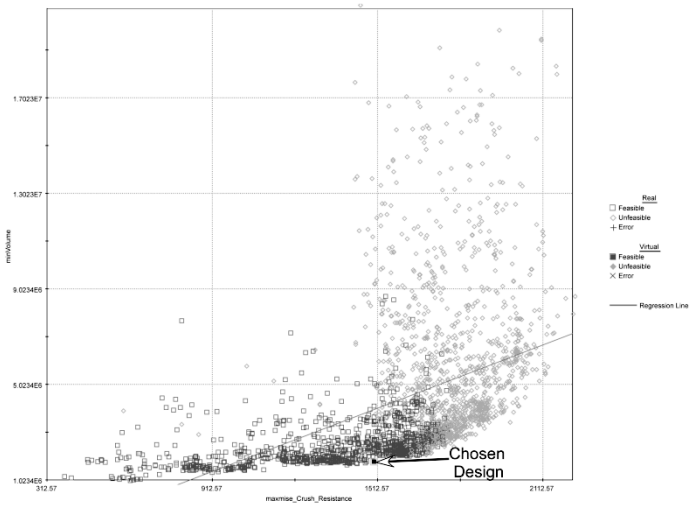

Fig. 5. Pareto Frontier

In a multi-objective problem, such as this one, a notion of optimum changes as the aim is to find good compromises rather than a single solution. Therefore, the study produced a set of solutions, called Pareto solutions or Pareto frontier. In the Pareto frontier, none of the objectives can be improved without deterioration of at least one of the other objectives. As the Pareto optimal solutions can be regarded as equally desirable, in the mathematical sense, a trade-off study was necessary. A design, indicated in **Fig 5.,** was identified as the most preferred one among the solutions – representing an acceptable trade-off between the objectives.

In contrast to the baseline model (see **Fig. 6.**), the chosen optimum (see **Fig. 7.**) improved the crush resistance by more than 80%, while reducing the mass by 1.2%. However, the material volume increased by 80% and material utilisation decreased by 7%. Such incomparable change in the volume and mass was possible due to the alternative materials. The optimisation converged to lighter and sufficiently strong materials such as wrought aluminium and zinc-aluminium general casting alloys.

5 Conclusion

An optimization study of a door reinforcing assembly was presented. The objective of the study, apart from an alternative material search, was to find an optimal assembly configuration and an optimal topology, whereby the topology optimisation allows for topologies to be produced by unconventional manufacturing processes. A factor analysis was conducted to investigate the effects of multiple input parameters. The thicknesses of the components were observed to be the most influential input parameters. The chosen optimum improved the crush resistance by more than 80%, while reducing the mass by 1.2%. However, the material volume increased by 80% and material utilisation decreased by 7%.

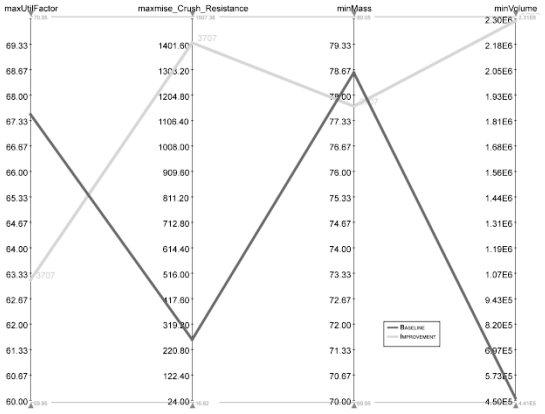

Fig. 6. Comparison against the baseline model

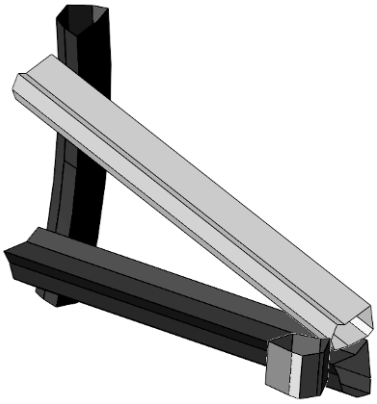

Fig. 7. Optimal assembly

References

[1] Blöcker, A. and U. Jürgens (2009). 'Changes in the German Car Design and Development Sector and the Challenge of Sustainability'. *16th GERPISA International Colloquium*.

[2] Gibson, T. L. (2000). 'Life Cycle Assessment of Advanced Materials for Automotive Applications'. *Society of Automotive Engineers (SAE)* 2000-01-1486.

[3] Brooke, L. and H. Evans (2009). 'Lighten Up!' Automotive Engineering International, *SAE International:* 3.

[4] Finkbeiner, M. and R. Hoffmann (2006). 'Application of Life Cycle Assessment for the Environmental Certificate of the Mercedes-Benz S-Class' *The International Journal of Life Cycle Assessment* 11(4): 240-246.

[5] Leibrecht, S. (2005). 'Fundamental Principles for CAD-based Ecological Assessments'. *The International Journal of Life Cycle Assessment* 10 (6): 436-444.

[6] Schäper, S. (2006). 'Sustainability-Optimised Material Selection and Product Design at Audi'. *Sustainable Metals Management*: 535-562.

[7] Schiavone, F., M. Pierini and V. Eckert (2008). 'Strategy-based approach to eco-design: an innovative methodology for systematic integration of ecologic/economic considerations into product development process'. *Int. J. Sustainable Design* 1(1): 15.

[8] Kajtaz, M., Subic, A., Takla, M. (2010). 'A collaborative FEA platform for rapid design of lightweight vehicle structures'. *Int. J. Vehicle Design* 53(1/2): p. 110.

[9] ADR (2006). Vehicle Standard (Australian Design Rule 29/00 – Side Door Strength); Available from: http://www.comlaw.gov.au

[10] SIMULIA. Simulia Products - Abaqus FEA. 2010; Available from: http://www.simulia.com/products/abaqus_fea.html.

[11] ESTECO. ESTECO Products :: modeFrontier. 2010; Available from: http://www.esteco.com/products.jsp.

[12] Poles S. (2003). 'MOGA-II An improved Multi-Objective Genetic Algorithm'. *ESTECO Technical Report* 2003-006,

[13] Wu, C-H., C-P. Liang and J-H. Lee (2006). 'Optimization of Side Impact Bar for Crashworthiness'. *Society of Automotive Engineers (SAE)* 2006-01-0245.

RESEARCH AND DEVELOPMENT OF A NEW AND SUSTAINABLE COMPOSITE: "NATURAL STONE LAMINATE"

L. Müller[1], J. Wellnitz[1,2]

[1]Private Institute for technique and artistic design e.V., Marie Curie Straße 6, 85055 Ingolstadt,Germany; Email: lars.mueller@itd-in.de

[2] University of Applied Sciences Ingolstadt, Esplanade 10, 85049 Ingolstadt, Germany; Email: joerg.wellnitz@haw-ingolstadt.de

Abstract NSL (Natural Stone Laminate) is a new sandwich material combining the favorable properties of natural stone and metal. Using two widely available and low priced components, the laminate will reach a competitive price level. The fields of application include construction, security and design. The current research is mainly working on the optimisation by running several tests. Finding different values for Tensile strength, Young's Modulus Bending- and impact behaviour are just a short overview of our work. Further development especially in the fields of forming and processing NSL will certainly open up even more possibilities for this competitive sandwich material. By regulating the used layers and materials NSL perfectly fits to the consumers needs.

1 Introduction

Light construction is the philosophy of gaining maximum reduction in weight. Especially in times of raising ecological damage, R&D efforts are on their way to find *lighter constructions*. On the one hand this is achieved through weight optimization of existing materials, on the other hand through engineering *totally new materials*. Variable sandwich- and laminate-structures combine different materials in order to *create optimized material behavior*. Besides material properties*, availability and price* play a major role in the development process of new materials.

Strengthening plastics using carbon fibre herein surely was one of the most interesting ideas in former times. The developed combinations turned out to be suitable for usage and are certainly very useful in their field of application. Also combinations of plastics and glass fibre are well known, and GLARE® was a further development in using aluminum. Figure 1 shows the material mix in a modern airplane and underlines the extensive usage of composite structures.

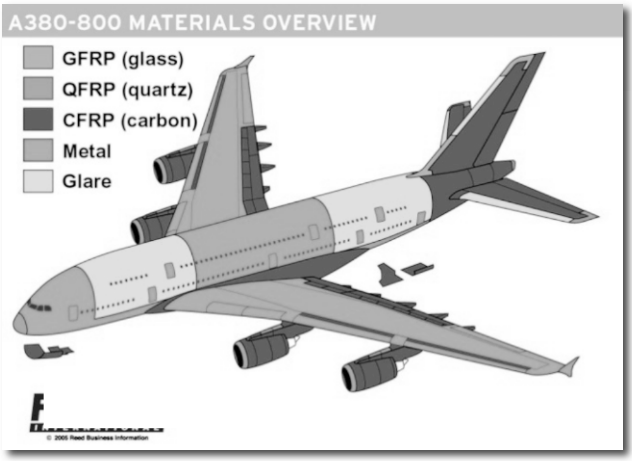

Fig. 1 Material overview in long distance airplanes [1].

2 Approach

To consider availability and price being the major focus in developing *a new material* a new idea needs to be found.

In the field of metallic materials a lot of realisable variants have been created and are still in use. Especially in *modern Airplanes* aluminium is often used as a light and stable metal in a lot of fields. The problem of difficulties in *availability* is negligible and one can count on the experiences in using aluminium and steel as it creates reliable and save constructions. To minimize damage in cases of debris containment a combination with an impact resistant material is very rewarding and surely opens interesting fields of application.

Earth is a terrestrial planet, meaning that it is a rocky body. It is the largest of the four solar terrestrial planets, both in terms of size and total mass. Considering availability issues stone as a new *"material"* is quiet obvious.

The "*Private Institute for technique and artistic design e.V*" and the "*University of Applied Sciences Ingolstadt*" are intensively working on developing a *brand new composite*. A thin foil of stone is brought to a metal carrier which is the source for creating a laminate of several coatings. The result is called "*Natural Stone Laminate*" (NSL – Figure 2) and *combines advantages* of both of the different elements.

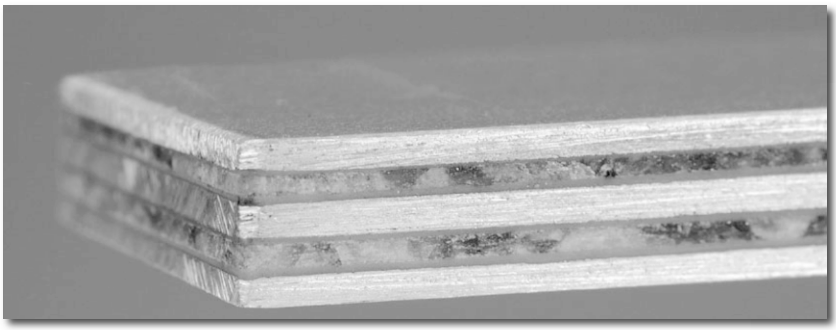

Fig. 2 Natural stone laminate.

By changing the properties of the three constituents - metal, stone and the way of bonding - the behaviour of the laminate can be adjusted to the users' requirements. There is no need for temperature treatment on the material and no difficulties of machining. By using high temperature resistant adhesives it even could be used in hot environments *(up to 500°C and higher)*.

A density of 2,7 kg/dm^3 with simultaneously very good *bending behaviour, acoustic damping, impact resistance and many more*, the NSL reaches different fields of the market.

3 Production

The pilot production is laboratory work. Layers of an "AB" combination - consisting of metal and stone - are produced in different types depending on their needs. By bringing several layers together symmetrical and asymmetrical plates can be created and formed, always allowing for construction issues.

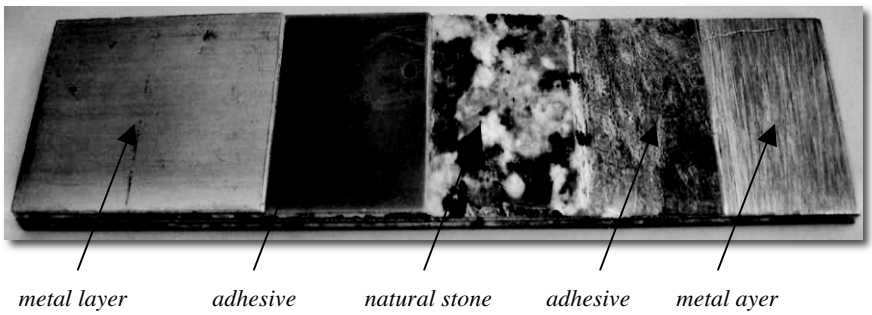

Fig. 3 Schematic of natural stone laminate.

Figure 3 shows the first "ABA" Layer of a *symmetrical assembly*. The used material is a combination of *Bianco Sardo* and *aluminium* using an *adhesive*. Investigation is also working on alternative possibilities of bonding (e.g Ceramic, Ultrasonic) and optimisation of serial production.

4 Experimental and numerical investigations and validation

4.1 Bending behavior

For a better understanding of the materials behaviour several experimental and numerical testing are planned within the projected research. One of the steps is the comparison of a mathematical model with *laboratory work* which is done in cooperation with the *University of Applied Sciences in Ingolstadt*. Within a *three-point-bending test* a specimen is bent while data of force and elongation are collected.

As it can be seen in Figure 4, a compressive loaded *AB – Laminate* reaches distinctly better results considering bending behaviour – stiffness and strength. That's not exciting, knowing the good values of comprehensive strength of the natural stone.

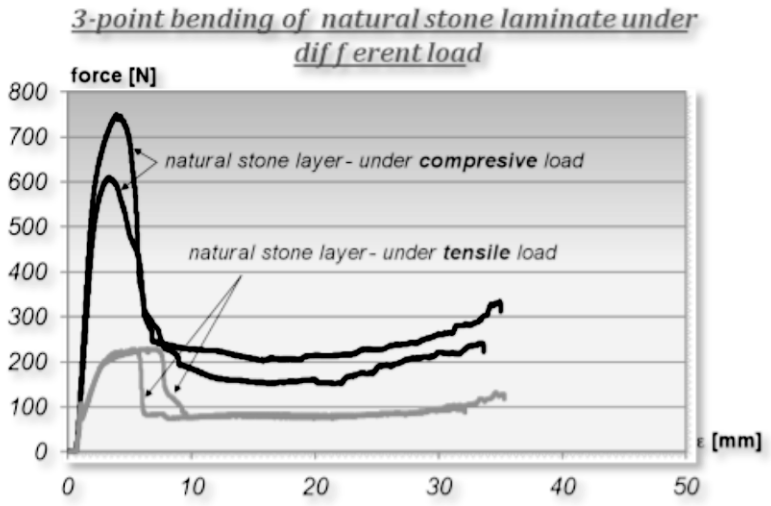

Fig. 4 Bending behavior under selected loads.

Although stone is very brittle, the fact that it is used in thin foils and set between aluminium provides it with a *very good bending behaviour*. That even allows a certain *amount of bending the stone*, without loosing the function of the composite. In Figure 5 that effect is shown.

Fig. 5 layer of NSL using "Bianco Sardo" after bending.

By calculating a *Young´s Modulus* of the entire laminate a model can be built for FE methods to integrate the CMA in engineering construction methods. For supporting the theory several laminate theories have been applied to composite laminates. The classical laminate theory is an extension of the Love-Kirchhoff assumption for isotopic plates and can be applied if the laminate is thin because transverse shear stresses are not considered [2]. As the problem of shear stress cannot be neglected, there is a need for a higher order shear deformation theory. In this case the third order theory of Reddy [3] will be used to describe the inner activities.

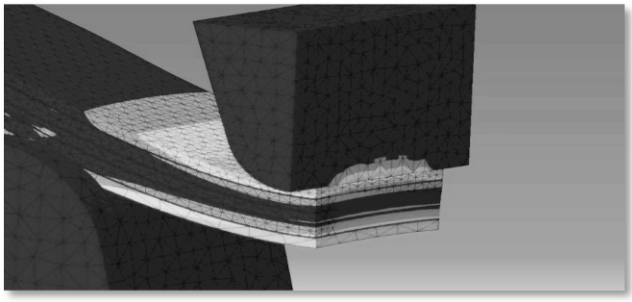

Fig. 6 FE simulation of a 5 layer natural stone laminate resistance.

4.2 Acoustic testing

Besides very good compressive properties the natural stone offers *excellent values of noise insulation*. In a test in cooperation with the *Fraunhofer Institute* at

Stuttgart, sound transmission values were evaluated. Therefore an aluminium sandwich (Figure 7) was compared with a natural stone laminate plate of the *same weight*.

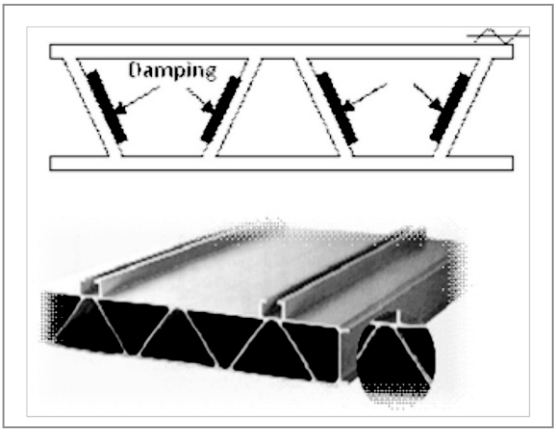

Fig. 7 Aluminum sandwich test specimen for noise insulation.

For the acoustic tests a natural stone called "*Nero Assoluto Zimbabwe*", a magmatic plutonic rock was chosen in an "ABA" composite with aluminium.

With *over 3dB* in the middle, natural stone laminate reaches a *far better insulation level*, than the aluminium sandwich does.

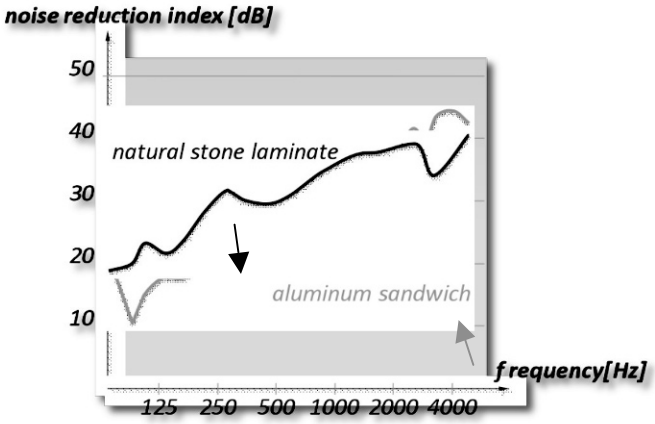

Fig. 8 Noise reduction index of selected testees.

5 Outlook

Next steps are to continue the evaluation of NSL. Therefore the ITD is working together with the University in Ingolstadt which allows the use of very modern laboratories. The ITD has built up a *slow speed impact testing* system for penetrating materials with different projectiles like ice and stone.

Possibilities of the system are:

Maximum of projectile size 300x300
Projectile: ice 50 g, stone 10 g
Distance of acceleration 5 m
Work pressure 8 bar
Maximum of velocity 250 m/s

Another point is to determinate substitutes to the used adhesives, e.g. the procedure of *ultrasonic welding*, that shows great results in first tests and even allows operation in high temperature areas. Exceeding investigation must be done in scope of manufacturing *complex shaped structures*.

References

[1] FlightGlobal, www.flightglobal.com, accessed on Oct 19th, 2009, http://www.flightglobal.com/assets/getAsset.aspx?ItemID=9116
[2] Altenbach H., Altenbach J., Rikards R. (1996), Einführung in die Mechanik der Laminat- und Sandwichtragwerke, Deutscher Verlag für Grundstoffindustrie Stuttgart, Erlangen.
[3] Reddy J.N.(1996), Mechanics of Laminated Composite Plates, CRC Press, USA.

VI VEHICLE SYSTEMS

IN-WHEEL COUPLED SUSPENSION AND DRIVE: DESIGN, DEVELOPMENT, AND MODELING

R. Clippard, J. Ziegert

Department of Automotive Engineering, Clemson University, 4 Research Drive, Greenville, SC 29607 U. S. A.; Email: rclippa@clemson.edu

Abstract: Vehicle propulsion systems are evolving to include more hybrid and purely electric systems. This trend has revived interest in hub-motor technology where the electric motor providing traction torque is integrated into the wheel, providing space saving and packaging advantages and enabling enhanced vehicle stability control through torque vectoring. The disadvantage of this approach is a significant increase in unsprung mass, which may detract from ride quality. This paper describes the development of a novel in-wheel coupled active suspension and drive system. This system utilizes two motors per wheel and a two degree of freedom kinematic mechanism that allows their torque to be utilized for both vertical suspension actuation as well as rotational actuation of the wheel. The system is designed such that when the motors are providing equal torque in the same direction, all energy is directed to traction and longitudinal propulsion of the vehicle. When the torque output of the motors is unequal, a net vertical force is applied to the wheel causing the suspension to move vertically and enabling active control of ride quality as well as control of vehicle attitude in acceleration, braking, and cornering. This paper will discuss the design of the system including kinematic synthesis, drive component selection, and simulation using multi-body dynamics software. Vertical, longitudinal, and combined actuation was tested and analyzed using multiple torque combinations and loading conditions. Although this integrated propulsion drive and active suspension architecture inherently tightly couples the longitudinal and vertical dynamics of the vehicle, the results of the simulations show that the system is capable of actuating in either degree of freedom independently, or in a coupled mode where it actuates in both modes simultaneously. The simulations showed that the system was capable of actively controlling the vertical wheel position while maintaining constant drive torque and rotational velocity of the wheel.

1 Introduction

Increases in electrically based vehicles are quickly penetrating the marketplace and are winning a spot in consumer's hearts. Many of these are based around a similar architecture to current internal combustion powered vehicles with a main drive motor, transmission, and then the power is delivered to the wheels. An alternate architecture under consideration is to locate the motor(s) inside the wheels to eliminate the transmissions and driveshafts. A downfall of hubcentric drives is the increase in unsprung mass. Increases in unsprung mass relative to the sprung mass of a vehicle increases the transmissibility ratio between the two masses, and this leads to a lower vibration isolation efficiency of the suspension [1]. This paper describes a novel design that allows the drive motors to also be utilized to actuate the vertical motion of the suspension to enable active control of vehicle attitude as well as potential improvements in ride quality. This design incorporates dual electric motors inside each wheel, coupled with a two degree of freedom kinematic mechanism to replace both the drive and suspension of a vehicle.

2 Kinematic Synthesis and Operational Modes

The system consists of two coupled slider crank mechanisms combined with a dual electric motor drive. The two motors can be linked to the main drive by any number of methods, but for the initial system the actual drive connections were treated as a friction connection with zero slip. This removed the potential noise that gears or a timing belt would add to the system while also reducing the simulation time and resources needed. The slider crank shown in Fig. 1 represents the right side of the entire system and provides a single degree of freedom. The motor pivots around the main drive connection maintaining a constant distance between the main drive and motor so that the drive coupling will remain in contact. The mass is connected to the motor mount via a control link and is also constrained to purely vertical motion by a slider connection. As the motor is actuated it walks around the main gear pushing and pulling on the vehicle body. When two of these systems are connected together to form a symmetric mechanism the main drive can be allowed to rotate and thus a second degree of freedom introduced. The coupled configuration also utilizes a spring and damper to support the vehicles mass.

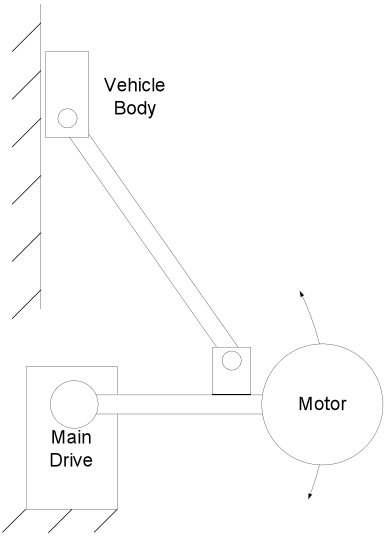

Fig. 1 Slider Crank Mechanism

The system has the ability to actuate in the vertical direction, rotationally, or both at the same time. These three different actuations are the operational modes of the symmetric mechanism. The operational modes are defined by the relative direction and magnitude of torques T_1 and T_2 (

Fig. **2**). When both motors are providing equal torques in both magnitude and direction the system acts as only a drive system for the wheel. Forces F_1 and F_2 are equal and opposite so there is a zero net force acting on the vehicle body so no vertical actuation takes place and all the actuation effort is utilized in driving the rotation of the tire and wheel. When the torques are of equal magnitude but opposite directions the system works solely in the vertical direction. In this situation forces F_1 and F_2 are equal in both magnitude and direction and the vehicle body is moved, but the net torque on the main drive, T_3 is zero so there is no rotational actuation. When any other torque condition exists, the system operates in both the vertical and rotational degrees of freedom.

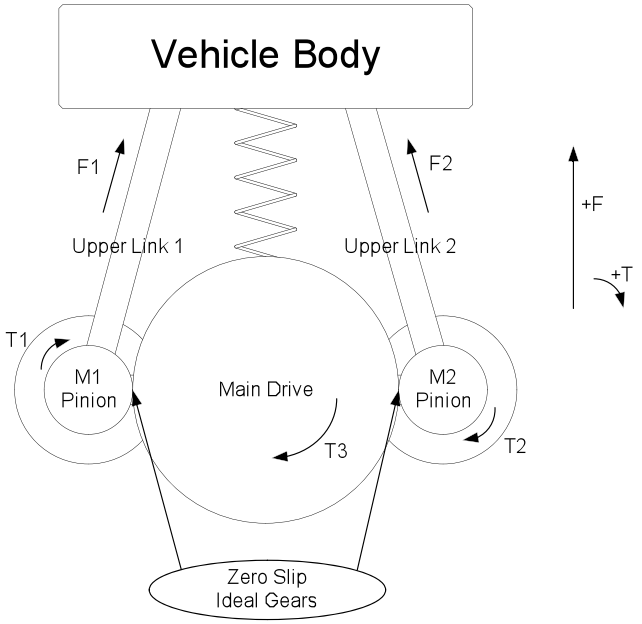

Fig. 2 Full System Diagram

3 Drive Sizing and Tradeoffs

As with any design there are a couple of obvious tradeoffs that can be made to allow for some adjustment in the overall sizing, performance, and configuration. The first major tradeoff is the physical size of the motor versus the size of the wheel. The torque of the motors versus the gear reduction is another tradeoff although this is closely linked to the physical size of the motors. The third tradeoff is the upper control link mount position on the motors. These design considerations allow for the system to be adjusted for different applications and performance metrics.

Currently, the power density of electric motors limits their ability to produce large amounts of torque from a small package size. Advances are being made, liquid cooling and stronger magnetic fields are allowing overall size to be reduced while the torque is increased [2-4]. The inner wheel diameter limits the amount of space that can be occupied by the two electric motors, and the actual vehicle design can limit the overall length of the motor. The system relies on the motors ability to rotate around the same axis as the wheel and main drive gear. As such there is some space that must be occupied by the rotational mechanism. So the two motors are limited to the space that is defined by the wheel inner diameter

minus the rotational mechanism diameter. This sets the spacing and limits the available reduction ratio between the motors and the main drive.

The reduction between the motors and the main drive defines the available motor vertical travel as well as the maximum speed available. To increase the maximum velocity of the vehicle a lower reduction ratio is desired, but this hurts the acceleration performance as well as reducing the vertical travel of the motors. In order to combat the reduction of vertical travel it is possible to adjust the upper control link mount on the motor.

This control link allows the overall travel to be adjusted as well as providing a mechanism for mechanical advantage for actuating the system vertically. As the upper links mounts are moved closer to the center of the wheel there is a larger mechanical advantage and this generates larger actuation forces, but it also reduces the available vertical travel. The motors have limited rotation around the central rotational axis before they encounter a collision with another part of the mechanism. By moving the upper control link mounts further away from the central rotational axis the mechanical advantage is reduced, but the overall vertical travel is increased.

As with every system, the end design is a compromise between these tradeoffs. The overall design goals will help to weigh the effect of one design choice over another. The goals for this system were to prove that both motions were possible utilizing the mechanism, that adequate vertical and rotational accelerations could be obtained by current motor technology, and that the coupled actuation could be achieved with the available torque.

4 Simulation

Simulation of the quarter vehicle model was performed utilizing Simpack© multibody dynamic simulation software. The vertical displacement and acceleration were tested to determine the system's ability to perform vibration isolation and attitude control. The longitudinal acceleration was tested to determine potential braking and acceleration performance. Finally the coupled system was simulated by applying time varying torque signals to the system to induce different rotational and vertical operating conditions.

The vertical actuation was tested by applying equal but opposite torques to the two motors. The results are shown in Fig. 3. The system is sized with two DC electric motors capable of delivering 75 Nm peak torque. With opposing torques the motors were able to actuate the vehicle body vertically by 60mm when pushing up and 32mm when pulling down. The reduced downward travel is due to the support spring that holds the mass up when there is no actuation. The additional displacement towards the maximum vertical position is due to the increased mechanical advantage as the motors near the top of the main drive.

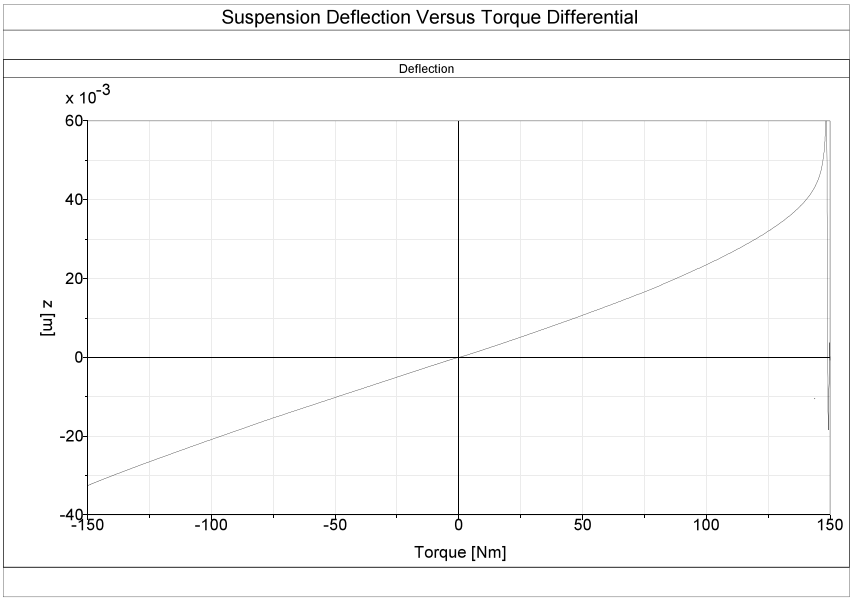

Fig. 3 Vertical Position versus Torque

Utilizing the 75 Nm motors and a 5:1 drive ratio between the motor pinion and the main gear, the peak available vertical acceleration is just over 3.5 m/s^2 in both directions. Higher vertical accelerations can be achieved if the upper link connection points are moved closer to the spindle axis the spindle at the expense of reduced range of vertical motion. .

The rotational simulation utilized an equivalent inertia for the tire to simulate actuating the actual mass of the vehicle longitudinally. The motors are driven with equal torques in both magnitude and direction. The calculated peak acceleration of the vehicle is 5.5 m/s^2. This can be adjusted by the design tradeoffs also. An increased drive ratio will increase peak acceleration performance at the cost of a reduced maximum speed.

Fig. 4 shows the system operating in a coupled mode. The rotational actuation was held constant so that there was no rotational acceleration, i.e. the vehicle speed is constant. At 0.5 seconds a torque differential of 20 Nm was applied to the existing torque signal. This differential allowed the vertical actuation of 6mm which is what is expected when referring back to the pure vertical simulations. There was still a positive torque on the main drive which maintained the rotational velocity.

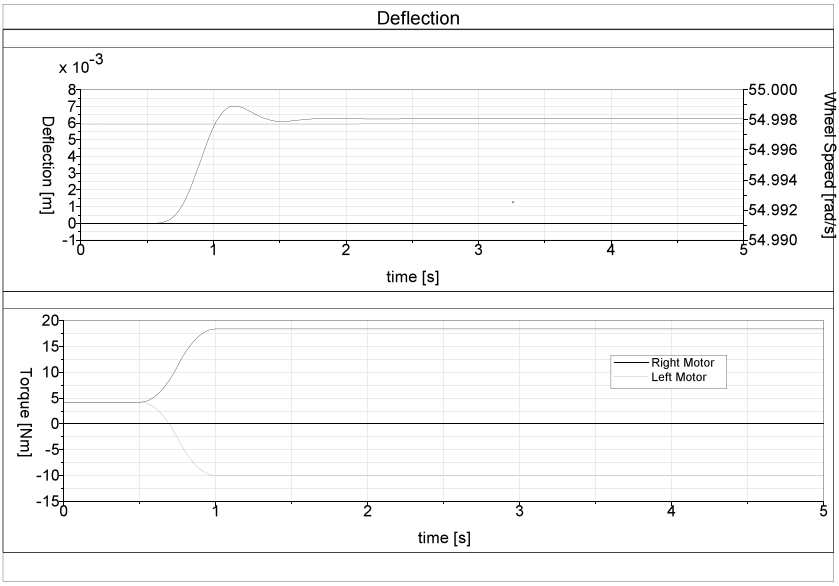

Fig. 4 Coupled Actuation

5 Conclusion

The coupled mechanism has the ability to provide actuation in both the rotational and vertical degrees of freedom with equivalent inertias and masses of a quarter vehicle model. Peak accelerations of over 3.5m/s^2 vertically and 5.5m/s^2 longitudinally are possible when only actuating the mechanism in a single DOF. The vertical actuation opens the door for use as an active suspension and/or attitude control actuator for vehicles while still providing longitudinal actuation of the vehicle. This actuation is possible with torque ranges that are available in commercial motors that fulfill initial packaging requirements of a compact vehicle.

References

[1] Wong, J.Y., *Theory of Ground Vehicles*. 3rd ed. 2001, New York: John Wiley & Sons, Inc.

[2] Rahman, M.A. and M.A. Masrur. *Advances on IPM technology for hybrid electric vehicles*. 2009. Piscataway, NJ, USA: IEEE.

[3] Fang Lin, L. and Y. Hock Guan. *Advanced PM brushless DC motor control and system for electric vehicles*. 2000. Piscataway, NJ, USA: IEEE.

[4] Chan, C.C. and K.T. Chau, *An advanced permanent magnet motor drive system for battery-powered electric vehicles*. IEEE Transactions on Vehicular Technology, 1996. **45**(1): p. 180-8.

OPTIMISATION OF AUTOMOTIVE SEAT KINEMATICS

M. Leary, M. Mazur, T. Mild, A. Subic

RMIT University, Bundoora, Victoria 3083, Australia
Phone: +61 3 9925 6177; Email: martin.leary@rmit.edu.au

Abstract Automotive seating structures have evolved over an extended period of development, resulting in convergence of practical embodiments to a planar kinematic chain, typically based on a four-bar linkage. Seating structures are subject to a stringent set of constraints and objectives, including: allowable envelope of motion, structural integrity, modularity and product cost. Although four-bar linkage kinematics is well understood, the large design space, combined with multiple constraints and objectives, impose significant challenges to design optimisation. The following work illustrates a practical method to resolve these conflicting design requirements by mapping the feasible design space and quantifying the relative merit of feasible designs for various objectives.

1 The design problem

The automotive seat structure is required to accommodate the anthropometric variation of users while meeting minimum safety standards under low and high speed crash scenarios [1]. Seating position is adjusted in multiple degrees of freedom (DoF) to locate the user with respect to vehicle controls (pedals and steering wheel). The design problem is further constrained by the allowable spatial envelope and allowable actuating effort for each DoF. Commercial competitiveness requires the minimisation of manufacturing cost and system weight.

The design task is a multi-objective optimisation problem consisting of identifying the set of dimensional parameters that achieve the required range of motion in each DoF without violating the design constraints. This work illustrates a practical method of identifying the set of feasible and optimal seat parameters.

2 Fundamental model

Benchmarking of automotive seating structures has identified that practical embodiments have converged to a planar kinematic chain [1]. This kinematic chain may exist in several variants, each with their own unique performance attributes. Of these observed kinematic chains, the typical implementation is a four-bar linkage[1], "the simplest possible pin-jointed mechanism for single degree of freedom controlled motion" [2].

The behaviour of the four-bar linkage is well understood based on the Grashof condition (Fig.1) [3], which classifies kinematic behaviour based on the length of the shortest, s, longest, l, and other links, p and q. Depending on which of these links is shortest (Table 1), the grounded links will be will behave as a crank (rotary motion), or a rocker (reciprocating motion). Of these permutations, the parallelogram and crank-rocker are often observed in automotive seating structures. The latter is typical as it results in induced tilting as the seat lifts – desirable to accommodate different percentile users. For example, shorter users typically require a higher seating position and greater seat tilt and vice versa [1].

Table 1. Classification of four-bar mechanisms.

Type	Grashof condition	Shortest link	Behaviour
1	$l+s < p+q$	frame	double-crank
2	$l+s < p+q$	grounded link	crank-rocker
3	$l+s < p+q$	coupler	double-rocker
4	$l+s > p+q$	any	double-rocker
5	$l+s = p+q$	any	double-crank (parallelogram)

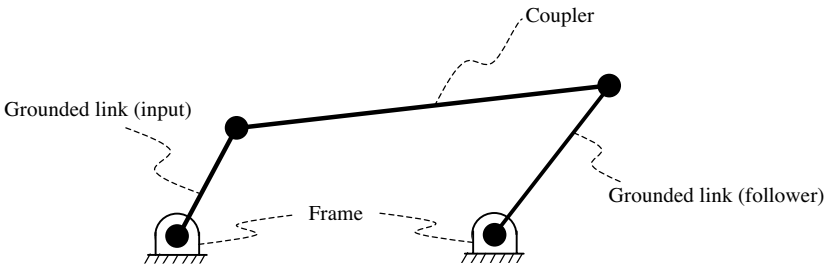

Fig 1. Four-bar linkage and associated nomenclature.

[1] Other embodiments include five-bar linkages and independent rocker actuation. The four-bar linkage may include an additional crank-slider to enable seat tilting [1].

3 Simulation

Despite the apparent simplicity of a four-bar linkage system, the number of input parameters (link lengths and frame position) and allowable permutations results in a very large design space. Furthermore, automotive seating structures are subject to multiple constraints and objectives which stymie systematic optimisation efforts. Historically, such problems are solved by inspection, or with graphical [4], or numeric [2] aids. The following work illustrates a practical method to resolve these conflicting design requirements by mapping the feasible design space and quantifying the relative merit of feasible designs for various objectives.

An algebraic model of four-bar linkage kinematics [3] was interfaced with a process integration and design optimisation (PIDO) tool (Fig. 2). PIDO software has the capability to facilitate automated analysis by the integration of standalone CAE tools to enable automated design of experiments (DOE), parametric analysis, multi-objective optimization, and statistical evaluation of system models [90, 120]. The optimisation approach consisted of two phases.

An initial analysis was developed to explore the design space using a DOE approach. Due to the analytical nature of the kinematic model, the computation cost of each evaluation was sufficiently low[2] to allow a high resolution experiment, providing the designer with a rapid overview of the feasible regions of the design space and aiding in the identification of local optima.

The second phase of the optimization approach addresses the multi-objective optimisation problem within the feasible regions of the design space. Genetic Algorithms are stochastic optimization algorithms modeled on the processes of evolutionary biology. A random population of problem input variables is evaluated to identify how well they satisfy problem objectives. The fitness of the population is subsequently improved through manipulations that are analogues for the mechanics of natural selection.

Stochastic optimization algorithms are suited to a large search space due to inherent robustness against objective function discontinuity and local optima stagnation. In contrast, deterministic algorithms (such as the Simplex approach) are more efficient at converging towards an optimum, but are typically only robust within localised regions of the search space and can stagnate at local optima [6]. For models which exhibit a high computation cost, it may be beneficial to refine the optimisation phase with deterministic algorithms prior to stochastic optimization [7]. Due to the low computational cost of the kinematic model used in this work, the direct application of a stochastic GA yielded acceptable results within a reasonable computation time.

[2] The basic four-bar linkage analysis required approximately 2.5 seconds on a 3GHz CPU.

4 Simulation results

The initial high resolution DOE analysis parameter space was populated using full factorial sampling of the model input parameters with an experiment size of 12,888 model evaluations. The subsequent multi-objective GA optimisation analysis was initialised with the feasible design space identified in the DOE results. The optimisation problem consisted of four competing objectives, and additional constraints. The GA was limited to 10 generations, resulting in a simulation size of 122,880 model evaluations. The total solution time was 3.5 days on a 3GHz CPU.

Table 2. Model input parameters.

Input parameter	Dimension
Input link length	mm
Follower link length	mm
Height of ground link and frame node	mm
Input link inclination	degrees
Follower link inclination	degrees
Included angle of follower rotation	degrees

Table 3. Model output parameters, dimension and objective.

Output parameter	Dimension	Objective
Vertical travel (at reference point)	mm	Minimise
Horizontal travel (at reference point)	mm	Minimise
Lift effort	N	Minimise
Pumps to achieve full lift	-	Minimise

The simulation identified 20,204 feasible designs with 304 designs being Pareto-optimal (Fig. 3). Without relative importance weighting of the competing design objectives there is no clearly optimal solution, as the set of Pareto-optimal designs offer equal performance in satisfying the design objectives; an improvement in one objective leads to a compromise in others. Designs of interest are identified with associated identification numbers (Fig. 3):

- Minimum peak force: #105908
- Minimum number of pumps to lift seat: #53684, #122063 and #105908
- Minimum horizontal travel: #50568

The other identified designs of Fig. 3 are balanced compromise between competing objectives.

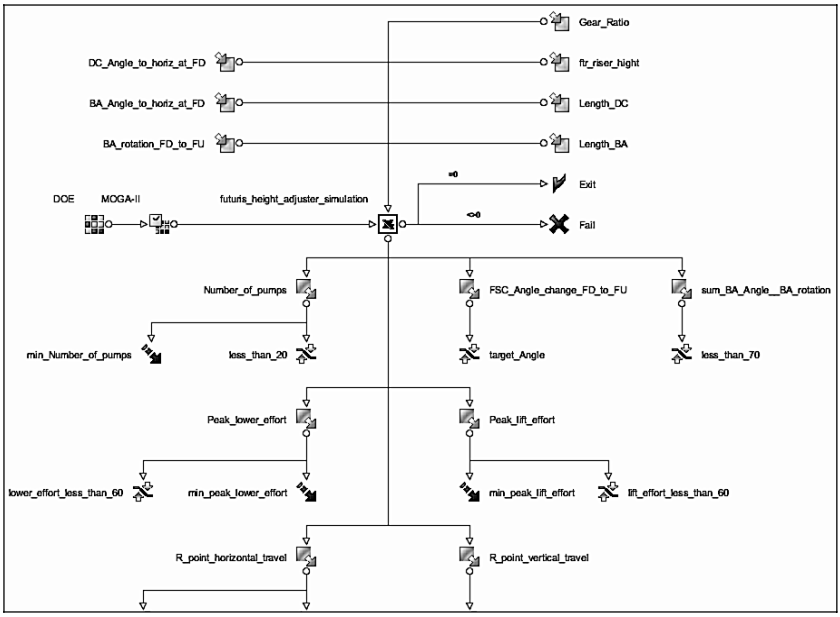

Fig. 2. Graphical process and logic workflow associated with the second phase of simulation.

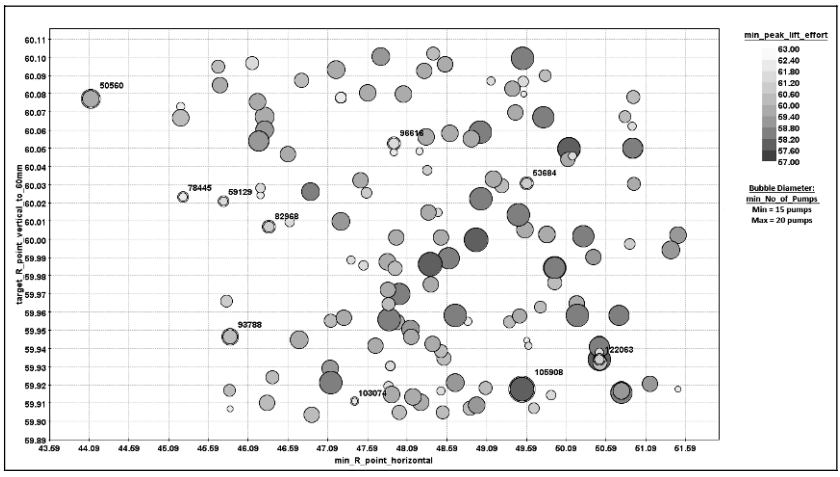

Fig. 3. Four dimensional chart indicating performance of Pareto-optimal solutions. Designs referred to in the discussion have been labeled with associated identification numbers.

5 Conclusion

Despite the apparent simplicity of the planar four-bar linkage, the large number of input parameters and possible permutations result in a very large design space. Furthermore, the presence of constraints and competing design objectives makes it difficult to identify regions of local and global optimum performance.

Due to the low cost of the analytical model a high-resolution DOE analysis combined with a stochastic optimization algorithm provide a practical method to resolve these conflicting design requirements by mapping the feasible design space and quantifying the relative merit of feasible designs for various objectives. PIDO tools lend themselves well to the rapid solution of this problem through embedded automated analysis, optimizations and decision making tools. Manual analysis would be impractical and significantly limited in comparison.

The proposed solution strategy can be extended to other problems for which the design space is large and the associated system model has low computational cost.

References

[1] Leary, M., Mazur, M. Gruijters, J., Subic. A. (2010). Benchmarking and Optimisation of Automotive Seat Structures. In Wellnitz, Subic, Leary (Ed.), *Sustainable Automotive Technologies 2010* (pp. 63–70). Berlin Heidelburg: Springer.

[2] Norton, R. (1999). *Design of Machinery*. 2nd Edition. USA: McGraw Hill.

[3] Barker, C. (1985). A complete classification of Planar Fourbar Linkages. Mechanisms and Machine theory, 20(6), 535–554.

[4] Bastow, D. (1976). *Kinematic and Dynamic Data for Crank-Rocker and Slider-Crank Linkages*. Engineering Sciences Data Unit, London.

[5] Flager F, Welle B, Bansal P, Soremekun, G, Haymaker J. Multidisciplinary process integration and design optimization of a classroom building. Electronic Journal of Information Technology in Construction 2009;14: 595-612.

[6] Deb, K., Pratap, A., Agarwal, S., and Meyarivan, T. 2000, A Fast and Elitist Multi-Objective Genetic Algorithm-NSGA-II, KanGAL Report Number 2000001.

[7] Deb, K., (2006) *Optimization for Engineering Design*, New Delhi: Prentice-Hall.

[8] Hiriyannaiah S, Mocko G. Information management capabilities of MDO frameworks. 2008 *Proceedings of the ASME International Design Engineering Technical Conferences and Computers and Information in Engineering Conference* 2008; A:635-645.